

**THE UNIVERSITY OF MICHIGAN**  
**COLLEGE OF ENGINEERING**  
**DEPARTMENT OF ELECTRICAL ENGINEERING**  
**Radiation Laboratory**

LOW FREQUENCY SCATTERING BY PLASMA COATED OBJECTS  
Final Report January 1969 - January 1970

By  
Ralph E. Kleinman, Thomas B.A. Senior and  
Piergiorgio L. E. Uslenghi

Prepared under  
ARPA Order 709, Program Code Number 8 E 40  
Contract DAAH01-69-C-0875

Each transmittal of this document outside the Department  
of Defense must have prior approval of U. S. Army Missile  
Command, Redstone Arsenal, Alabama 35809, ATTN: AMSMI-RNA.



This research was sponsored by the ADVANCED RESEARCH  
PROJECTS AGENCY and was monitored by the U. S. ARMY  
MISSILE COMMAND under Contract DAAH01-69-C-0875.

**Ann Arbor, Michigan**



## TABLE OF CONTENTS

	Page
LIST OF ILLUSTRATIONS	iii
LIST OF TABLES	v
ABSTRACT	vi
CHAPTER I - INTRODUCTION	1
1.1 General Considerations	1
1.2 Outline of Research	2
1.3 List of Common Symbols	3
CHAPTER II - GENERAL FORMULATION OF LOW FREQUENCY SCATTERING	5
2.1 Low Frequency Methods	5
2.2 Rayleigh Scattering	7
2.3 Dipole Moments	9
2.4 Arbitrary Plane Wave Incidence on an Arbitrary Scatterer	12
2.5 Scattered Fields	14
CHAPTER III - DIPOLE MOMENTS FOR PLASMA-COATED BODIES	17
3.1 General Considerations	17
3.2 Discussion of Low-Frequency Expansions	17
3.3 Rayleigh Scattering by a Coated Conductor	25
3.4 The Eigenvalue Problem for the Coated Sphere	34
CHAPTER IV - DIPOLE MOMENTS FOR SPECIFIC GEOMETRIES	39
4.1 General Considerations	39
4.2 Results for Prolate Spheroids	40
4.3 Results for Round-backed Cones	45
4.4 Results by Numerical Method	46
4.5 The Rayleigh Term in Far-Field Plane Wave Scattering	51
CHAPTER V - RADAR CROSS SECTIONS OF VARIOUS PLASMA-COATED BODIES	58
5.1 Choice of Shapes	58
5.2 Diagrams in the H-Plane	59
5.3 Diagrams in the E-Plane	61
5.4 Discussion of Results	61

Table of Contents continued	Page
<b>CHAPTER VI - CONCLUSIONS</b>	<b>73</b>
6.1 Summary of Results	73
6.2 Recommendations for Further Study	75
<b>REFERENCES</b>	<b>77</b>
<b>APPENDIX A - DIPOLE MOMENTS FOR THE ROUND-BACKED CONE</b>	<b>79</b>
A.1 Round-backed Cone	79
A.2 Transverse Electric Dipole Moment	83
A.3 Transverse Magnetic Dipole Moment	86
A.4 Axial Magnetic Dipole Moment	89
A.5 Axial Electric Dipole Moment	93
A.6 Some Legendre Function Relations	96
A.7 The Hemisphere	102
A.8 Numerical Solution	105
A.9 References	110
<b>APPENDIX B - NUMERICAL DETERMINATION OF SURFACE CURRENTS AND FAR FIELDS FOR BODIES OF REVOLUTION</b>	<b>111</b>
B.1 Introduction	111
B.2 Surface Currents	112
B.3 Low-Frequency Approximation	117
B.4 Far-Field Expansion	119
B.5 Dipole Contributions to the Backscattered Field	122
B.6 Comparison with Siegel's Formula	124
B.7 Numerical Formulation	127
B.8 Computer Program	133
B.9 References	146
<b>APPENDIX C - INTEGRAL EQUATION FORMULATION OF LOW- FREQUENCY SCATTERING FROM A SLENDER CONE SURROUNDED BY A PENETRABLE OVERDENSE PLASMA SHEATH</b>	<b>147</b>
C.1 The Fundamental Integral Equation	147
C.2 The Jump Condition	152
C.3 Reference	156

DD Form 1473

## LIST OF ILLUSTRATIONS

		Page
3-1	Geometry for Plasma Coated Re-entry Vehicle.	18
3-2	Geometry for the Derivations of Section 3.3.	27
4-1	Normalized Dipole Moment Coefficients for Oblate and Prolate Spheroids as Functions of Length-to-Width Ratio $l/w$ : $-a_1^{(1)}/V$ ( - - - ); $-a_1^{(3)}/V$ ( - . - ); $b_1^{(1)}/V$ ( — ) , where $V$ is the volume.	44
4-2	Exact (normalized) Dipole Moment Coefficients for a Round-Backed Cone ( — ) Compared with Those for a Spheroid ( - - - ) of the Same Length-to-Width Ratio.	47
5-1	Normalized Backscattering Cross Section in the H-Plane. B = Bare Round-Backed Cone ( $\pi - \theta_0 = 10^\circ$ ), E = Plasma-Coated Cone, C = Conducting Cone-Sphere.	63
5-2	Normalized Backscattering Cross Section in the H-Plane. B = Bare Round-Backed Cone ( $\pi - \theta_0 = 20^\circ$ ), E = Plasma-Coated Cone, C = Conducting Cone-Sphere.	64
5-3	Normalized Backscattering Cross Section in the H-Plane. B = Bare Flat-Base Cone, E = Plasma-Coated Cone, C = Conducting Cone-Sphere.	65
5-4	Normalized Backscattering Cross Section in the H-Plane. B = Bare Flat-Base Cone, E = Plasma-Coated Cone, C = Conducting Sphere-Cone-Sphere.	66
5-5	Normalized Backscattering Cross Section in the H-Plane. B = Bare Flat-Base Cone with Rounded Nose, E = Plasma-Coated Cone, C = Conducting Sphere-Cone-Sphere.	67
5-6	Normalized Backscattering Cross Section in the H-Plane. B = Bare Flat-Base Cone with Rounded Nose, E = Plasma-Coated Cone, C = Conducting Prolate Spheroid.	68
5-7a	Normalized Backscattering Cross Section in the H-Plane. B = Bare Round-Backed Cone ( $\pi - \theta_0 = 15^\circ$ ), E = Plasma-Coated Cone, C = Conducting Prolate Spheroid.	69
5-7b	Normalized Backscattering Cross Section in the E-Plane. B = Bare Round-Backed Cone ( $\pi - \theta_0 = 15^\circ$ ), E = Plasma-Coated Cone, C = Conducting Prolate Spheroid.	70

List of Illustrations continued

	Page
5-8a Normalized Backscattering Cross Section in the H-Plane. B = Bare Round-Backed Cone ( $\pi - \theta_0 = 30^\circ$ ), E = Plasma-Coated Cone, C = Conducting Prolate Spheroid.	71
5-8b Normalized Backscattering Cross Section in the E-Plane. B = Bare Round-Backed Cone ( $\pi - \theta_0 = 30^\circ$ ), E = Plasma Coated Cone, C = Conducting Prolate Spheroid.	72
A-1 Cone Geometry.	80
A-2 Computed Dipole Moments: $-a_1^{(1)}/d^3$ , —; $-a_1^{(3)}/d^3$ , - · -; $b_1^{(1)}/d^3$ , - - -; and $b_1^{(3)}/d^3$ , - - - .	109
B-1 Geometry for Body of Revolution.	113
B-2 Unit Vectors at the Point P.	114
B-3 Geometry for the Far-field Expansion.	114
B-4 Geometry for Numerical Computations.	128
B-5 Amplitude of Surface Currents on a Sphere with $ka = 0.1$ . Comparison Between our Numerical Results with $N=30$ (+++  f ; o o o  g  ) and the Exact Results (Ducmanis and Liepa, 1965).	132
C-1 Geometry of the Problem.	148
C-2 Convention for Unit Normals.	148
C-3 Geometry for Jump Condition.	148

## LIST OF TABLES

	<b>Page</b>
4-1 Ratios of Legendre Functions with Argument $\xi$ .	43
4-2 Dipole Moment Coefficients for Prolate Spheroids.	43
4-3 Dipole Moment Coefficients for Round-backed Cones.	45
4-4 Axial Backscattering from Round-backed Cones.	48
4-5 Dipole Moment Coefficients.	52
5-1 Choice of Shapes.	58
A-1 Computed Dipole Moments.	108

## ABSTRACT

The scattered field produced by a plane electromagnetic wave incident on a plasma coated re-entry vehicle is studied, in the low-frequency limit. When the collision frequency is large with respect to the operational frequency, the determination of the electric and magnetic dipole moments of the scatterer is reduced to the solution of two standard potential problems for perfect conductors.

For axially symmetric bodies, only three of the six dipole moment coefficients are independent. The dipole moments are found for a variety of scattering shapes, and the low-frequency radar cross section is obtained for any direction of incidence and for different combinations of the shapes of the bare vehicle and of the outer surface of the plasma sheath.



## CHAPTER I

### INTRODUCTION

#### 1.1 General Considerations

At low frequencies, the field scattered by a finite body when an electromagnetic wave is incident upon it can be expanded in a series of powers of the free-space wave number  $k$ , which series is absolutely convergent for sufficiently small  $k$ . The leading term is produced by the electric and magnetic dipole contributions, and if the incident wavelength  $\lambda = 2\pi/k$  is much greater than all the dimensions of the body, the scattered field can be approximated by the leading term alone. The result is Rayleigh scattering for which the cross section is  $\sigma = Ck^4$ .

For metallic bodies, Siegel (1959) reasoned that the coefficient  $C$  should be proportional to  $V^2$ , where  $V$  is the volume of the body, and from an examination of the known expression for the backscattering cross section of a prolate spheroid at axial incidence, Siegel was led to an empirical formula for the constant of proportionality in terms of the shape (length-to-width ratio) of the body. The resulting expression for  $\sigma$  has found considerable utility, but it should be noted that it applies only to axial backscattering from a body of revolution, that it is most accurate when the body is long and thin, and that its derivation assumes that the body is metallic.

Hiatt et al.(1960) subsequently claimed that since the effect of conductivity is enhanced at low frequencies, any body made of a material with non-zero conductivity appears perfectly conducting if the frequency is sufficiently low. Thus, it seemed reasonable to conclude that Siegel's formula would still be applicable to plasma (or absorber) coated bodies by considering the whole scatterer (body plus plasma coating) as perfectly conducting. Therefore, when a body re-enters

the atmosphere and a plasma is formed around it, the low-frequency cross section should increase as a consequence of the increased scattering volume.

However, experimental data later showed that the cross section does not increase nearly as much as would be expected on the basis of the reasoning in the preceding paragraph. Although in the experiments the overall length of the body and near wake were such as to violate the criterion for Rayleigh scattering, a rigorous analysis of the scattering phenomenon in the Rayleigh limit appeared desirable. Thus, the main task of this report is the theoretical investigation and computation of the low-frequency (Rayleigh) backscattering cross section of a perfectly conducting, axially symmetric, cone-like space vehicle under atmospheric re-entry conditions.

## 1.2 Outline of Research

After a survey of low-frequency methods and of Rayleigh scattering, the electric and magnetic dipole contributions to the far field scattered by an arbitrary object under plane wave incidence are discussed in Chapter II.

A detailed investigation of the dipole moments of plasma-coated metallic bodies is performed in Chapter III, where the cases in which the collision frequency  $\nu_c$  is either much larger or much smaller than the operating frequency  $\omega$  are considered. It is shown that in the former case the low-frequency scattering phenomenon can be reduced to the solution of two standard potential problems for perfect conductors. In the latter case, however, the success of the method depends on the existence of a continuous spectrum of solutions for a boundary-value problem for a wave equation with imaginary wave number.

The following two chapters are devoted to the case  $\nu_c \gg \omega$ . The dipole moments of various scattering shapes are studied in Chapter IV, where spheroids, round-backed cones, flat-base cones and cone-spheres with or without a rounded nose are considered. From these dipole moments, the backscattering cross

section for a variety of shapes of the bare body and of the plasma outer surface is obtained in Chapter V, for all angles of incidence and two different polarizations.

Appendix A is devoted to the determination by analytic means of the dipole moment coefficients of all round-backed cones. A computer program which yields all dipole moment coefficients but one for any roll-symmetric, perfectly conducting scatterer is developed in Appendix B. These coefficients determine the backscattering cross section in the entire H-plane. Finally, an alternative approach to the problem is explored in Appendix C, where a new integral equation is derived for the jump current at the surface of an overdense plasma sheath surrounding a thin conical shell.

### 1.3 List of Common Symbols

Vectors are underlined (e. g.  $\underline{E}$ ), unit vectors are indicated by carets (e. g.  $\hat{n}$ ), scalar products by dots (e. g.  $\hat{n} \cdot \underline{E}$ ), and vector products by wedges (e. g.  $\hat{n} \wedge \underline{E}$ ). The rationalized MKSA system of units is adopted.

$x, y, z,$  = rectangular cartesian coordinates

$r, \theta, \phi$  = spherical polar coordinates

$\nabla$  = gradient operator

$\nabla \cdot$  = divergence operator

$\nabla \wedge$  = curl operator

$\epsilon_0$  = permittivity of free space

$\mu_0$  = permeability of free space

$Z = \sqrt{\mu_0 / \epsilon_0}$  = intrinsic impedance of free space (=  $120 \pi$  ohm)

$Y = Z^{-1}$  = intrinsic admittance of free space

$\omega$  = operating (angular) frequency

$k = \omega \sqrt{\epsilon_0 \mu_0}$  = wave number in free space

$\omega_p$  = plasma frequency

$\nu_c$  = collision frequency

$\underline{E}^i, \underline{H}^i$  = incident electric and magnetic fields

$\underline{E}^s, \underline{H}^s$  = scattered electric and magnetic fields.

## CHAPTER II

### GENERAL FORMULATION OF LOW FREQUENCY SCATTERING

#### 2.1 Low Frequency Methods

The first attempt to obtain low-frequency solutions of the steady-state wave equation from the solutions of the corresponding static problems is due to Strutt, Lord Rayleigh (1897); a comprehensive survey of Strutt's contributions to scattering theory is presented by Twersky (1964). In general, the term "Rayleigh scatterer" is applied to a body whose characteristic dimensions are small compared to the wavelength, but authors often disagree with one another on the precise definition. Thus, for example, to Born and Wolf (1959) a Rayleigh scatterer is one that does not change the frequency of the incident field in forming the scattered field, whereas to other authors it is one whose scattered far field is linearly polarized, or is proportional to  $k^2$ . For our purposes a satisfactory definition of Rayleigh scattering has been given by Kleinman (1965a): for a given scatterer, the "Rayleigh region" is that range of values of  $k$  for which the quantity of interest, e.g. the scattered far field, can be expanded in convergent series in positive integral powers of  $k$ . For three-dimensional scattering by smooth finite objects, such series exist and have finite radii of convergence, as proved by Kleinman (1965b) in the scalar case and by Werner (1963) in the electromagnetic case. These expansions are known as "Rayleigh series", or "quasi-static series", or "low-frequency expansions".

In the scalar case, the determination of the low-frequency expansion consists of two steps: the terms of the expansion are found for the near field, and then they are continued into the far field. The details of this procedure may be found, for example, in Noble (1962) and Kleinman (1965a). When applied to soft (hard) scatterers, the method consists of a series of steps which require the solution of the same Dirichlet (Neumann) potential problem, but with

different boundary values at each step. This inconvenience has been eliminated in a new method developed by Kleinman (1965b) (see also Ar and Kleinman (1966)), which produces successive terms iteratively, without requiring the solution of a new problem at each step.

In both Rayleigh's and Kleinman's methods, the solution of the potential problem, i. e. the static Green's function for the scatterer under consideration must be known. For a limited number of shapes, potential problems can be solved by separation of variables. Darling (1960) has proposed a method of solving potential problems for surfaces which are intersections of separable surfaces, and Darling and Senior (1965) have applied it to a round-backed cone. A detailed study of the dipole moments of the round-backed cone is performed in Appendix A.

The extension of Rayleigh's method to electromagnetic scattering by penetrable three-dimensional bodies was performed by Stevenson (1953a). The calculations required for obtaining each successive term in the low-frequency series, however, rapidly become so intolerable (see, for example, Stevenson (1953b)) that Stevenson's technique does not seem to have been employed in deriving more than three terms. Kleinman (1965c, 1967) has achieved some simplification and removed some of the ambiguities in Stevenson's work. Low frequency electromagnetic scattering by two-dimensional bodies has been studied by Van Bladel (1963).

The extension of the method of Kleinman (1965b) to three-dimensional electromagnetic problems has been achieved by Asvestas (1968), who has derived two coupled integral equations for the scattered field vectors. The kernels of the equations are dyadic functions of position and can be derived from the solutions of standard interior and exterior potential problems. Once these

dyadic kernels are determined for a particular surface geometry, the integral equations can be solved by iteration, when  $k$  is sufficiently small. Alternatively, the scattered fields in the integral equations may be expanded in a power series of the wave number  $k$  and recursion formulas may be found for the unknown coefficients by equating equal powers of  $k$ .

## 2.2 Rayleigh Scattering

In keeping with Rayleigh's original work, some authors restrict the Rayleigh region to the wavelength range in which the Rayleigh series is not only convergent but is well approximated by its first term. To this order, the backscattering cross section of a thin, elongated, perfectly conducting body of revolution on which a plane electromagnetic wave is axially incident is

$$\sigma = \frac{4}{\pi} k^4 V^2 , \quad (2.1)$$

where  $V$  is the volume of the body. As the body is made less elongated, the approximation (2.1) becomes worse; however, it can be improved somewhat by multiplying the right-hand side of (2.1) by a shape factor  $G^2$  (Siegel 1959). With this modification, (2.1) becomes

$$\sigma = \frac{4}{\pi} k^4 V^2 G^2 , \quad (2.2)$$

where  $G$  can be written as

$$G = 1 + \frac{1}{\pi y} e^{-y} \quad (2.3)$$

and  $y$  is a ratio of characteristic dimensions (characteristic length to characteristic width) of the scatterer. For a long thin body,  $y \rightarrow \infty$  and therefore  $G \approx 1$ . Approximate values of  $G$  for various scattering shapes are given by Siegel (1959).

Formula (2.2) is heuristic in nature, and it is based on the observation that the details of the structure of the body cannot be revealed when the wavelength is large compared to the dimensions of the body. What we observe depends more on the size of the body than on its shape, so that the knowledge of the volume of the scatterer modified by a rough indication of its shape should yield a reasonable approximation to the Rayleigh cross section. Thus, the Rayleigh-Siegel formula (2.2) suffers from two limitations: it only predicts the monostatic cross section for axial incidence, and it is not always very accurate. For these reasons, we have developed alternative approaches in this report, that allow us to accurately estimate the Rayleigh cross section of any body of revolution for axial incidence (Appendix B), and both the monostatic and bistatic Rayleigh cross sections of round-backed cones (Appendix A) and spheroids (section 4-2) for any direction and polarization of the incident plane wave.

These approaches are based on the fact that the low-frequency far scattered field can be approximated by a series of radiating multipoles (electric and magnetic dipoles, electric and magnetic quadrupoles, etc) located at the scatterer; a precise formulation is presented in section B.4 of Appendix B. In the Rayleigh limit, the dominant contribution arises from the dipoles; the electric and magnetic dipole contributions are of the same order of magnitude for a metal body, and become nearly equal for a long thin body of revolution and axial incidence.

Thus, the main effort must consist in deriving the electric and magnetic dipoles for a given body; these are functions of the shape of the scatterer but not of the incident field. Once the dipoles are known, it is a simple matter to derive the Rayleigh far field in any given direction, for any preassigned direction and polarization of the incident plane wave.



It should be noted that the dipole terms give a good approximation to the far field scattered by a body which is small compared to the wavelength, but do not accurately describe the field near the body: the relative magnitude of terms in the multipole expansion varies with the distance of the observer from the scatterer.

### 2.3 Dipole Moments

We wish to explore the dipole moments associated with the low frequency scattering of a plane electromagnetic wave by a perfectly conducting body of revolution. Particular attention will be devoted to axial incidence on a long thin body.

Given an electric dipole of moment  $\underline{P}$ , the electric Hertz vector is

$$\underline{\pi}^{(e)} = \underline{P} \frac{e^{ikr}}{4\pi\epsilon_0 r} , \quad (2.4)$$

whereas for a magnetic dipole of moment  $\underline{M}$  the magnetic Hertz vector is

$$\underline{\pi}^{(m)} = \underline{M} \frac{e^{ikr}}{4\pi r} . \quad (2.5)$$

The quantity  $\epsilon_0$  is the permittivity (dielectric constant) of free space, and  $\underline{P}$  and  $\underline{M}$  are, of course, independent of  $r$ . These definitions of electric and magnetic dipole moments are the standard ones (see, for example, Bowman et al, 1969), but differ by factors  $k/(4\pi\epsilon_0)$  and  $k/(4\pi)$  respectively from those employed by Kleinman (1965a).

The electric and magnetic fields resulting from (2.4) and (2.5) are:

$$\underline{E} = \nabla_{\wedge} \nabla_{\wedge} \left( \underline{P} \frac{e^{ikr}}{4\pi\epsilon_0 r} \right) + ikZ \nabla_{\wedge} \left( \underline{M} \frac{e^{ikr}}{4\pi r} \right), \quad (2.6)$$

$$\underline{H} = -ikY \nabla_{\wedge} \left( \underline{P} \frac{e^{ikr}}{4\pi\epsilon_0 r} \right) + \nabla_{\wedge} \nabla_{\wedge} \left( \underline{M} \frac{e^{ikr}}{4\pi r} \right). \quad (2.7)$$

Now if  $\underline{a}$  is any constant vector,

$$\nabla_{\wedge} \left( \underline{a} \frac{e^{ikr}}{r} \right) = \nabla \left( \frac{e^{ikr}}{r} \right) \wedge \underline{a} = \left( ik - \frac{1}{r} \right) \frac{e^{ikr}}{r} \left( \hat{r} \wedge \underline{a} \right), \quad (2.8)$$

from which the precise form of the magnetic dipole contribution to the electric field, and the electric dipole contribution to the magnetic field, follow. Moreover:

$$\begin{aligned} \nabla_{\wedge} \nabla_{\wedge} \left( \underline{a} \frac{e^{ikr}}{r} \right) &= \nabla \left\{ \left( \frac{ik}{r} - \frac{1}{r^2} \right) \frac{e^{ikr}}{r} \right\} \wedge \left( \hat{r} \wedge \underline{a} \right) + \\ &+ \left( \frac{ik}{r} - \frac{1}{r^2} \right) \frac{e^{ikr}}{r} \nabla_{\wedge} \left( \hat{r} \wedge \underline{a} \right). \end{aligned}$$

But  $\nabla_{\wedge} (\hat{r} \wedge \underline{a}) = -2\underline{a}$  and

$$\nabla \left\{ \left( \frac{ik}{r} - \frac{1}{r^2} \right) \frac{e^{ikr}}{r} \right\} = \left( \frac{3}{r^3} - \frac{3ik}{r^2} - \frac{k^2}{r} \right) \frac{e^{ikr}}{r} \hat{r}.$$

Hence

$$\begin{aligned} \nabla_{\wedge} \nabla_{\wedge} \left( \underline{a} \frac{e^{ikr}}{r} \right) &= \left[ \frac{1}{r^2} \left\{ 3 \hat{r} \wedge (\hat{r} \wedge \underline{a}) + 2 \underline{a} \right\} - \frac{ik}{r} \left\{ 3 \hat{r} \wedge (\hat{r} \wedge \underline{a}) + 2 \underline{a} \right\} - \right. \\ &\quad \left. -k^2 \hat{r} \wedge (\hat{r} \wedge \underline{a}) \right] \frac{e^{ikr}}{r}, \quad (2.9) \end{aligned}$$

from which the electric dipole contribution to the electric field, and the magnetic dipole contribution to the magnetic field, follow immediately.

In the far field ( $r \rightarrow \infty$ ), expressions (2.6) and (2.7) become

$$\underline{E} \sim \frac{e^{ikr}}{kr} \frac{k^3}{4\pi} \left\{ \frac{1}{\epsilon_0} \left[ \hat{r} \wedge (\underline{P} \wedge \hat{r}) \right] - Z (\hat{r} \wedge \underline{M}) \right\}, \quad (2.10)$$

$$\underline{H} \sim \frac{e^{ikr}}{kr} Y \frac{k^3}{4\pi} \left\{ \frac{1}{\epsilon_0} (\hat{r} \wedge \underline{P}) + Z \left[ \hat{r} \wedge (\underline{M} \wedge \hat{r}) \right] \right\}, \quad (2.11)$$

whereas the dominant terms  $\underline{E}_0$  and  $\underline{H}_0$  in the near field and at low frequencies are

$$\underline{E}_0 = \frac{1}{4\pi\epsilon_0} \frac{3\hat{r} \wedge (\hat{r} \wedge \underline{P}) + 2\underline{P}}{r^3}, \quad (2.12)$$

$$\underline{H}_0 = \frac{1}{4\pi} \frac{3\hat{r} \wedge (\hat{r} \wedge \underline{M}) + 2\underline{M}}{r^3}; \quad (2.13)$$

we point out the decoupling of the electric and magnetic near fields:  $\underline{E}_0$  depends on  $\underline{P}$  only, and  $\underline{H}_0$  on  $\underline{M}$  only.

If we use the relation

$$\nabla \left( \frac{\hat{r} \cdot \underline{P}}{r^2} \right) = -\frac{1}{r^3} \left\{ 3\hat{r} \wedge (\hat{r} \wedge \underline{P}) + 2\underline{P} \right\},$$

then (2.12) and (2.13) may be rewritten as

$$\underline{E}_0 = -\frac{1}{4\pi\epsilon_0} \nabla \left( \frac{\hat{r} \cdot \underline{P}}{r^2} \right), \quad (2.14)$$

$$\underline{H}_0 = -\frac{1}{4\pi} \nabla \left( \frac{\hat{r} \cdot \underline{M}}{r^2} \right). \quad (2.15)$$

Therefore, in a scattering problem in which  $\underline{P}$  and  $\underline{M}$  are generated by the incidence of a particular field on a particular scatterer,  $\underline{P}$  and  $\underline{M}$  can be obtained from the solutions of certain (static) potential problems for the geometry in question.

#### 2.4 Arbitrary Plane Wave Incidence on an Arbitrary Scatterer

Let us consider the incident plane wave

$$\underline{E}^i = (\ell_1 \hat{x} + m_1 \hat{y} + n_1 \hat{z}) e^{ik(\ell x + my + nz)}, \quad (2.16)$$

$$\underline{H}^i = Y (\ell_2 \hat{x} + m_2 \hat{y} + n_2 \hat{z}) e^{ik(\ell x + my + nz)}, \quad (2.17)$$

where

$$\hat{\ell}_1 = \hat{\ell}_2 \wedge \hat{\ell},$$

$$\hat{\ell}_2 = \hat{\ell} \wedge \hat{\ell}_1,$$

$$\hat{\ell} = \hat{\ell}_1 \wedge \hat{\ell}_2,$$

with  $\hat{\ell}_1 = \ell_1 \hat{x} + m_1 \hat{y} + n_1 \hat{z}$ , etc. The  $\ell_i$ ,  $m_i$ , and  $n_i$  ( $i=1, 2, 3$ ) are direction cosines.

To the first order at low frequencies

$$\underline{E}^i \sim \underline{E}_0^i = \ell_1 \hat{x} + m_1 \hat{y} + n_1 \hat{z}, \quad (2.18)$$

which can be written as

$$\underline{E}_0^i = \nabla(\ell_1 x + m_1 y + n_1 z). \quad (2.19)$$

Since this is independent of  $\hat{\ell}_1$  and  $\hat{\ell}_2$ ,  $\ell_1$ ,  $m_1$  and  $n_1$  can be chosen independently of one another. It follows that the corresponding scattered electric vector can be written as

$$\underline{E}_0^s = \nabla \Phi^s, \quad (2.20)$$

with

$$\Phi^s = \sum_{n=1}^{\infty} r^{-n-1} \left\{ \ell_1 a_n^{(1)} P_n^1(\cos \theta) \cos \phi + \right. \\ \left. + m_1 a_n^{(2)} P_n^1(\cos \theta) \sin \phi + n_1 a_n^{(3)} P_n^0(\cos \theta) \right\}, \quad (2.21)$$

where  $a_n^{(1)}$ ,  $a_n^{(2)}$  and  $a_n^{(3)}$  are independent of  $\hat{\ell}_1$ ,  $\hat{\ell}_1$  and  $\hat{\ell}_2$  and can be obtained from the solutions of three separate and elementary potential problems for the body in question. In terms of the  $a_n^{(j)}$ ,

$$\underline{P} = -4\pi\epsilon_0 (\ell_1 a_1^{(1)} \hat{x} + m_1 a_1^{(2)} \hat{y} + n_1 a_1^{(3)} \hat{z}). \quad (2.22)$$

Similarly

$$\underline{H}^i \sim \underline{H}_0^i = Y (\ell_2 \hat{x} + m_2 \hat{y} + n_2 \hat{z}) = Y \nabla (\ell_2 x + m_2 y + n_2 z) \quad (2.23)$$

and the corresponding scattered magnetic vector is

$$\underline{H}_0^s = Y \nabla \psi^s, \quad (2.24)$$

with

$$\psi^s = \sum_{n=1}^{\infty} r^{-n-1} \left\{ \ell_2 b_n^{(1)} P_n^1(\cos \theta) \cos \phi + m_2 b_n^{(2)} P_n^1(\cos \theta) \sin \phi + \right. \\ \left. + n_2 b_n^{(3)} P_n^0(\cos \theta) \right\}. \quad (2.25)$$

The solutions of three more separate but elementary potential problems serve to determine the  $b_n^{(j)}$ , in terms of which

$$\underline{M} = -4\pi Y (\ell_2 b_1^{(1)} \hat{x} + m_2 b_1^{(2)} \hat{y} + n_2 b_1^{(3)} \hat{z}). \quad (2.26)$$

In general, therefore, six separate potential problems must be solved to completely determine  $\underline{P}$  and  $\underline{M}$ . However, if the body is one of revolution about the  $z$  axis (say), then

$$a_n^{(2)} = a_n^{(1)}, \quad b_n^{(2)} = b_n^{(1)}, \quad (2.27)$$

and the number of potential problems is reduced to four.

## 2.5 Scattered Fields

Knowing  $\underline{P}$  and  $\underline{M}$ , the scattered field can be obtained from Eqs. (2.6) and (2.7). In the far zone the results simplify to the forms shown in Eqs. (2.10) and (2.11).

The back scattered field is of particular interest. This can be obtained by putting  $\hat{r} = -\hat{\ell}$ , and the direct and cross polarized components are then

$$\underline{E}^s \cdot \hat{\ell}_1 \Big|_{\hat{r} = -\hat{\ell}} = \frac{e}{kr} S_{||}, \quad (2.28)$$

$$\underline{E}^s \cdot \hat{\ell}_2 \Big|_{\hat{r} = -\hat{\ell}} = \frac{e}{kr} S_{\perp}, \quad (2.29)$$

respectively, where, from Eqs. (2.10) and (2.11):

$$S_{||} = \frac{k^3}{4\pi} \left\{ \frac{1}{\epsilon_0} (\underline{P} \cdot \hat{\ell}_1) - Z (\underline{M} \cdot \hat{\ell}_2) \right\}, \quad (2.30)$$

$$S_{\perp} = \frac{k^3}{4\pi} \left\{ \frac{1}{\epsilon_0} (\underline{P} \cdot \hat{\ell}_2) + Z (\underline{M} \cdot \hat{\ell}_1) \right\}. \quad (2.31)$$

Substituting the expressions for  $\underline{P}$  and  $\underline{M}$  given by Eqs. (2.22) and (2.26) respectively, we have

$$S_{\parallel} = -k^3 \left\{ \ell_1^2 a_1^{(1)} + m_1^2 a_1^{(2)} + n_1^2 a_1^{(3)} - \ell_2^2 b_1^{(1)} - m_2^2 b_1^{(2)} - n_2^2 b_1^{(3)} \right\}, \quad (2.32)$$

$$S_{\perp} = -k^3 \left\{ \ell_1 \ell_2 (a_1^{(1)} + b_1^{(1)}) + m_1 m_2 (a_1^{(2)} + b_1^{(2)}) + n_1 n_2 (a_1^{(3)} + b_1^{(3)}) \right\} \quad (2.33)$$

and in terms of  $S_{\parallel}$  and  $S_{\perp}$ , the direct and cross polarized components of the back scattering cross section are

$$\sigma_{\parallel} = \frac{4\pi}{k^2} \left| S_{\parallel} \right|^2, \quad \sigma_{\perp} = \frac{4\pi}{k^2} \left| S_{\perp} \right|^2. \quad (2.34)$$

If the body is one of revolution about the  $z$  axis (so that Eq. (2.27) obtains), the expressions for  $S_{\parallel}$  and  $S_{\perp}$  reduce to

$$S_{\parallel} = -k^3 \left\{ a_1^{(1)} - b_1^{(1)} - n_1^2 (a_1^{(1)} - a_1^{(3)}) + n_2^2 (b_1^{(1)} - b_1^{(3)}) \right\}, \quad (2.35)$$

$$S_{\perp} = k^3 n_1 n_2 \left\{ a_1^{(1)} - a_1^{(3)} + b_1^{(1)} - b_1^{(3)} \right\}. \quad (2.36)$$

Observe that only the direction cosines  $n_1$  and  $n_2$  enter into these equations. If, therefore, the incident plane wave has either  $\underline{E}^i$  perpendicular to  $\hat{z}$  (so that  $n_1 = 0$ ) or  $\underline{H}^i$  perpendicular to  $\hat{z}$  (so that  $n_2 = 0$ ),  $S_{\perp} = 0$ . This is

a general result, true at all frequencies. Note also that (i) if  $n_1 = 0$ :

$$S_{||} = -k^3 \left\{ a_1^{(1)} - (1-n_2^2) b_1^{(1)} - n_2^2 b_1^{(3)} \right\}, \quad (2.37)$$

so that  $a_1^{(3)}$  does not appear; whereas (ii) if  $n_2 = 0$ :

$$S_{||} = +k^3 \left\{ b_1^{(1)} - (1-n_1^2) a_1^{(1)} - n_1^2 a_1^{(3)} \right\}, \quad (2.38)$$

so that  $b_1^{(3)}$  does not appear.

In the particular case of nose-on incidence ( $n_1=n_2=0$ ),

$$S_{||} = -k^3 (a_1^{(1)} - b_1^{(1)}), \quad (2.39)$$

and this is the situation under which the empirical formula (2.2) of Siegel (1959) is relevant.



## CHAPTER III

### DIPOLE MOMENTS FOR PLASMA-COATED BODIES

#### 3.1 General Considerations

In order to permit the detailed analysis of the low-frequency cross section of the re-entry vehicle, the plasma sheath and the near wake are idealized through the assumption that both can be represented by a homogeneous, isotropic material having permeability  $\mu$  equal to the free-space value  $\mu_0$  and permittivity  $\epsilon$  given by

$$\epsilon = \epsilon_0 \left[ 1 - \frac{\omega_p^2}{\omega(\omega + i\nu_c)} \right], \quad (3.1)$$

where  $\omega_p$  is the plasma frequency,  $\nu_c$  is the collision frequency, and  $\omega = k\sqrt{\epsilon_0\mu_0}$  is the frequency of the incident field. In the following section 3.2 we investigate the low-frequency expansions of the electromagnetic field for a lossless plasma ( $\nu_c = 0$ ), and for a lossy plasma when either  $\nu_c \gg \omega$  or  $\nu_c \ll \omega$ . In the case  $\nu_c \gg \omega$ , the determination of the dipole moments  $\underline{P}$  and  $\underline{M}$  is reduced to the solution of two standard potential problems, as shown in section 3.3. In the other two cases ( $\nu_c \ll \omega$  and, in particular,  $\nu_c = 0$ ), the determination of  $\underline{P}$  is still easy, but some difficulties arise in the determination of  $\underline{M}$ : they are examined in detail for a plasma-coated sphere, in section 3.4.

#### 3.2 Discussion of the Low-Frequency Expansions

The geometry of the problem is illustrated in Fig. 3-1. A perfectly conducting re-entry vehicle with surface B is embedded in a plasma with outer surface C. The volume of the plasma is indicated by  $V^{(i)}$ , whereas  $V^{(e)}$  is the free-space volume surrounding C. We denote the total fields interior and exterior to the plasma coating by  $\underline{E}^{(i)}$ ,  $\underline{H}^{(i)}$  and  $\underline{E}^{(e)}$ ,  $\underline{H}^{(e)}$ , respectively. We shall discuss three cases: lossless plasma coating and lossy coating where

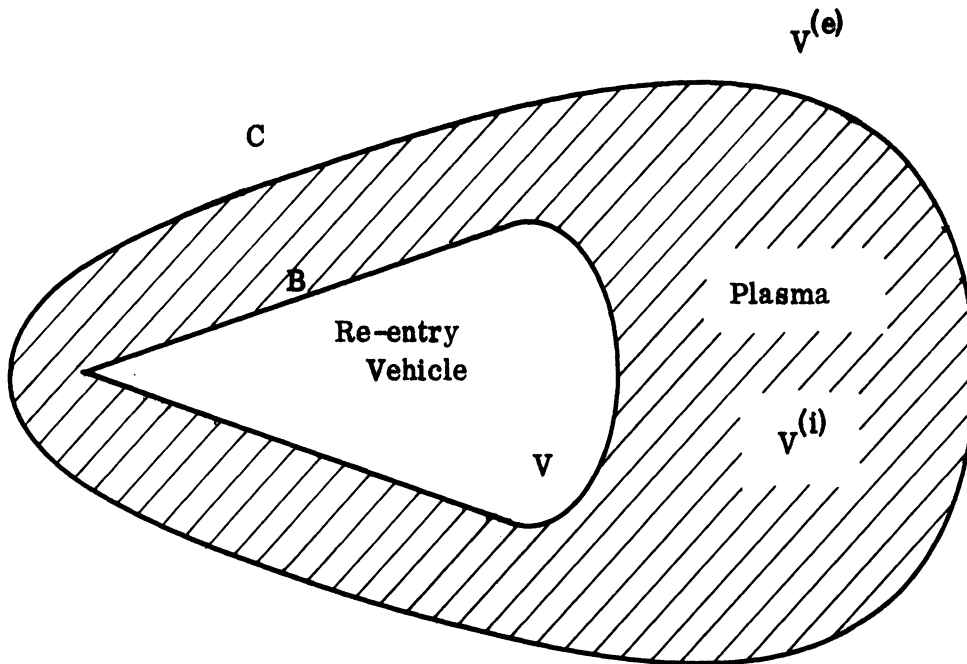


FIG. 3-1: Geometry for Plasma Coated Re-entry Vehicle.

the collision frequency is either much smaller or much larger than the operating frequency.

**Case 1: Lossless Coating**

Consider the case when the plasma coating is homogeneous, isotropic, overdense, with negligible collision frequency such that it may be characterized by an equivalent dispersive permittivity

$$\epsilon = \epsilon_0 \left( 1 - \frac{\omega_p^2}{\omega^2} \right) , \quad (3.2)$$

obtained by setting  $\nu_c=0$  in equation (3.1). The equations governing the propagation phenomena then take the form:

$$\begin{aligned} \nabla_{\wedge} \underline{E}^{(i)} &= i\omega\mu_0 \underline{H}^{(i)} , \\ \nabla_{\wedge} \underline{H}^{(i)} &= -i\omega\epsilon_0 \left( 1 - \frac{\omega_p^2}{\omega^2} \right) \underline{E}^{(i)} \\ \nabla_{\wedge} \underline{E}^{(e)} &= i\omega\mu_0 \underline{H}^{(e)} , \\ \nabla_{\wedge} \underline{H}^{(e)} &= -i\omega\epsilon_0 \underline{E}^{(e)} , \end{aligned} \quad (3.3)$$

with boundary conditions

$$\left. \begin{aligned} \hat{n}_{\wedge} \underline{E}^{(i)} &= 0 \\ \hat{n} \cdot \underline{H}^{(i)} &= 0 \end{aligned} \right\} \text{ on B ,} \quad (3.4)$$

$$\left. \begin{aligned} \hat{n}_{\wedge} (\underline{E}^{(e)} - \underline{E}^{(i)}) &= 0 \\ \hat{n}_{\wedge} (\underline{H}^{(e)} - \underline{H}^{(i)}) &= 0 \\ \hat{n} \cdot (\underline{H}^{(e)} - \underline{H}^{(i)}) &= 0 \\ \hat{n} \cdot \left[ \underline{E}^{(e)} - \left( 1 - \frac{\omega_p^2}{\omega^2} \right) \underline{E}^{(i)} \right] &= 0 \end{aligned} \right\} \text{ on C,} \quad (3.5)$$

where  $\hat{n}$  is the unit normal to the surface considered (B or C).

Now we assume that all field quantities may be expanded in powers of  $\omega$  in the form

$$\underline{E}^{(i)} = \sum_{n=0}^{\infty} (i\omega)^n \underline{E}_n^{(i)}, \text{ etc.}, \quad (3.6)$$

we substitute these expansions in Maxwell's equations (3.3) and in the boundary conditions (3.4) and (3.5), and equate like powers of  $\omega$  to obtain:

$$\left. \begin{aligned} \nabla \wedge \underline{E}_n^{(i)} &= \mu_0 \underline{H}_{n-1}^{(i)}, \\ \nabla \wedge \underline{H}_n^{(i)} &= -\epsilon_0 \underline{E}_{n-1}^{(i)} - \epsilon_0 \omega^2 \underline{E}_{n+1}^{(i)}, \quad \underline{E}_0^{(i)} = 0, \\ \nabla \wedge \underline{E}_n^{(e)} &= \mu_0 \underline{H}_{n-1}^{(e)}, \\ \nabla \wedge \underline{H}_n^{(e)} &= -\epsilon_0 \underline{E}_{n-1}^{(e)}, \end{aligned} \right\} \quad (3.7)$$

$$\left. \begin{aligned} \hat{n} \wedge \underline{E}_n^{(i)} &= 0 \\ \hat{n} \cdot \underline{H}_n^{(i)} &= 0 \end{aligned} \right\} \text{ on B,} \quad (3.8)$$

$$\left. \begin{aligned} \hat{n} \wedge (\underline{E}_n^{(e)} - \underline{E}_n^{(i)}) &= 0 \\ \hat{n} \wedge (\underline{H}_n^{(e)} - \underline{H}_n^{(i)}) &= 0 \\ \hat{n} \cdot (\underline{H}_n^{(e)} - \underline{H}_n^{(i)}) &= 0 \\ \hat{n} \cdot (\underline{E}_n^{(e)} - \underline{E}_n^{(i)} - \omega^2 \underline{E}_{n+2}^{(i)}) &= 0, \\ \hat{n} \cdot \underline{E}_0^{(i)} &= 0, \\ \hat{n} \cdot \underline{E}_{-1}^{(i)} &= 0. \end{aligned} \right\} \text{ on C.} \quad (3.9)$$

In the above formulas, coefficients with negative subscripts are identically zero.

If we concern ourselves only with the problem of finding  $\underline{E}_0^{(e)}$  and  $\underline{H}_0^{(e)}$ , from which we can determine the Rayleigh term in the far field, things are much simplified. The relevant equations are:

$$\begin{aligned}
\underline{E}_0^{(i)} &= 0, \quad \mu_0 \underline{H}_0^{(i)} = \nabla \wedge \underline{E}_1^{(i)}, \\
\nabla \wedge \underline{H}_0^{(i)} &= -\epsilon_0 \omega_p^2 \underline{E}_1^{(i)}, \\
\nabla \wedge \underline{E}_0^{(e)} &= 0, \\
\nabla \wedge \underline{H}_0^{(e)} &= 0, \tag{3.10} \\
\hat{n} \cdot \underline{H}_0^{(i)} &= 0, \quad \text{on } B, \\
\left. \begin{aligned}
\hat{n} \wedge \underline{E}_0^{(e)} &= 0, \\
\hat{n} \wedge (\underline{H}_0^{(e)} - \underline{H}_0^{(i)}) &= 0, \\
\hat{n} \cdot (\underline{H}_0^{(e)} - \underline{H}_0^{(i)}) &= 0.
\end{aligned} \right\} \text{ on } C.
\end{aligned}$$

Obviously  $\underline{E}_0^{(e)}$  is exactly the same as it would be had  $C$  been a perfectly conducting boundary, that is

$$\underline{E}_0^{(e)} = \nabla \Phi + \underline{E}_0^i, \tag{3.11}$$

where  $\underline{E}_0^i$  is the  $\omega=0$  value of the incident electric field, and

$$\left. \begin{aligned}
\nabla^2 \Phi &= 0, \quad \text{in } V^{(e)} \\
\hat{n} \wedge \nabla \Phi &= -\hat{n} \wedge \underline{E}_0^i, \quad \text{on } C, \\
\Phi &\text{ regular at infinity.}
\end{aligned} \right\} \tag{3.12}$$

To obtain the magnetic field terms, however, is a bit more complicated. If  $\underline{E}_1^{(i)} = 0$ , it follows that  $\underline{H}_0^{(i)}$  also vanishes and this fact in turn may be used to show that both normal and tangential components of  $\underline{H}_0^{(e)}$  vanish on  $C$ . This implies that  $\underline{H}_0^{(e)}$  vanishes in  $V^{(e)}$ , which is inconsistent with the fact that  $\underline{H}_0^{(e)}$  consists of a non-zero contribution from the incident field as well as a regular part. One suspects, therefore, that  $\underline{E}_1^{(i)} \neq 0$ ; however, it is easily shown that

$$\left. \begin{aligned} (\nabla^2 - \omega_p^2 \mu_0 \epsilon_0) \underline{E}_1^{(i)} &= 0, & \text{in } V^{(i)}, \\ \hat{n} \wedge \underline{E}_1^{(i)} &= 0, & \text{on } B, \\ \hat{n} \cdot \underline{E}_1^{(i)} &= 0, & \text{on } C, \end{aligned} \right\} \quad (3.13)$$

and  $\underline{E}_1^{(i)} \equiv 0$  is certainly a solution of this homogeneous problem. The existence of non-trivial solutions has to be investigated, and if there are non-trivial solutions it is of interest to know whether the spectrum is continuous or discrete. We remark that a discrete spectrum would be of little interest because the frequencies would be critical functions of the geometry and even a slight loss (or inhomogeneity) in the plasma could affect the results. Although it is unlikely that any members of a discrete spectrum would be excited, there could sometimes occur a sharp variation in the observed scattering from the body, at those altitudes where the plasma properties would lead to the excitation of a member of a discrete spectrum. A study of problem (3.13) for a plasma-coated sphere is performed in section 3.4.

Case 2: Lossy Coating with  $\omega \ll \nu_c$

In this case the permittivity within the plasma is written in the form (3.1).

Maxwell's equations are now:

$$\begin{aligned}
 \nabla \wedge \underline{E}^{(i)} &= i\omega \mu_0 \underline{H}^{(i)} , \\
 \nabla \wedge \underline{H}^{(i)} &= -i\omega \epsilon_0 \left[ 1 - \frac{i\omega_p^2}{\omega(-\nu_c + i\omega)} \right] \underline{E}^{(i)} , \\
 \nabla \wedge \underline{E}^{(e)} &= i\omega \mu_0 \underline{H}^{(e)} , \\
 \nabla \wedge \underline{H}^{(e)} &= -i\omega \epsilon_0 \underline{E}^{(e)} ,
 \end{aligned} \tag{3.14}$$

and the boundary conditions are

$$\left. \begin{aligned}
 \hat{n} \wedge \underline{E}^{(i)} &= 0 \\
 \hat{n} \wedge \underline{H}^{(i)} &= 0
 \end{aligned} \right\} \text{ on B ,} \tag{3.15}$$

$$\left. \begin{aligned}
 \hat{n} \wedge (\underline{E}^{(e)} - \underline{E}^{(i)}) &= 0 \\
 \hat{n} \wedge (\underline{H}^{(e)} - \underline{H}^{(i)}) &= 0 \\
 \hat{n} \cdot (\underline{H}^{(e)} - \underline{H}^{(i)}) &= 0 \\
 \hat{n} \cdot \left\{ \underline{E}^{(e)} - \left[ 1 - \frac{i\omega_p^2}{\omega(-\nu_c + i\omega)} \right] \underline{E}^{(i)} \right\} &= 0
 \end{aligned} \right\} \text{ on C .} \tag{3.16}$$

As done previously (see eq. (3.6) ), we assume power series expansions of all field quantities in powers of  $\omega$  , substitute in the above relations (3.14) - (3.16), equate like powers of  $\omega$  and obtain finally:

$$\left. \begin{aligned}
\nabla_{\wedge} \underline{E}_n^{(i)} &= \mu_0 \underline{H}_{n-1}^{(i)} , \\
\nabla_{\wedge} \underline{H}_n^{(i)} &= \nu_c^{-1} \nabla_{\wedge} \underline{H}_{n-1}^{(i)} - \epsilon_0 \underline{E}_{n-1}^{(i)} + \frac{\epsilon_0}{\nu_c} \underline{E}_{n-2}^{(i)} + \frac{\epsilon_0 \omega_p^2}{\nu_c} \underline{E}_n^{(i)} , \\
\nabla_{\wedge} \underline{E}_n^{(e)} &= \mu_0 \underline{H}_{n-1}^{(e)} , \\
\nabla_{\wedge} \underline{H}_n^{(e)} &= -\epsilon_0 \underline{E}_{n-1}^{(e)} ,
\end{aligned} \right\} (3.17)$$

$$\left. \begin{aligned}
\hat{n}_{\wedge} \underline{E}_n^{(i)} &= 0 \\
\hat{n} \cdot \underline{H}_n^{(i)} &= 0
\end{aligned} \right\} \text{ on B ,} \quad (3.18)$$

$$\left. \begin{aligned}
\hat{n}_{\wedge} (\underline{E}_n^{(e)} - \underline{E}_n^{(i)}) &= 0 , \\
\hat{n}_{\wedge} (\underline{H}_n^{(e)} - \underline{H}_n^{(i)}) &= 0 , \\
\hat{n} \cdot (\underline{H}_n^{(e)} - \underline{H}_n^{(i)}) &= 0 , \\
\hat{n} \cdot (\nu_c \underline{E}_{n-1}^{(e)} - \underline{E}_{n-2}^{(e)} - \nu_c \underline{E}_{n-1}^{(i)} + \underline{E}_{n-2}^{(i)} + \omega_p^2 \underline{E}_0^{(i)}) &= 0
\end{aligned} \right\} \text{ on C .} \quad (3.19)$$

Again concerning ourselves only with the problem of finding  $\underline{E}_0^{(e)}$  and  $\underline{H}_0^{(e)}$  (which necessitates consideration of the interior fields as well), we have that

$$\begin{aligned}
\nabla_{\wedge} \underline{E}_0^{(i)} &= 0 , \\
\nabla_{\wedge} \underline{H}_0^{(i)} &= + \frac{\epsilon_0 \omega_p^2}{\nu_c} \underline{E}_0^{(i)} , \\
\nabla_{\wedge} \underline{E}_0^{(e)} &= 0 , \\
\nabla_{\wedge} \underline{H}_0^{(e)} &= 0 , \\
\left. \begin{aligned}
\hat{n}_{\wedge} \underline{E}_0^{(i)} &= 0 \\
\hat{n} \cdot \underline{H}_0^{(i)} &= 0
\end{aligned} \right\} \text{ on B ,} \\
\left. \begin{aligned}
\hat{n}_{\wedge} (\underline{E}_0^{(e)} - \underline{E}_0^{(i)}) &= 0 \\
\hat{n}_{\wedge} (\underline{H}_0^{(e)} - \underline{H}_0^{(i)}) &= 0 \\
\hat{n} \cdot (\underline{H}_0^{(e)} - \underline{H}_0^{(i)}) &= 0 \\
\hat{n} \cdot \underline{E}_0^{(i)} &= 0
\end{aligned} \right\} \text{ on C .}
\end{aligned} \quad (3.20)$$



It may be shown that again  $\underline{E}_0^{(i)} = 0$ , which simplifies the problem immensely by reducing the case to that of a dielectric coating. Also,  $\underline{E}_0^{(e)}$  is exactly the same as it would be if the coating were perfectly conducting and may be found by solving a standard Dirichlet potential problem for the surface C, whereas  $\underline{H}_0^{(e)}$  is exactly the same as it would be if the coating were not there and may be found as the solution of a standard Neumann potential problem for the surface B. Detailed proofs of these statements are given in section 3.3.

Case 3: Lossy Coating with  $\nu_c \ll \omega$ .

The permittivity in the plasma, the Maxwell equations and the boundary conditions are given by the same expressions considered in Case 2. However, an expansion in  $\omega$  about  $\omega = 0$  is not possible, since the equivalent permittivity has a pole at  $\omega = -i\nu_c$ . We may then assume that

$$\nu_c = \delta \omega, \quad (3.21)$$

where  $\delta$  is small compared to unity, and introduce the complex plasma frequency

$$\tilde{\omega}_p = \frac{\omega_p}{\sqrt{1+i\delta}}. \quad (3.22)$$

The analysis developed in Case 1 is directly applicable to this case, by replacing  $\omega_p$  with  $\tilde{\omega}_p$ .

### 3.3 Rayleigh Scattering by a Coated Conductor

In this section we consider the Rayleigh scattering of a plane electromagnetic wave by a perfectly conducting finite three-dimensional object coated with a homogeneous, isotropic, non-dispersive material of constitutive parameters  $\epsilon$  (permittivity),  $\mu$  (permeability) and  $\sigma$  (conductivity). Geometry and symbols have been defined in the previous section. The only limitations on the shapes of the outer surfaces B of the object and C of the coating is that they be sufficiently smooth for the use of Green's theorem. The incident plane wave propagates in the direction  $\hat{a}$  and its electric field is linearly polarized in the direction  $\hat{a}$ ,

so that

$$\underline{E}^i(\underline{r}) = \hat{a} e^{ik\hat{\alpha}\cdot\underline{r}}, \quad \underline{H}^i(\underline{r}) = Y\hat{\alpha}\wedge\hat{a} e^{ik\hat{\alpha}\cdot\underline{r}}. \quad (3.23)$$

The positive unit normals  $\hat{n}$  on B and C are directed into  $V^{(i)}$  and  $V^{(e)}$ , respectively (see Fig. 3-2).

The particular case we are interested in, namely that of a lossy plasma coating with  $\nu_c \gg \omega$ , is obtained from the results of this section by letting

$$\epsilon \rightarrow \epsilon_0, \quad \mu \rightarrow \mu_0, \quad \sigma \rightarrow +\frac{\omega^2}{\nu_c} \epsilon_0. \quad (3.24)$$

We must solve Maxwell's equations

$$\left. \begin{aligned} \nabla_{\wedge} \underline{E}^S(\underline{r}) &= i\omega\mu_0 \underline{H}^S(\underline{r}) \\ \nabla_{\wedge} \underline{H}^S(\underline{r}) &= -i\omega\epsilon_0 \underline{E}^S(\underline{r}) \end{aligned} \right\} \underline{r} \text{ in } V^{(e)} \quad (3.25)$$

and

$$\left. \begin{aligned} \nabla_{\wedge} \underline{E}^{(i)}(\underline{r}) &= i\omega\mu \underline{H}^{(i)} \\ \nabla_{\wedge} \underline{H}^{(i)}(\underline{r}) &= (-i\omega\epsilon + \sigma) \underline{E}^{(i)}(\underline{r}) \end{aligned} \right\} \underline{r} \text{ in } V^{(i)}, \quad (3.26)$$

subject to the boundary conditions

$$\left. \begin{aligned} \hat{n} \wedge \underline{E}^{(i)}(\underline{r}) &= 0 \\ \hat{n} \cdot \underline{H}^{(i)}(\underline{r}) &= 0 \end{aligned} \right\} \underline{r} \text{ on } B, \quad (3.27)$$

the continuity conditions

$$\left. \begin{aligned} \hat{n} \wedge [\underline{E}^S(\underline{r}) + \underline{E}^i(\underline{r}) - \underline{E}^{(i)}(\underline{r})] &= 0 \\ \hat{n} \cdot [\epsilon_0 \underline{E}^S(\underline{r}) + \epsilon_0 \underline{E}^i(\underline{r}) - \left(\epsilon + \frac{i\sigma}{\omega}\right) \underline{E}^{(i)}(\underline{r})] &= 0 \\ \hat{n} \wedge [\underline{H}^S(\underline{r}) + \underline{H}^i(\underline{r}) - \underline{H}^{(i)}(\underline{r})] &= 0 \\ \hat{n} \cdot [\mu_0 \underline{H}^S(\underline{r}) + \mu_0 \underline{H}^i(\underline{r}) - \mu \underline{H}^{(i)}(\underline{r})] &= 0 \end{aligned} \right\} \underline{r} \text{ on } C, \quad (3.28)$$

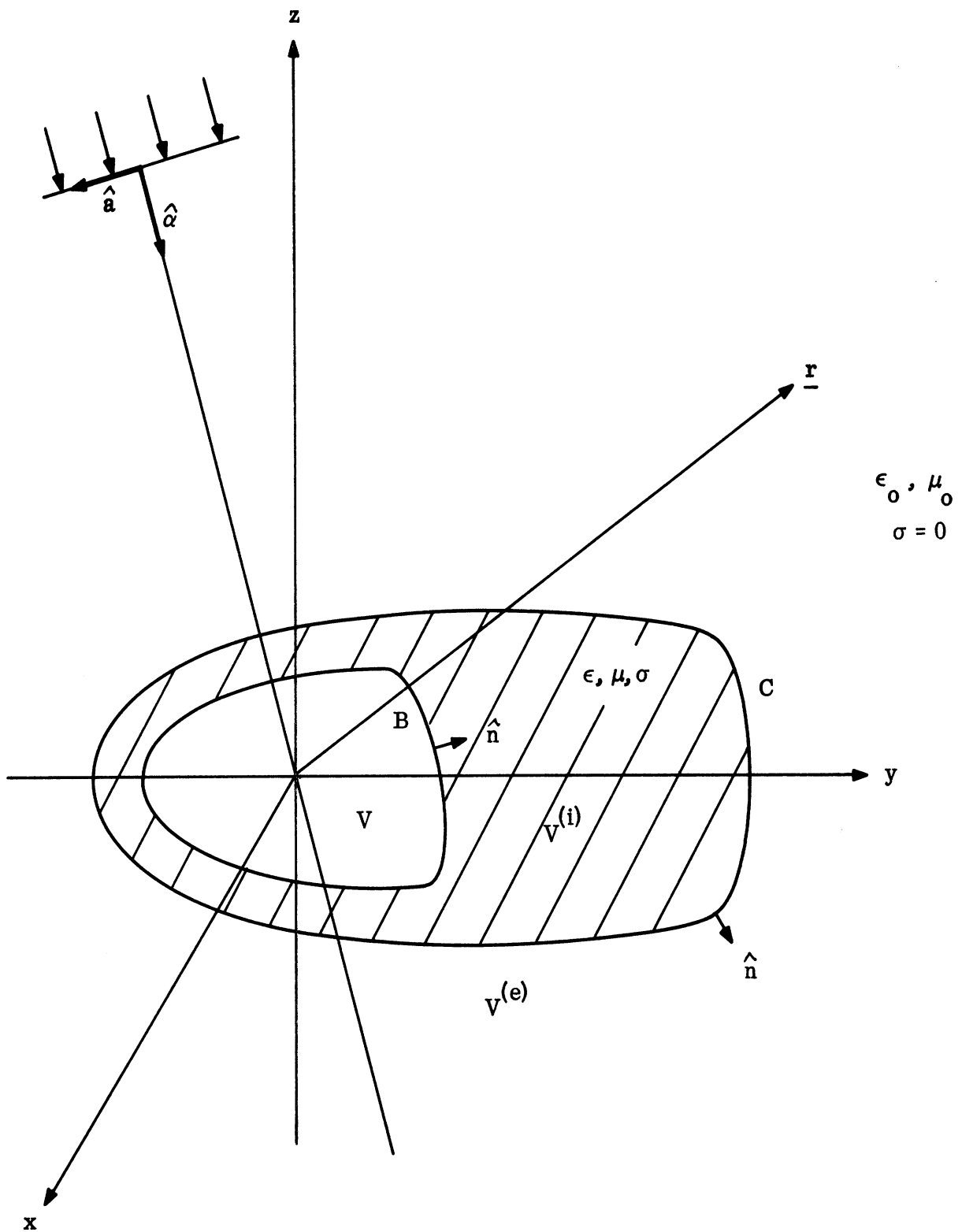


FIG. 3-2: Geometry for the Derivations of Section 3.3.

and the Silver-Müller radiation condition

$$\begin{aligned} \lim_{\underline{r} \rightarrow \infty} \underline{r} \wedge \left[ \nabla \wedge \underline{E}^S(\underline{r}) \right] + ikr \underline{E}^S(\underline{r}) &= 0, \\ \lim_{\underline{r} \rightarrow \infty} \underline{r} \wedge \left[ \nabla \wedge \underline{H}^S(\underline{r}) \right] + ikr \underline{H}^S(\underline{r}) &= 0. \end{aligned} \quad (3.29)$$

The total field is  $\underline{E}^{(i)}(\underline{r})$ ,  $\underline{H}^{(i)}(\underline{r})$  for  $\underline{r}$  in  $V^{(i)}$ , and

$$\left. \begin{aligned} \underline{E}^{(e)}(\underline{r}) &= \underline{E}^i(\underline{r}) + \underline{E}^S(\underline{r}) ; \\ \underline{H}^{(e)}(\underline{r}) &= \underline{H}^i(\underline{r}) + \underline{H}^S(\underline{r}) , \end{aligned} \right\} \text{for } \underline{r} \text{ in } V^{(e)}. \quad (3.30)$$

In order to find a low frequency solution in the near field, we assume that all field components have convergent power series representations of the type (3.6). In particular, for the incident fields,

$$\underline{E}^i(\underline{r}) = \hat{a} \sum_{n=0}^{\infty} \frac{(ik\hat{\alpha} \cdot \underline{r})^n}{n!}, \quad \underline{H}^i(\underline{r}) = Y\hat{\alpha} \wedge \hat{a} \sum_{n=0}^{\infty} \frac{(ik\hat{\alpha} \cdot \underline{r})^n}{n!}, \quad (3.31)$$

where  $k = \omega \sqrt{\epsilon_0 \mu_0}$ . By substituting these series in (3.25) - (3.28) and by equating equal powers of  $\omega$ , we obtain a set of equations for each power. In the Rayleigh limit, we are interested only in  $\underline{E}_0^S$ ,  $\underline{H}_0^S$ ,  $\underline{E}_0^{(i)}$  and  $\underline{H}_0^{(i)}$ , which must satisfy the equations:

$$\left. \begin{aligned} \nabla \wedge \underline{E}_0^S(\underline{r}) &= 0 \\ \nabla \wedge \underline{H}_0^S(\underline{r}) &= 0 \end{aligned} \right\} \underline{r} \text{ in } V^{(e)}, \quad (3.32)$$

$$\left. \begin{aligned} \nabla \wedge \underline{E}_0^{(i)}(\underline{r}) &= 0 \\ \nabla \wedge \underline{H}_0^{(i)}(\underline{r}) &= \sigma \underline{E}_0^{(i)}(\underline{r}) \end{aligned} \right\} \underline{r} \text{ in } V^{(i)}, \quad (3.33)$$

$$\left. \begin{aligned} \hat{\mathbf{n}} \wedge \underline{\mathbf{E}}_0^{(i)}(\underline{\mathbf{r}}) &= 0 \\ \hat{\mathbf{n}} \cdot \underline{\mathbf{H}}_0^{(i)}(\underline{\mathbf{r}}) &= 0 \end{aligned} \right\} \underline{\mathbf{r}} \text{ on } B, \quad (3.34)$$

$$\left. \begin{aligned} \hat{\mathbf{n}} \wedge [\underline{\mathbf{E}}_0^S(\underline{\mathbf{r}}) + \hat{\mathbf{a}} - \underline{\mathbf{E}}_0^{(i)}(\underline{\mathbf{r}})] &= 0 \\ \hat{\mathbf{n}} \cdot \underline{\mathbf{E}}_0^{(i)}(\underline{\mathbf{r}}) &= 0 \\ \hat{\mathbf{n}} \wedge [\underline{\mathbf{H}}_0^S(\underline{\mathbf{r}}) + Y \hat{\alpha} \wedge \hat{\mathbf{a}} - \underline{\mathbf{H}}_0^{(i)}(\underline{\mathbf{r}})] &= 0 \\ \hat{\mathbf{n}} \cdot [\mu_0 \underline{\mathbf{H}}_0^S(\underline{\mathbf{r}}) + \mu_0 Y \hat{\alpha} \wedge \hat{\mathbf{a}} - \mu \underline{\mathbf{H}}_0^{(i)}(\underline{\mathbf{r}})] &= 0 \end{aligned} \right\} \underline{\mathbf{r}} \text{ on } C. \quad (3.35)$$

In addition, the fact that all the field quantities satisfy Maxwell's equations means that these quantities have zero divergence, which in turn implies that all terms in a low frequency expansion are also divergence free. In particular,

$$\left. \begin{aligned} \nabla \cdot \underline{\mathbf{E}}_0^S(\underline{\mathbf{r}}) &= 0 \\ \nabla \cdot \underline{\mathbf{H}}_0^S(\underline{\mathbf{r}}) &= 0 \end{aligned} \right\} \underline{\mathbf{r}} \text{ in } V^{(e)}, \quad (3.36)$$

$$\left. \begin{aligned} \nabla \cdot \underline{\mathbf{E}}_0^{(i)}(\underline{\mathbf{r}}) &= 0 \\ \nabla \cdot \underline{\mathbf{H}}_0^{(i)}(\underline{\mathbf{r}}) &= 0 \end{aligned} \right\} \underline{\mathbf{r}} \text{ in } V^{(i)} \quad (3.37)$$

Firstly, consider the problem of finding  $\underline{\mathbf{E}}_0^{(i)}(\underline{\mathbf{r}})$ . The first of (3.33) implies that  $\underline{\mathbf{E}}_0^{(i)}(\underline{\mathbf{r}})$  is the gradient of a scalar function, i. e. that

$$\underline{\mathbf{E}}_0^{(i)}(\underline{\mathbf{r}}) = \nabla \Phi^{(i)}(\underline{\mathbf{r}}), \quad (3.38)$$

and from (3.37):

$$\nabla^2 \Phi^{(i)}(\underline{r}) = 0 \quad , \quad \underline{r} \text{ in } V^{(i)} \quad . \quad (3.39)$$

The second continuity condition (3.35) is actually a boundary condition for  $\underline{E}_0^{(i)}$ , namely,

$$\left. \frac{\partial \Phi^{(i)}(\underline{r})}{\partial n} \right|_{\underline{r} \text{ on } C} = 0 \quad . \quad (3.40)$$

Furthermore, the boundary condition (3.34) states that

$$\left. \hat{n} \wedge \nabla \Phi^{(i)}(\underline{r}) \right|_{\underline{r} \text{ on } B} = 0 \quad ; \quad (3.41)$$

it can be shown that this is equivalent to the condition

$$\Phi^{(i)}(\underline{r}) = A, \quad \underline{r} \text{ on } B, \quad (3.42)$$

where  $A$  is an arbitrary constant. Conditions (3.39) - (3.42) may be used to show that  $\Phi^{(i)}(\underline{r})$  is constant throughout  $V^{(i)}$  by reasoning in the following manner. The divergence theorem applied to the function  $\nabla \Phi^{(i)}(\underline{r})$  in  $V^{(i)}$  states that

$$\int_{\bar{C}} \hat{n} \cdot \nabla \Phi^{(i)}(\underline{r}) \, dS - \int_B \hat{n} \cdot \nabla \Phi^{(i)}(\underline{r}) \, dS = \int_{V^{(i)}} \nabla^2 \Phi^{(i)}(\underline{r}) \, dV \quad . \quad (3.43)$$

The sign difference on the left-hand side of (3.43) results from the choice of normal direction ( $\hat{n}$  into  $V^{(i)}$  from B but out of  $V^{(i)}$  from C). The facts that  $\Phi^{(i)}(\underline{r})$  is a potential function and has vanishing normal derivative on C imply that

$$\int_B \hat{n} \cdot \nabla \Phi^{(i)}(\underline{r}) \, dS = 0 \quad . \quad (3.44)$$

Now we again employ the divergence theorem applied to the function

$\Phi^{(i)}(\underline{r}) \nabla \Phi^{(i)}(\underline{r})$  in  $V^{(i)}$ , obtaining

$$\int_C \hat{n} \cdot \Phi^{(i)} \nabla \Phi^{(i)} \, dS - \int_B \hat{n} \cdot \Phi^{(i)} \nabla \Phi^{(i)} \, dS = \int_{V^{(i)}} \left[ (\nabla \Phi^{(i)})^2 + \Phi^{(i)} \nabla^2 \Phi^{(i)} \right] \, dV \quad . \quad (3.45)$$

But (3.40) implies that

$$\int_C \hat{n} \cdot \Phi^{(i)} \nabla \Phi^{(i)} \, dS = 0 \quad ,$$

whereas (3.42) and (3.44) imply that

$$\int_B \hat{n} \cdot \Phi^{(i)} \nabla \Phi^{(i)} \, dS = A \int_B \hat{n} \cdot \nabla \Phi^{(i)} \, dS = 0, \quad (3.46)$$

and (3.39) states that  $\nabla^2 \Phi^{(i)} = 0$ . Hence equation (3.45) reduces to

$$\int_{V^{(i)}} (\nabla \Phi^{(i)})^2 \, dV = 0 \quad . \quad (3.47)$$

From this we conclude that

$$\nabla \Phi^{(i)}(\underline{r}) = 0 \quad , \quad \underline{r} \text{ in } V^{(i)} \quad (3.48)$$

and therefore from (3.38):

$$\underline{E}_0^{(i)}(\underline{r}) = 0, \quad \underline{r} \text{ in } V^{(i)} \quad . \quad (3.49)$$

A similar result was obtained by Van Bladel (1964) under somewhat different conditions.

Turning now to the problem of finding  $\underline{E}_0^S(\underline{r})$ , we see that with the interior electric field identically zero, this reduces to the problem of finding the Rayleigh term of the electric field exterior to a perfectly conducting surface C. Explicitly,

$$\underline{E}_0^S(\underline{r}) = \nabla \Phi^S(\underline{r}) \quad , \quad (3.50)$$

where  $\Phi^S(\underline{r})$  is an exterior potential function satisfying the boundary condition

$$\Phi^S(\underline{r}) + \hat{\mathbf{a}} \cdot \underline{r} = \text{constant}, \quad \underline{r} \text{ on } C. \quad (3.51)$$

The ambiguity introduced by the arbitrary constant in (3.51) is removed with the additional condition (for details see Kleinman, 1965c):

$$\int_C \hat{\mathbf{n}} \cdot \nabla \Phi^S(\underline{r}) \, dS = 0 \quad . \quad (3.52)$$

The fact that  $\underline{E}_0^{(i)} = 0$  also simplifies the problem of determining the magnetic field terms. Equations (3.32) and (3.36) imply that

$$\underline{H}_0^S(\underline{r}) = \nabla \psi^S(\underline{r}) \quad (3.53)$$



where  $\psi^S(\underline{r})$  is a regular exterior potential function. Equations (3.33) and (3.37) imply that  $\underline{H}_0^{(i)}(\underline{r})$  is also the gradient of a regular potential function, but it is convenient to exhibit explicitly a term corresponding to the incident field, viz. ,

$$\underline{H}_0^{(i)}(\underline{r}) = \nabla(Y \hat{\alpha} \wedge \hat{a} \cdot \underline{r} + \psi^{(i)}), \quad \underline{r} \text{ in } V^{(i)} . \quad (3.54)$$

This is legitimate since  $\hat{\alpha} \wedge \hat{a} \cdot \underline{r}$  is a regular potential function in  $V^{(i)}$ .

The boundary conditions become

$$\frac{\partial \psi^{(i)}}{\partial n} = -Y \hat{n} \cdot \hat{\alpha} \wedge \hat{a} , \quad \underline{r} \text{ on } B , \quad (3.55)$$

and the continuity conditions

$$\left. \begin{aligned} \hat{n} \wedge \nabla [\psi^S(\underline{r}) - \psi^{(i)}(\underline{r})] &= 0 \\ \hat{n} \cdot \left\{ \nabla [\mu_0 \psi^S(\underline{r}) - \mu \psi^{(i)}(\underline{r})] + (\mu_0 - \mu) Y \hat{\alpha} \wedge \hat{a} \right\} &= 0 \end{aligned} \right\} \underline{r} \text{ on } C. \quad (3.56)$$

This constitutes a well posed potential problem which cannot be solved in general, but can be solved for particular choices of  $B$  and  $C$ .

In the special case when  $\mu = \mu_0$ , the conditions (3.56) require that  $\psi^S(\underline{r})$  and  $\psi^{(i)}(\underline{r})$  have continuous normal as well as tangential derivatives at  $C$ . This means that it is unnecessary to consider separately the two regions of space  $V^{(e)}$  and  $V^{(i)}$ . That is,

$$\begin{aligned} \underline{H}_0^{(i)}(\underline{r}) &= Y \hat{\alpha} \wedge \hat{a} + \nabla \psi(\underline{r}) , & \underline{r} \text{ in } V^{(i)} , \\ \underline{H}_0^S(\underline{r}) &= \nabla \psi(\underline{r}) , & \underline{r} \text{ in } V^{(e)} , \end{aligned} \quad (3.57)$$

where  $\psi(\underline{r})$  is a regular potential function exterior to B,

$$\nabla^2 \psi(\underline{r}) = 0, \quad \underline{r} \text{ in } V^{(i)} \text{ or } V^{(e)}, \quad (3.58)$$

and satisfies the boundary condition

$$\frac{\partial \psi(\underline{r})}{\partial \underline{n}} = -Y \hat{\underline{n}} \cdot \hat{\underline{\alpha}} \hat{\underline{a}}, \quad \underline{r} \text{ on } B. \quad (3.59)$$

But this is exactly the problem of finding the Rayleigh term of the magnetic field exterior to a perfectly conducting surface B.

In conclusion, we have shown that the problem of finding the Rayleigh term for the electric field when a coated object is illuminated by a plane wave is completely solved for points in the coating, i. e.,  $\underline{E}_0^{(i)}(\underline{r}) = 0$ , and is the same as that posed if the coating were perfectly conducting for points exterior to the coating. Furthermore the determination of the Rayleigh term in the magnetic field has been formulated as a potential problem which takes into account both object and coating; however, in the special case when the permeability of the coating is the same as that of free space, the effects of the coating disappear and the field exterior to the body is precisely that which would be found were the coating completely absent.

#### 3.4 The Eigenvalue Problem for the Coated Sphere

In the following we investigate the existence of solutions of the problem (3.13) for the particular case of a concentric spherical system. The perfectly conducting sphere of surface B (radius  $r = b$ ) is surrounded by a plasma layer of constant thickness ( $c - b$ ) and outer surface C (radius  $r = c$ ); ( $r, \theta, \phi$ ) are spherical polar coordinates with origin at the center of the sphere. The boundary conditions are

$$\begin{aligned} \hat{\underline{\theta}} \cdot \underline{E}_1^{(i)} = \hat{\underline{\phi}} \cdot \underline{E}_1^{(i)} = 0, \quad \text{for } r = b, \\ \hat{\underline{r}} \cdot \underline{E}_1^{(i)} = 0, \quad \text{for } r = c. \end{aligned} \quad (3.60)$$

Following the method of Hansen and Stratton, let us consider first the vector wave function

$$\underline{M}_o e_{mn}^{(z_n)} = + \frac{m}{\sin \theta} z_n(\tilde{kr}) P_n^m(\cos \theta) \frac{\sin m \phi}{\cos \phi} \hat{\theta} - z_n(\tilde{kr}) \frac{\partial P_n^m(\cos \theta)}{\partial \theta} \frac{\cos m \phi}{\sin \phi} \hat{\phi}, \quad (3.61)$$

where  $m$  and  $n$  are integers,  $z_n$  is any spherical Bessel or Hankel function (i.e.,  $j_n$ ,  $y_n$ ,  $h_n^{(1)}$  or  $h_n^{(2)}$ ), and

$$\tilde{k} = -i \omega_p \sqrt{\epsilon_0 \mu_0}. \quad (3.62)$$

Observe that the boundary condition at  $r = c$  is automatically satisfied when  $E_1^{(i)}$  is any linear combination of wavefunctions (3.61). The boundary conditions at  $r = b$  are satisfied by any wavefunction of the type

$$\underline{M}_o e_{mn}^{(j_n)} - \frac{j_n(\tilde{kb})}{h_n^{(1)}(\tilde{kb})} \underline{M}_o e_{mn}^{(h_n^{(1)})}. \quad (3.63)$$

Thus, an admissible solution is

$$\underline{E}_1^{(i)} = \sum_{n=1}^{\infty} \sum_{m=0}^n A_{mn}^{(e,o)} \left[ \underline{M}_o e_{mn}^{(j_n)} - \frac{j_n(\tilde{kb})}{h_n^{(1)}(\tilde{kb})} \underline{M}_o e_{mn}^{(h_n^{(1)})} \right]. \quad (3.64)$$

where the coefficients  $A_{mn}^{(e,o)}$  are arbitrary; the spectrum of this solution is continuous.

There is also a discrete spectrum of solutions based on the  $\underline{M}_o e_{mn}$ .

Note that

$$h_1^{(1)}(\rho) = -\rho^{-2} (\rho + i) e^{i\rho}, \quad (\rho = \tilde{kr}), \quad (3.65)$$

has a zero at  $\rho = -i$ . Thus  $\underline{M}_{e_{m1}}^{(h_1^{(1)})}$  is a solution if

$$b \omega_p \sqrt{\epsilon_0 \mu_0} = 1 . \quad (3.66)$$

Similarly,  $\underline{M}_{e_{mn}}^{(h_n^{(1)})}$  has a negative pure imaginary zero for any odd  $n$ . All of these constitute solutions, each for a single discrete (real positive) value of  $\omega_p$ . Therefore, we have proved that the  $\underline{M}_{e_{mn}}$  originate both a continuous and discrete spectrum of solutions.

Let us now consider the wavefunctions

$$\begin{aligned} \underline{N}_{e_{mn}}(z_n) &= \frac{n(n+1)}{\tilde{kr}} z_n(\tilde{kr}) P_n^m(\cos \theta) \frac{\cos m \phi}{\sin \theta} \hat{r} + \\ &+ \frac{1}{\tilde{kr}} \left[ \tilde{kr} z_n(\tilde{kr}) \right]' \frac{\partial P_n^m(\cos \theta)}{\partial \theta} \frac{\cos m \phi}{\sin \theta} \hat{\theta} + \\ &- \frac{m}{\tilde{kr}} \left[ \tilde{kr} z_n(\tilde{kr}) \right]' \frac{P_n^m(\cos \theta)}{\sin \theta} \frac{\sin n \phi}{\cos \phi} \hat{\phi} , \end{aligned} \quad (3.67)$$

where the prime indicates the derivative with respect to the argument  $\tilde{kr}$ . If  $n = 0$  (implying  $m = 0$ ) the radial component vanishes. Moreover,

$P_0^0(\cos \theta) = 1$ , so that  $\frac{\partial P_0^0}{\partial \theta} = 0$ . Hence  $\underline{N}_{e_{00}} \equiv 0$  and the solution is null.

The radial component also vanishes for  $m = 0$ , and the odd function

$$\underline{N}_{e_{0n}} = 0 ,$$

so that here again we have a null function. Since we cannot use a linear combination of two  $\underline{N}_{e_{mn}}$  based on different radial functions to cancel both

the radial and tangential components at  $r = c$  and  $r = b$  respectively, we conclude that there is no continuous spectrum based on the  $\underline{N}_{e\ mn}^0$ . Similarly, no discrete spectrum exists, since the use of a linear combination of radial functions to cancel the  $\hat{\theta}$  and  $\hat{\phi}$  components at  $r = b$  does not enable the  $\hat{r}$  component to be cancelled at  $r = c$ , for discrete values of  $\omega_p$ .

From relation (3.64) and

$$\nabla_{\wedge} \underline{M}_{e\ mn}^0(z_n) = \tilde{k} \underline{N}_{e\ mn}^0(z_n) \quad (3.68)$$

it follows that (see the second of relations (3.10)):

$$\begin{aligned} \underline{H}_0^{(i)} &= \frac{1}{\mu_0} \nabla_{\wedge} \underline{E}_1^{(i)} \\ &= -i\omega_p Y \sum_{n=1}^{\infty} \sum_{m=0}^n A_{mn}^{(e,0)} \left[ \underline{N}_{e\ mn}^0(j_n) - \frac{j_n^{(kb)}}{h_n^{(1)}(kb)} \underline{N}_{e\ mn}^0(h_n^{(1)}) \right]. \end{aligned} \quad (3.69)$$

The coefficients  $A_{mn}^{(e,0)}$  are determined as follows. The known  $\theta$  and  $\phi$  dependence of  $\underline{H}_0^i$  in  $V^{(e)}$  is used to choose the  $m$  and the  $n$  for which  $A_{mn}$  is non-zero; all other coefficients are equal to zero. The remaining non-zero coefficient is found by using the fact that  $\underline{H}_0^s$  in  $V^{(e)}$  is determinable from a regular potential. Specifically,  $\underline{H}_0^i = Y \hat{y}$ , and the only non-zero coefficient is  $A_{11}^{(o)}$ , which has the value:

$$A_{11}^{(o)} = \frac{3 (\tilde{k}b)^2 \tilde{k}c h_1^{(1)}(\tilde{k}b)}{2\omega_p \left\{ \sin [\tilde{k}(c-b)] + \tilde{k}b \cos [\tilde{k}(c-b)] \right\}}. \quad (3.70)$$

In conclusion we have been able to prove that, at least in the particular case of spherical symmetry, the system (3.13) has a non-trivial solution. It is therefore intuitive that the same result should be arrived at in the general

case, i. e. for any shapes of B and C, but we have not derived such general proof. Also, it should be pointed out that the success of the method employed in this section is due to the particularly simple geometry of the system; in fact, the method would fail if spherical symmetry were not present (e. g, when B and C are two confocal spheroids).

## CHAPTER IV

### DIPOLE MOMENTS FOR SPECIFIC GEOMETRIES

#### 4.1 General Considerations

It has been shown in the previous chapter that when the collision frequency of the plasma coating is large compared with the operating frequency ( $\nu_c \gg \omega$ ), the Rayleigh scattered field near the body can be obtained by solving two potential problems for perfect conductors. Specifically, the coefficients  $a_1^{(j)}$  ( $j = 1, 2, 3$ ) which appear in the expression (2.22) of the electric dipole moment  $\underline{P}$  are the same that would obtain if the outer surface of the plasma coating were perfectly conducting. Similarly, the coefficients  $b_1^{(j)}$  which appear in the expression (2.26) of the magnetic dipole moment  $\underline{M}$  are the same that would obtain if only the bare conducting body were present (no plasma coating). Thus, in the case  $\nu_c \gg \omega$  the problem of finding the scattered field in the Rayleigh limit is reduced to the determination of the magnetic dipole moment coefficients  $b_1^{(j)}$  for the bare metallic body and of the electric dipole moment coefficients  $a_1^{(j)}$  for a perfectly conducting scatterer whose surface coincides with the outer surface of the plasma coating. It is the purpose of this chapter to present analytic and/or numerical expressions of these dipole coefficients for a variety of scattering shapes. Since we limit our considerations to bodies of revolution about the z axis, only the four dipole coefficients  $a_1^{(1)}$ ,  $a_1^{(3)}$ ,  $b_1^{(1)}$  and  $b_1^{(3)}$  are independent (see relations (2.27)).

The only previously known results are for ellipsoids (see, for example, Stevenson (1953b) and references therein). These results are summarized in section 4.2 for the particular case of prolate spheroids. Section 4.3 contains the numerical values of dipole moment coefficients for round-backed cones; the detailed derivation is presented in Appendix A. For more complicated cone-like shapes, such as the flat-base cone, the cone-sphere, the sphere-cone-sphere and the flat-base cone with a rounded nose, which are not easily subjected to

analytical treatment, the numerical approach developed in Appendix B has been applied, and the results obtained are exhibited in section 4.4.

The limitations of the Rayleigh-Siegel formula (2.2) for bodies that are not thin have been touched upon in section 2.2 and are discussed again in section B.6. An alternate approach, which is especially useful when the scatterer is nearly spherical, is developed in section 4.5. It is there shown that the low-frequency scattered far field can be written as the sum of three terms; the first term is the field that would be scattered by the smallest sphere containing the body, whereas the other two terms are written as integrals over the volume exterior to the scatterer but interior to the smallest sphere surrounding it.

#### 4.2 Results for Prolate Spheroids

For a perfectly conducting prolate spheroid of interfocal distance  $2d$ , semi-major axis  $d\xi$  and semi-minor axis  $d\sqrt{\xi^2-1}$ , having the  $z$ -axis as axis of symmetry, the dipole moments  $\underline{P}$  and  $\underline{M}$  are immediately obtained from the results of Senior and Knott (1967, pp. 75 et seq.):

$$\underline{P} = -\frac{8\pi}{3} \epsilon_0 d^3 \left\{ \left( \ell_1 \hat{x} + m_1 \hat{y} \right) \frac{P_1^1(\xi)}{Q_1^1(\xi)} - \frac{1}{2} n_1 \hat{z} \frac{P_1^0(\xi)}{Q_1^0(\xi)} \right\}, \quad (4.1)$$

$$\underline{M} = -\frac{8\pi}{3} Y d^3 \left\{ \left( \ell_2 \hat{x} + m_2 \hat{y} \right) \frac{P_1^{1'}(\xi)}{Q_1^{1'}(\xi)} - \frac{1}{2} n_2 \hat{z} \frac{P_1^{0'}(\xi)}{Q_1^{0'}(\xi)} \right\}, \quad (4.2)$$

where  $(\ell_1, m_1, n_1)$  and  $(\ell_2, m_2, n_2)$  are the direction cosines of the incident electric and magnetic fields (see Eqs. (2.16) and (2.17)), and the prime denotes differentiation with respect to  $\xi$ . Since



$$\frac{P_1^{0'}(\xi)}{Q_1^{0'}(\xi)} = \frac{P_1^1(\xi)}{Q_1^1(\xi)}, \quad (4.3)$$

it follows by comparison of (4.1) and (4.2) with (2.22) and (2.26) that

$$a_1^{(1)} = a_1^{(2)} = \frac{2}{3} d^3 \frac{P_1^1(\xi)}{Q_1^1(\xi)}, \quad a_1^{(3)} = -\frac{1}{3} d^3 \frac{P_1^0(\xi)}{Q_1^0(\xi)}, \quad (4.4)$$

$$b_1^{(1)} = b_1^{(2)} = \frac{2}{3} d^3 \frac{P_1^{1'}(\xi)}{Q_1^{1'}(\xi)}, \quad b_1^{(3)} = -\frac{1}{3} d^3 \frac{P_1^1(\xi)}{Q_1^1(\xi)}.$$

The analogous results for an oblate spheroid can be obtained by replacing  $d$  and  $\xi$  by  $-id$  and  $i\xi$ , respectively.

For any prolate or oblate spheroid, the  $a_1^{(j)}$  and  $b_1^{(j)}$  are independent of all direction cosines (they are functions of  $\xi$  and  $d$  only); also,

$$b_1^{(3)} = -\frac{1}{2} a_1^{(1)} \quad (4.5)$$

but  $a_1^{(3)}/a_1^{(1)}$  varies drastically with the length-to-width ratio.

We point out the following limiting cases:

(i) the sphere ( $\xi \rightarrow \infty$ ;  $d \rightarrow 0$ ;  $d\xi \rightarrow a$ , the radius):

$$\frac{P_1^1(\xi)}{Q_1^1(\xi)} \sim -\frac{3}{2} \xi^3, \quad \frac{P_1^{1'}(\xi)}{Q_1^{1'}(\xi)} \sim \frac{3}{4} \xi^3, \quad \frac{P_1^0(\xi)}{Q_1^0(\xi)} \sim 3\xi^3, \quad (4.6)$$

and therefore

$$a_1^{(1)} = a_1^{(2)} = a_1^{(3)} = -a^3, \quad b_1^{(1)} = b_1^{(2)} = b_1^{(3)} = \frac{1}{2}a^3; \quad (4.7)$$

(ii) the spindle ( $\xi = 1 + \delta$ ;  $\delta \rightarrow 0$ ):

$$\frac{P_1^1(\xi)}{Q_1^1(\xi)} \sim -2\delta, \quad \frac{P_1^{1'}(\xi)}{Q_1^{1'}(\xi)} \sim 2\delta, \quad \frac{P_1^0(\xi)}{Q_1^0(\xi)} \sim -\frac{2}{\ell \ln \delta}, \quad (4.8)$$

and therefore

$$a_1^{(1)} = a_1^{(2)} = b_1^{(1)} = b_1^{(2)} = b_1^{(3)} = 0, \quad a_1^{(3)} = \frac{2}{3}d^3(\ell \ln \delta)^{-1}; \quad (4.9)$$

(iii) the disk ( $\xi \rightarrow 0$ ;  $a = \text{disk radius}$ ):

$$\frac{P_1^1(i\xi)}{Q_1^1(i\xi)} \sim \frac{2i}{\pi}, \quad \frac{P_1^{1'}(i\xi)}{Q_1^{1'}(i\xi)} \sim 0, \quad \frac{P_1^0(i\xi)}{Q_1^0(i\xi)} \sim 0, \quad (4.10)$$

and therefore

$$a_1^{(1)} = a_1^{(2)} = -\frac{4a^3}{3\pi}, \quad a_1^{(3)} = 0, \quad b_1^{(1)} = b_1^{(2)} = 0, \quad b_1^{(3)} = \frac{2a^3}{3\pi}. \quad (4.11)$$

For intermediate values of  $\xi$ , corresponding to prolate spheroids with different length-to-width ratios, some values of the Legendre functions ratios are listed in Table 4-1. Of more direct use is Table 4-2, in which  $(d\xi)^{-3} a_1^{(1)}$  and  $a_1^{(3)}/a_1^{(1)}$ ,  $b_1^{(1)}/a_1^{(1)}$  are given. The dipole moment coefficients, normalized to the volume  $V$  of the body, are plotted as functions of the length-to-width ratio for oblate and prolate spheroids in Fig. 4-1. Observe that

$$V_{\text{oblate}} = \frac{4}{3} \pi d^3 \xi (\xi^2 + 1), \quad V_{\text{prolate}} = \frac{4}{3} \pi d^3 \xi (\xi^2 - 1). \quad (4.12)$$

TABLE 4-1

Ratios of Legendre Functions With Argument  $\xi$ .

$\xi$	length/width	$P_1^1/Q_1^1$	$P_1^{1'}/Q_1^{1'}$	$P_1^0/Q_1^0$
2	1.155	-8.5208	4.6301	20.2812
1.2	1.809	-0.6543	0.4426	2.7353
1.1	2.400	-0.2691	0.2023	1.6308
1.05	3.281	-0.1192	0.09808	1.1062
1.025	4.556	-0.05540	0.04880	0.8191
1.01	7.124	-0.02101	0.01963	0.6007
1.0075	8.211	-0.01560	0.01476	0.5502
1.005	10.040	-0.01028	0.00988	0.5179

TABLE 4-2

Dipole Moment Coefficients for Prolate Spheroids.

$\xi$	$(d\xi)^{-3} a_1^{(1)}$	$a_1^{(3)}/a_1^{(1)}$	$b_1^{(1)}/a_1^{(1)}$
2	-0.7101	1.1901	-0.5434
1.2	-0.2524	2.0903	-0.6764
1.1	-0.1348	3.0299	-0.7519
1.05	-0.0687	4.6390	-0.8226
1.025	-0.0343	7.3926	-0.8809
1.01	-0.0136	14.296	-0.9343
1.0075	-0.0102	17.635	-0.9462
1.005	-0.0068	25.190	-0.9611

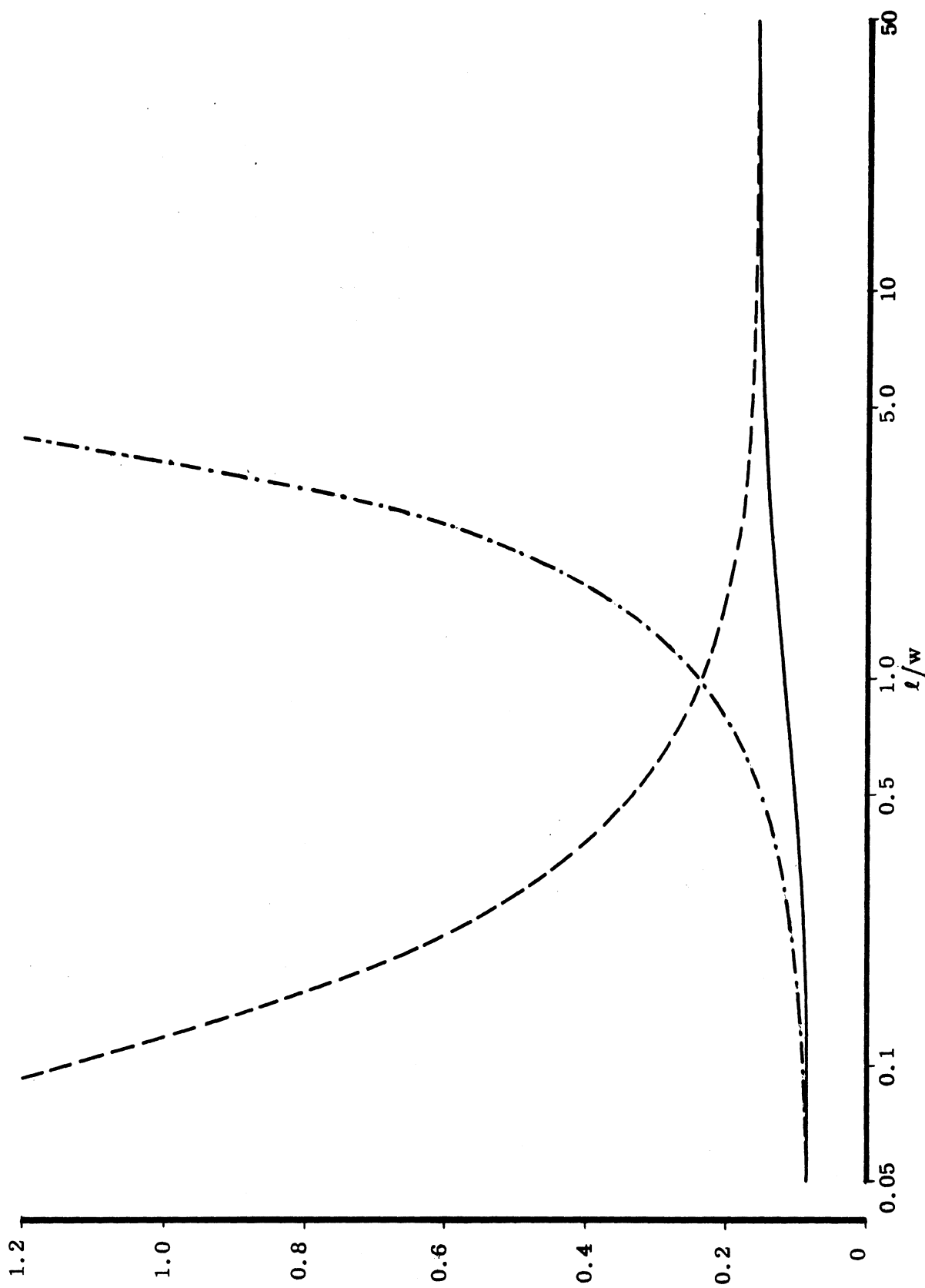


FIG. 4-1: Normalized Dipole Moment Coefficients for Oblate and Prolate Spheroids as Functions of Length-to-Width Ratio  $l/w$ :  $-a_1^{(1)}/V$  (---);  $-a_1^{(3)}/V$  (---);  $b_1^{(1)}/V$  (-·-·-), where  $V$  is the volume.

### 4.3 Results for Round-backed Cones

The scattering body is a perfectly conducting circular cone with semi-aperture angle  $(\pi - \theta_0)$ , truncated by a spherical surface of radius  $d$  whose center is at the tip of the cone. The four distinct dipole moment coefficients  $a_1^{(1)} = a_1^{(2)}$ ,  $a_1^{(3)}$ ,  $b_1^{(1)} = b_1^{(2)}$  and  $b_1^{(3)}$  have been determined in Appendix A by solving four distinct potential problems. The numerical values of the normalized coefficients are reproduced in Table 4-3, for narrow cones. More extensive results are to be found in Table A-1.

TABLE 4-3

Dipole Moment Coefficients for Round-Backed Cones

$\pi - \theta_0$ degrees	$-a_1^{(1)}/d^3$	$-a_1^{(3)}/d^3$	$b_1^{(1)}/d^3$	$b_1^{(3)}/d^3$
2.5	0.0003	0.0144	0.0003	0.0001
5.0	0.0014	0.0210	0.0011	0.0007
7.5	0.0035	0.0274	0.0025	0.0017
10.0	0.0066	0.0332	0.0041	0.0033
12.5	0.0108	0.0383	0.0062	0.0054
15.0	0.0163	0.0438	0.0084	0.0082
17.5	0.0234	0.0491	0.0111	0.0117
20.0	0.0318	0.0545	0.0139	0.0159

It should be noted that the result (4.5), which has been rigorously proven for all spheroids, is also valid for all round-backed cones, as seen from Tables 4-3 and A-1. Therefore, we advance the hypothesis (which we put to use in Chapter V) that relation (4.5) is valid for all bodies of revolution.

The exact dipole moment coefficients (normalized to the volume  $V$  of the scatterer) for a round-backed cone are compared with those of a spheroid of the same length-to-width ratio in Fig. 4-2. Observe that for a round-backed cone of semi-aperture angle  $(\pi - \theta_0)$ :

$$V = \frac{2}{3} \pi (1 + \cos \theta_0) d^3 . \quad (4.13)$$

For nose-on incidence, the back scattering cross section is determined by  $a_1^{(1)}$  and  $b_1^{(1)}$  alone; specifically, the far-field coefficient  $S_{||}$  is given by equation (2.39). According to Siegel's formula (2.2),

$$\left| S_{||} \right| \approx \frac{k^3}{\pi} VG , \quad (4.14)$$

where  $V$  is given by (4.13), and  $G$  by (2.3) in which now (Siegel, 1963):

$$y = \frac{1}{4} \operatorname{cosec} \theta_0 . \quad (4.15)$$

A comparison of  $(kd)^{-3} S_{||}$  as obtained from (2.39) and Table A-1 with the approximate values provided by Siegel's formula is shown in Table 4-4. As expected, Siegel's approximation is quite accurate for narrow-angle cones ( $\theta_0$  near  $180^\circ$ ) but becomes rather poor for wide-angle cones ( $\theta_0$  near  $90^\circ$ ).

#### 4.4 Results by Numerical Method

The analytical determination of the dipole moment coefficients is possible whenever the surface of the body is either a complete coordinate surface in a system of coordinates for which the Laplace equation is separable (e.g. a spheroid), or is made of portions of such surfaces so that a mode matching technique is applicable (e.g. a round-backed cone). In all other cases, some dipole coefficients can be found numerically by the method developed in Appendix B.

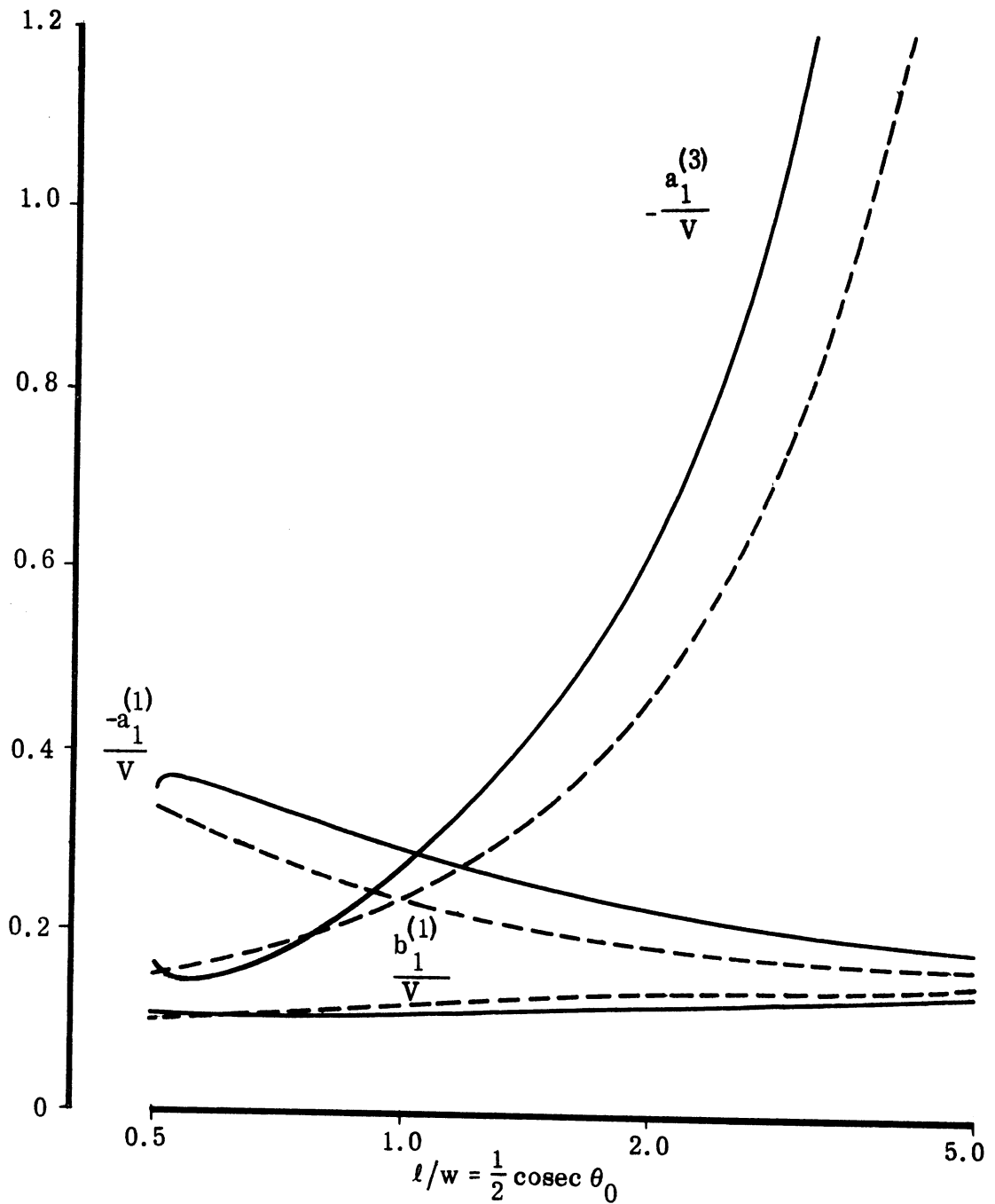


FIG. 4-2: Exact (normalized) Dipole Moment Coefficients for a Round-Backed Cone (—) Compared with Those for a Spheroid (- - -) of the Same Length to Width Ratio.

TABLE 4-4

Axial Backscattering From Round-backed Cones

$\pi-\theta_0$ degrees	$(kd)^{-3} S_{  }$		ratio
	exact	Siegel	
5	0.0005(6)	0.0006(3)	-----
10	0.0105	0.0107	1.02
15	0.0258	0.0256	0.99
20	0.0482	0.0488	1.01
30	0.1122	0.1238	1.10
40	0.2080	0.2425	1.17
50	0.3270	0.4057	1.24
60	0.4810	0.6106	1.27
70	0.6367	0.8408	1.32
80	0.8072	1.0867	1.35

When the plane wave

$$\underline{E}^i = \hat{x} e^{ikz}, \quad \underline{H}^i = \hat{y} e^{ikz} \quad (4.16)$$

is axially incident on a perfectly conducting body of revolution, it produces a backscattered electric field

$$\underline{E}^{b.s.} = \hat{x} (F_e + F_m) \frac{e^{ikr}}{kr}, \quad (4.17)$$

where  $F_e$  and  $F_m$  are the contributions due to the electric and magnetic dipoles  $\underline{P}$  and  $\underline{M}$ , and are related to the x-component of  $\underline{P}$  and to the y-component of  $\underline{M}$  by:

$$F_e = \frac{k^3}{4\pi\epsilon_0} P_x, \quad F_m = -\frac{k^3 Z}{4\pi} M_y. \quad (4.18)$$



The quantities  $F_e$  and  $F_m$  are to be found numerically through the computer program of section B. 8; for any given scattering shape, they can be considered as known. From relations (2.22) with  $\ell_1 = 1$ ,  $m_1 = n_1 = 0$ , and (2.26) with  $m_2 = 1$ ,  $\ell_2 = n_2 = 0$ , it follows that ( $b_1^{(1)} = b_1^{(2)}$ ):

$$P_x = -4\pi\epsilon_0 a_1^{(1)}, \quad M_y = -4\pi Y b_1^{(1)}. \quad (4.19)$$

From (4.18) and (4.19) :

$$\frac{a_1^{(1)}}{3} = -(ka)^{-3} F_e, \quad \frac{b_1^{(1)}}{3} = (ka)^{-3} F_m \quad (4.20)$$

and

$$F_e + F_m = S \Big|_{n_1 = n_2 = 0} = -k^3 (a_1^{(1)} - b_1^{(1)}), \quad (4.21)$$

where  $a$  is a characteristic dimension of the scatterer. Rigorously speaking, relations (4.20) and (4.21) are valid only if  $F_e$  and  $F_m$  are computed in the limit  $k \rightarrow 0$ . In practice, however, it is sufficient that  $ka \ll 1$  (e.g.  $ka = 0.1$ ), as is evident from the following two examples.

Consider first a sphere of radius  $a$  for which the exact values are given by (4.7):

$$\frac{a_1^{(1)}}{3} = -1, \quad \frac{b_1^{(1)}}{3} = \frac{1}{2}.$$

For  $ka = 0.1$  the computer program of Appendix B gives the surface currents of Fig. B-5 and the far-field coefficients

$$\left. \begin{aligned} F_e &= 1.0084482 \times 10^{-3} + i 0.70283909 \times 10^{-6}, \\ F_m &= 0.49690390 \times 10^{-3} - i 0.16412946 \times 10^{-6}; \end{aligned} \right\} ka = 0.1$$

it is seen that the agreement between (4.20) and the exact values is indeed excellent.

Secondly, consider a round-backed cone with semi-aperture  $\pi - \theta_0 = 30^\circ$  and base radius  $d$  (equal to the length of a generator) for which, from Tables A-1 and 4-4:

$$\frac{a_1^{(1)}}{d^3} = -0.0814, \quad \frac{b_1^{(1)}}{d^3} = 0.0306, \quad (kd)^{-3} S_{\parallel} = 0.1122.$$

For  $kd = 0.1$  (and choosing a total  $N = 20$  of sampling points for the surface currents, ten along a generator and ten on the rounded base), the computer program yields the far-field coefficients,

$$\left. \begin{aligned} F_e &= 0.079801248 \times 10^{-3} + i 0.035802121 \times 10^{-3}, \\ F_m &= 0.032452983 \times 10^{-3} + i 0.050564468 \times 10^{-4}, \end{aligned} \right\} kd = 0.1$$

from which

$$F_e + F_m = (0.11225423 + i 0.04085856) \times 10^{-3};$$

again, the use of (4.20) and (4.21) leads to rather precise results.

In conclusion, we may say that the computer program of Appendix B and the formulas (4.20) and (4.21) give reliable values of  $a_1^{(1)}$  and  $b_1^{(1)}$  provided that  $ka \lesssim 0.1$  and that a sufficient number of sampling points is chosen for the surface currents on the body (at least 20, and preferably 30). The imaginary parts of  $F_e$  and  $F_m$  may be neglected.

If we accept the relation (4.5) which has been proven valid for spheroids and round-backed cones, also for all other bodies of revolution, then the only dipole moment coefficient that cannot be numerically obtained by the method of Appendix B is  $a_1^{(3)}$ ; this is because the method has been developed for axial incidence only.

A variety of numerical results are exhibited in Table 4-5, together with the profiles of the scatterers in a plane through the axis  $z$  of symmetry. In all cases, the computations of  $F_e$  and  $F_m$  have been carried out for  $ka = 0.1$ , formulas (4.20) have been used, and the imaginary parts have been neglected.

#### 4.5 The Rayleigh Term in Far-Field Plane Wave Scattering

The purpose of this section is to present some new results on the Rayleigh term in an expansion of the far electric field scattered when a plane wave is incident upon a finite three dimensional perfectly conducting object.

The expression of the far field in terms of surface integrals of the static, near field terms is (Kleinman, 1967):

$$\underline{E}^s = \frac{e^{ikr}}{4\pi r} k^2 \hat{r} \int_B \left[ \hat{r} \wedge \underline{r}_B (Z \hat{r} \cdot \hat{n} \wedge \underline{H}_0 - \hat{n} \cdot \underline{E}_0^s) - \underline{r}_B (\hat{r} \cdot \hat{n} \wedge \underline{E}_0^s + Z \hat{n} \cdot \underline{H}_0^s) \right] dS, \quad (4.22)$$

where  $B$  is the surface of the scatterer,  $\underline{r}_B$  is the position vector of the integration point on  $B$ ,  $\hat{n}$  is the outward unit normal to  $B$  at  $\underline{r}_B$ ,  $\hat{r}$  is a unit vector directed from the origin of coordinates toward the observation point, and  $\underline{E}_0^s$  and  $\underline{H}_0^s$  are the Rayleigh terms in an expansion of the scattered electric and magnetic fields which satisfy the boundary conditions

$$\left. \begin{aligned} \hat{n} \wedge \underline{E}_0^s &= -\hat{n} \wedge \underline{E}_0^i \\ \hat{n} \cdot \underline{H}_0^s &= -\hat{n} \cdot \underline{H}_0^i \end{aligned} \right\} \text{ on } B. \quad (4.23)$$

TABLE 4-5: Dipole Moment Coefficients.

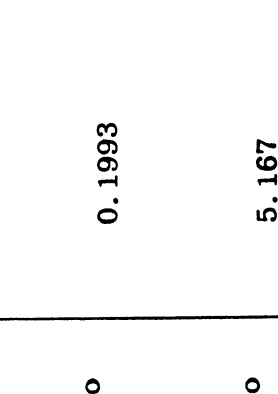
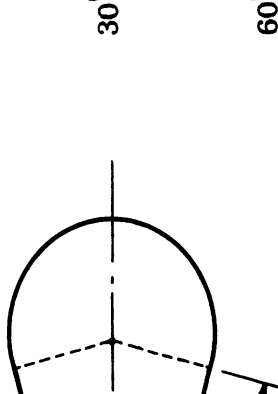
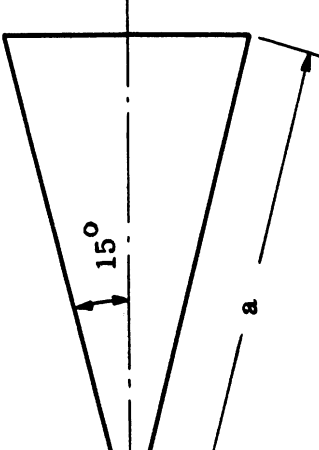
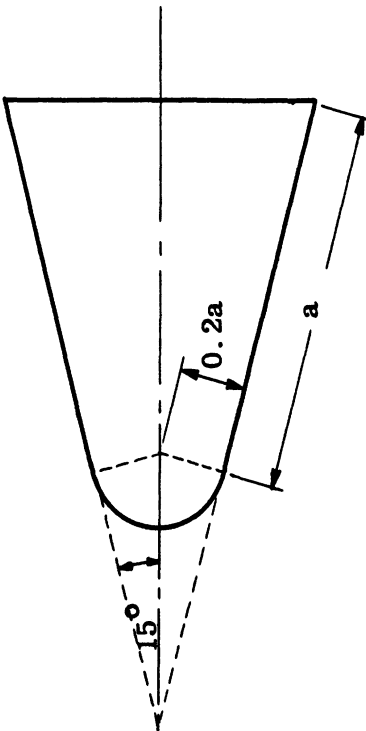
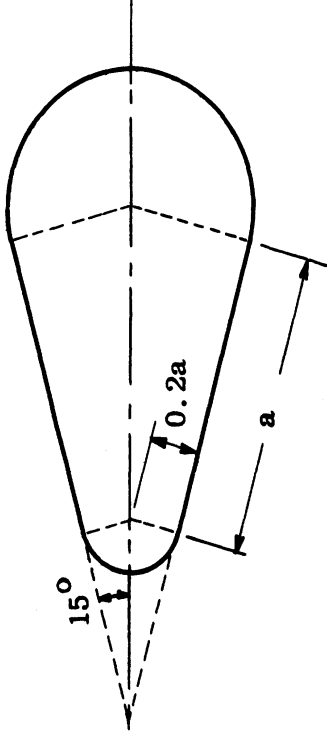
Scattering Body	$-a_1^{(1)}/a^3$	$b_1^{(1)}/a^3$
<p>1) Cone Spheres.</p> <p style="text-align: center;"><math>\pi - \theta_0 = 15^\circ</math></p>  <p style="text-align: center;"><math>30^\circ</math></p>  <p style="text-align: center;"><math>60^\circ</math></p>	<p>0.02371</p> <p>0.1993</p> <p>5.167</p>	<p>0.01671</p> <p>0.1133</p> <p>2.435</p>
<p>2) Flat-Base Cone.</p> 	<p>0.01409</p>	<p>0.008203</p>

TABLE 4-5 Continued

Scattering Body	$-a_1^{(1)}/a^3$	$b_1^{(1)}/a^3$
<p>3) Flat-Base Cone With Rounded Nose.</p> 	<p>0.08066</p>	<p>0.04240</p>
<p>4) Sphere-Cone-Sphere.</p> 	<p>0.1267</p>	<p>0.08340</p>

If the incident field is a plane wave, i. e.

$$\underline{\underline{E}}^i = \hat{\underline{a}} e^{ik\hat{\alpha} \cdot \underline{r}} , \quad \underline{\underline{H}}^i = \hat{\alpha} \wedge \hat{\underline{a}} Y e^{ik\hat{\alpha} \cdot \underline{r}} , \quad (4.24)$$

then

$$\underline{\underline{E}}_0^i = \hat{\underline{a}} , \quad \underline{\underline{H}}_0^i = \hat{\alpha} \wedge \hat{\underline{a}} Y , \quad (4.25)$$

and

$$\hat{\underline{n}} \wedge \underline{\underline{E}}_0^s = -\hat{\underline{n}} \wedge \hat{\underline{a}} \quad \hat{\underline{n}} \cdot \underline{\underline{H}}_0^s = -\hat{\underline{n}} \cdot \hat{\alpha} \wedge \hat{\underline{a}} Y . \quad (4.26)$$

Substitution of these results in the expression for the scattered field yields:

$$\underline{\underline{E}}^s = \frac{e^{ikr}}{4\pi r} k^2 \hat{\underline{r}} \wedge \int_B \left[ \hat{\underline{r}} \wedge \underline{r}_B (Z \hat{\underline{r}} \cdot \hat{\underline{n}} \wedge \underline{\underline{H}}_0^s - \hat{\underline{n}} \cdot \underline{\underline{E}}_0^s) + \underline{r}_B (\hat{\underline{r}} \cdot \hat{\underline{n}} \wedge \hat{\underline{a}} + \hat{\underline{n}} \cdot \hat{\alpha} \wedge \hat{\underline{a}}) \right] dS ; \quad (4.27)$$

but

$$\begin{aligned} & \int_B \underline{r}_B (\hat{\underline{r}} \cdot \hat{\underline{n}} \wedge \hat{\underline{a}} + \hat{\underline{n}} \cdot \hat{\alpha} \wedge \hat{\underline{a}}) dS \\ &= \int_B \underline{r}_B \hat{\underline{n}} \cdot (\hat{\alpha} \wedge \hat{\underline{a}} - \hat{\underline{r}} \wedge \hat{\underline{a}}) dS \\ &= \hat{\underline{x}} \left\{ (\hat{\alpha} \wedge \hat{\underline{a}} - \hat{\underline{r}} \wedge \hat{\underline{a}}) \cdot \int_B \hat{\underline{x}} \hat{\underline{n}} dS \right\} + \hat{\underline{y}} \left\{ (\hat{\alpha} \wedge \hat{\underline{a}} - \hat{\underline{r}} \wedge \hat{\underline{a}}) \cdot \int_B \hat{\underline{y}} \hat{\underline{n}} dS \right\} + \hat{\underline{z}} \left\{ (\hat{\alpha} \wedge \hat{\underline{a}} - \hat{\underline{r}} \wedge \hat{\underline{a}}) \cdot \int_B \hat{\underline{z}} \hat{\underline{n}} dS \right\} \\ &= \hat{\underline{x}} \left\{ (\hat{\alpha} \wedge \hat{\underline{a}} - \hat{\underline{r}} \wedge \hat{\underline{a}}) \cdot \int_V \nabla(\hat{\underline{x}}) dV \right\} + \hat{\underline{y}} \left\{ (\hat{\alpha} \wedge \hat{\underline{a}} - \hat{\underline{r}} \wedge \hat{\underline{a}}) \cdot \int_V \nabla(\hat{\underline{y}}) dV \right\} + \hat{\underline{z}} \left\{ (\hat{\alpha} \wedge \hat{\underline{a}} - \hat{\underline{r}} \wedge \hat{\underline{a}}) \cdot \int_V \nabla(\hat{\underline{z}}) dV \right\} \\ &= \left[ \hat{\underline{x}} \left\{ (\hat{\alpha} \wedge \hat{\underline{a}} - \hat{\underline{r}} \wedge \hat{\underline{a}}) \cdot \hat{\underline{x}} \right\} + \hat{\underline{y}} \left\{ (\hat{\alpha} \wedge \hat{\underline{a}} - \hat{\underline{r}} \wedge \hat{\underline{a}}) \cdot \hat{\underline{y}} \right\} + \hat{\underline{z}} \left\{ (\hat{\alpha} \wedge \hat{\underline{a}} - \hat{\underline{r}} \wedge \hat{\underline{a}}) \cdot \hat{\underline{z}} \right\} \right] \int_V dV \\ &= (\hat{\alpha} \wedge \hat{\underline{a}} - \hat{\underline{r}} \wedge \hat{\underline{a}}) \cdot \underline{\underline{V}} . \end{aligned} \quad (4.28)$$

Thus

$$\underline{E}^s = \frac{e^{ikr}}{4\pi r} k^2 \hat{r} \wedge \left\{ \int_B \hat{r} \wedge \underline{r}_B (Z \hat{r} \cdot \hat{n} \wedge \underline{H}_0^s - \hat{n} \cdot \underline{E}_0^s) dS + (\hat{\alpha} \wedge \hat{a} - \hat{r} \wedge \hat{a}) V \right\}, \quad (4.29)$$

where  $V$  is the volume of the scatterer.

The remaining terms involve  $\underline{E}_0^s$  and  $\underline{H}_0^s$  but following Rayleigh and his successors these may be written as gradients of potential functions, i. e.

$$\underline{E}_0^s = \nabla \bar{\Phi}, \quad \underline{H}_0^s = Y \nabla \psi. \quad (4.30)$$

where

$$\nabla^2 \bar{\Phi} = \nabla^2 \psi = 0 \text{ exterior to } B \quad (4.31)$$

and with the boundary conditions

$$\left. \begin{aligned} \hat{n} \wedge \nabla \bar{\Phi} &= -\hat{n} \wedge \hat{a} = -\hat{n} \wedge \nabla (\hat{a} \cdot \underline{r}) \\ \hat{n} \cdot \nabla \psi &= -\hat{n} \cdot \hat{\alpha} \wedge \hat{a} \end{aligned} \right\} \underline{r} \text{ on } B, \quad (4.32)$$

The first of these may be written as  $\hat{n} \wedge \nabla (\bar{\Phi} + \hat{a} \cdot \underline{r}) = 0$  which may be shown

to imply that  $\bar{\Phi} + \hat{a} \cdot \underline{r} = \text{constant on } B$ . The constant may be explicitly evaluated using the additional condition  $\int_B \hat{n} \cdot \nabla \bar{\Phi} dS = 0$ .

Thus

$$\underline{E}^s = \frac{e^{ikr}}{4\pi r} k^2 \hat{r} \wedge \left\{ \int_B \hat{r} \wedge \underline{r}_B \left[ \hat{r} \cdot \hat{n} \wedge \nabla_B \psi(\underline{r}_B) - \hat{n}_B \cdot \nabla_B \bar{\Phi}(\underline{r}_B) \right] dS + (\hat{\alpha} \wedge \hat{a} - \hat{r} \wedge \hat{a}) V \right\}. \quad (4.33)$$

This expression is rewritten with the help of the following

#### Lemma

If  $\psi$  is a differentiable scalar function defined everywhere on the closed surface  $B$ , then

$$\int_B \underline{r}_B \hat{r} \cdot \hat{n} \wedge \nabla_B \psi dS = -\hat{r} \wedge \int_B \hat{n} \psi dS. \quad (4.34)$$

Proof

Use the properties of the scalar triple product to write

$$\int_B \underline{r}_B \hat{r} \cdot \hat{n} \wedge \nabla_B \psi \, dS = \int_B \underline{r}_B \hat{n} \cdot \nabla_B \psi \wedge \hat{r} \, dS,$$

and since

$$\nabla_B \wedge \hat{r} = 0,$$

$$\int_B \underline{r}_B \hat{r} \cdot \hat{n} \wedge \nabla_B \psi \, dS = \int_B \underline{r}_B \hat{n} \cdot \nabla_B \psi \wedge \hat{r} \, dS .$$

Now employ the Lemma proved in Kleinman (1967) to obtain

$$\int_B \underline{r}_B \hat{r} \cdot \hat{n} \wedge \nabla_B \psi \, dS = \int_B \hat{n} \wedge \psi \hat{r} \, dS = -\hat{r}_\wedge \int_B \hat{n} \psi \, dS , \quad \text{Q. E. D.}$$

With this result the expression for the scattered field becomes:

$$\begin{aligned} \underline{E}^s = \frac{e}{4\pi r} k^2 \left\{ -\hat{r}_\wedge \hat{r}_\wedge \hat{r}_\wedge \int_B \hat{n} \psi \, dS - \hat{r}_\wedge \hat{r}_\wedge \int_B \underline{r}_B \hat{n} \cdot \nabla_B \psi \, dS + \right. \\ \left. + [\hat{r}_\wedge (\hat{\alpha}_\wedge \hat{a}) - \hat{r}_\wedge (\hat{r}_\wedge \hat{a})] \, \mathbf{V} \right\} , \end{aligned} \quad (4.35)$$

or

$$\begin{aligned} \underline{E}^s = \frac{e}{4\pi r} k^2 \left\{ \hat{r}_\wedge \int_B \hat{n} \psi \, dS - \hat{r}_\wedge \hat{r}_\wedge \int_B \underline{r}_B \hat{n} \cdot \nabla_B \psi \, dS + \right. \\ \left. + \hat{r}_\wedge (\hat{\alpha}_\wedge \hat{a}) \, \mathbf{V} - \hat{r}_\wedge (\hat{r}_\wedge \hat{a}) \, \mathbf{V} \right\} . \end{aligned} \quad (4.36)$$



An alternate and perhaps more revealing form of the far field expression may be obtained by using the following theorem, whose proof is here omitted:

If  $u$  is a regular potential function exterior to  $B$  and  $\delta V$  is the volume exterior to  $B$  but interior to the smallest sphere containing  $B$ , then:

$$\int_B \underline{\underline{r}}_B \hat{n} \cdot \nabla u \, dS + 2 \int_B \hat{n} u \, dS + 3 \int_{\delta V} \nabla u \, dV = 0 .$$

By identifying  $u$  first with  $\Phi$  and then with  $\psi$  and by using the boundary conditions it is found after some manipulation that

$$\underline{\underline{E}}^s = \frac{e^{ikr}}{4\pi r} k^2 \underline{\underline{r}}_A \left\{ \left( \frac{3}{2} \hat{\alpha} \wedge \hat{a} - 3 \hat{r} \wedge \hat{a} \right) \cdot \nabla - \frac{3}{2} \int_{\delta V} \nabla \psi \, dV + 3 \hat{r} \wedge \int_{\delta V} \nabla \Phi \, dV \right\} . \quad (4.37)$$

This last expression reduces to the first term in the curly brackets when the scatterer is a sphere.

## CHAPTER V

### RADAR CROSS SECTIONS OF VARIOUS PLASMA-COATED BODIES

#### 5.1 Choice of Shapes

The results presented below are valid for a plasma sheath with  $\nu_c \gg \omega$ . As shown in Chapter III, in this case the electric dipole moment coefficients  $a_1^{(j)}$  are those of a metal body whose surface coincides with the outer boundary of the plasma, whereas the magnetic dipole moment coefficients  $b_1^{(j)}$  are those pertaining to the bare re-entry vehicle. By choosing the shapes of the body and of the outer surface of the plasma among those whose dipole moment coefficients have been computed in Chapter IV, various possible combinations emerge for which the radar cross section has been obtained and plotted, as described in sections 5.2 and 5.3.

The choices of shapes are listed in the following table.

TABLE 5.1  
CHOICE OF SHAPES

bare body	outer plasma boundary	figures
round-backed cone	cone-sphere	5-1 , 5-2
flat-base cone	cone-sphere	5-3
flat-base cone	sphere-cone-sphere	5-4
flat-base cone with rounded nose	sphere-cone-sphere	5-5
flat-base cone with rounded nose	prolate spheroid	5-6
round-backed cone	prolate spheroid	5-7a, 5-7b, 5-8a, 5-8b.

Even though the shapes of the plasma outer boundary are not very realistic, certain general conclusions can be drawn for the behavior of the backscattering cross section (see section 5.4). It should be pointed out that, in general, we can calculate the backscattering cross section for all angles of incidence but only in the H-plane, i. e. for an incident plane wave whose magnetic field vector  $\underline{H}^i$  is parallel to the plane containing the axis of symmetry of the scatterer (taken as the z-axis) and the direction of propagation of the incident wave. Even with this limitation, we must postulate the validity of formula (4.5) for all bodies of revolution treated here .

The determination of the backscattering cross section for all other polarizations of the incident field requires the knowledge of all dipole moment coefficients. Since  $a_1^{(3)}$  cannot be obtained by the numerical technique of Appendix B and is therefore presently known for round-backed cones and spheroids only, the backscattering cross section in the E-plane (incident electric field vector  $\underline{E}^i$  parallel to the plane containing the symmetry axis z and the direction of incidence) is given only for round-backed cones coated by a plasma whose outer surface is a prolate spheroid.

For each scattering configuration, three curves of the backscattering cross section as a function of the angle of incidence are given. The curve B corresponds to the bare vehicle (no plasma coating) and therefore applies to the exo-atmospheric phase of re-entry. The curve C is obtained by taking the plasma as perfectly conducting for both the  $a_1^{(j)}$ 's and the  $b_1^{(j)}$ 's , i. e. by following the suggestion of Hiatt et al. (1960). The curve E is derived by applying the rigorous analysis of the previous chapters: the  $b_1^{(j)}$ 's are those of the bare body, but the  $a_1^{(j)}$ 's are those that would obtain if the plasma sheath were perfectly conducting.

## 5.2 Diagrams in the H-plane

When the incident magnetic field  $\underline{H}^i$  is parallel to the plane containing the axis z of symmetry and the direction of propagation of the incident plane wave, the cross-polarized component of the backscattering cross section is zero, and the direct polarized component is

$$\sigma(\alpha) = \frac{4\pi}{k^2} \left| S_{\parallel} \right|^2 \quad (5.1)$$

where  $S_{\parallel}$  is given by eq. (2.37) with  $n_2^2 = \sin^2 \alpha$ , and  $\alpha$  is the angle which the direction of incidence forms with the z-axis.

We normalize the cross section to the value  $\frac{4}{\pi} k^4 V^2$  ( $V$  = volume of bare body), i. e. to the Rayleigh approximate value of eq. (2.1) for the bare vehicle and axial incidence. Thus, we consider the normalized cross section

$$\sigma_n(\alpha) = \frac{\sigma(\alpha)}{\frac{4}{\pi} k^4 V^2} = A_h^2, \quad (5.2)$$

where

$$A_h = \left| \frac{b_1^{(1)}}{V/\pi} \cos^2 \alpha + \frac{b_1^{(3)}}{V/\pi} \sin^2 \alpha - \frac{a_1^{(1)}}{V/\pi} \right|. \quad (5.3)$$

Since

$$\sigma_n(\pi - \alpha) = \sigma_n(\alpha), \quad (5.4)$$

we may restrict our plot of  $\sigma_n$  to the range  $0 \leq \alpha \leq 90^\circ$ .

Various diagrams are presented in Figs. 5-1 to 5-6, 5-7a and 5-8a.

The vertical scale is in db, that is we plot

$$\sigma_n \text{ (in db)} = 20 \log_{10} A_h. \quad (5.5)$$

Although the sketches of the scattering shapes are self-explanatory, Figs. 5-7a and 5-8a deserve a particular comment. Here we have chosen the prolate spheroid (simulating the outer boundary of the plasma) to touch both the tip and the circular rim at the base of the round-backed vehicle, and we have further imposed that the volume of the spheroid be minimum. It then follows

that the minor axis of the spheroid is equal to the base diameter  $2b \sin(\pi - \theta_0)$  of the round-backed cone. Thus, the characteristic parameters of the minimum-volume spheroid are:

$$\begin{aligned} \text{major axis} &= 2b \cos(\pi - \theta_0), \\ \text{minor axis} &= 2b \sin(\pi - \theta_0), \\ \text{volume} &= \frac{4}{3} \pi b^3 \cos \beta \sin^2 \beta, \\ \text{length-to-width ratio} &= \cot \beta. \end{aligned}$$

### 5.3 Diagrams in the E-Plane

When the incident electric field  $\underline{E}^i$  is parallel to the plane containing the axis  $z$  of symmetry and the direction of propagation of the incident plane wave, the cross-polarized component of the backscattering cross section is zero. All considerations and formulas of section 5.3 still apply to the direct polarized component, provided that  $A_h$  is replaced throughout by

$$A_e = \left| \frac{b_1^{(1)}}{V/\pi} - \frac{a_1^{(1)}}{V/\pi} \cos^2 \alpha - \frac{a_1^{(3)}}{V/\pi} \sin^2 \alpha \right|. \quad (5.6)$$

Since  $a_1^{(3)}$  is known only for round-backed cones and spheroids, we have limited our diagrams to the two figures 5-7b and 5-8b.

### 5.4 Discussion of Results

The previous diagrams are confined to the direct polarized component in the H- and E-planes; for other polarizations, the cross section would exhibit an intermediate behavior between these two extreme cases, and a cross-polarized component would also appear, according to formulas (2.34)-(2.36).

In the H-plane, the rigorous value of the cross section (curve E) is always much larger than the bare vehicle value (curve B), so that the formation of the plasma sheath during re-entry always increases the monostatic cross

section, in the low-frequency limit. Also, the values of the correct curve E are always a few db's lower than the corresponding values obtained by considering the plasma outer boundary as perfectly conducting (curve C). For all practical purposes, the curve E yields a cross section which is independent of the angle  $\alpha$  of incidence. We again point out that these conclusions are subordinated to the validity of formula (4.5), which has been proven only for round-backed cones and spheroids.

It is more difficult to make statements of general validity for the cross section in the E-plane, due to the paucity of available theoretical results. However, from the results of Figs. 5-7b and 5-8b, it seems reasonable to conclude that in this case too the low-frequency cross section increases significantly as the vehicle re-enters the atmosphere, but its correct value is somewhat lower than what would be obtained by replacing the plasma with a perfect conductor. Also, the cross section in the E-plane varies markedly with the angle  $\alpha$  of incidence. For the shapes of vehicle and plasma considered here,  $\sigma_n(\alpha)$  increases with  $\alpha$  (see curve E on Figs. 5-7b and 5-8b), and the difference between  $\sigma_n(90^\circ)$  and  $\sigma_n(0^\circ)$  becomes more pronounced as the scatterer becomes more elongated.

For axial incidence ( $\alpha = 0^\circ$ ), the predictions based on the Rayleigh-Siegel formula (2.2) agree well with the values  $\sigma_n(0^\circ)$  of curves B and C if the corresponding scatterers are very elongated, but are more and more in error as the scatterers become fatter.

Finally, we observe that although the shapes and dimensions of the plasma outer surface considered here are rather idealistic, the conclusions of this section should remain valid in a realistic situation, since they were derived from features exhibited by a variety of shapes of the plasma sheath. If the dimensions of the plasma sheath are increased, the major consequence is simply an upward shift of curves E and C with respect to curve B.

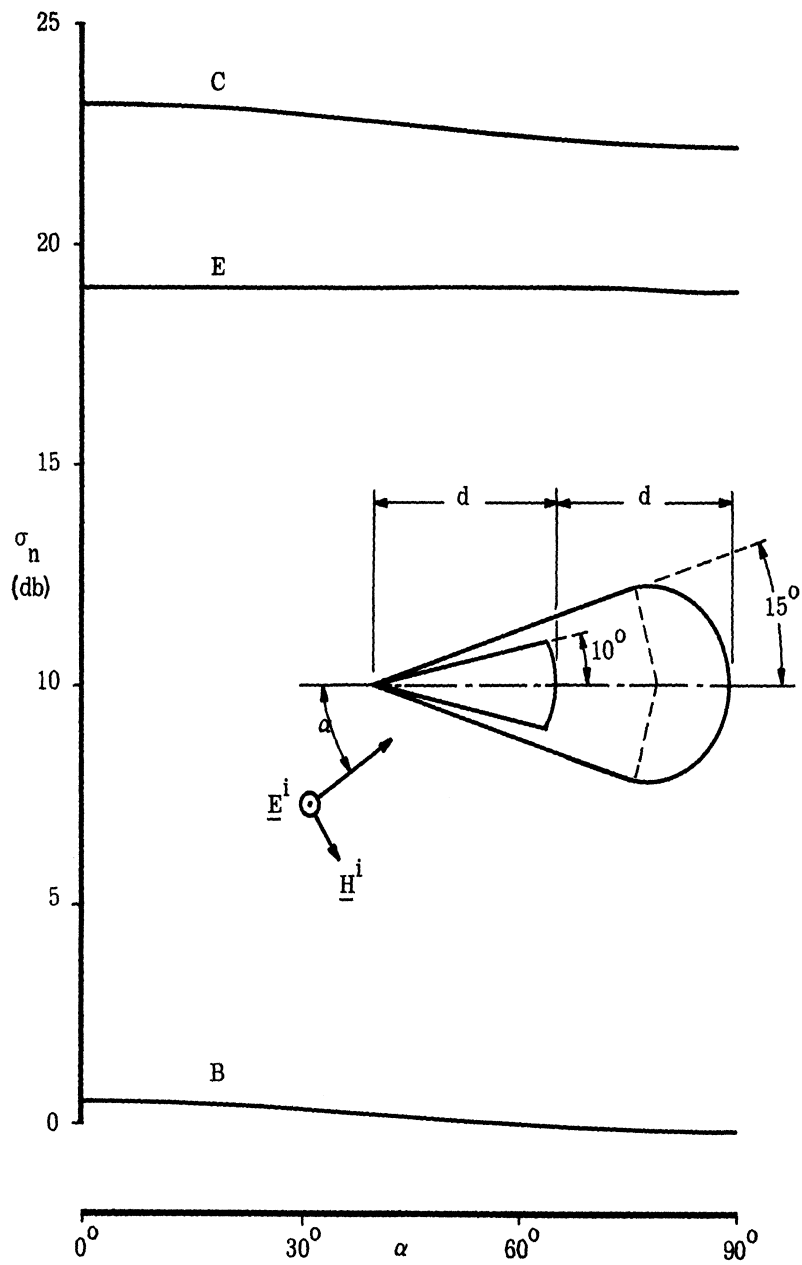


FIG. 5-1: Normalized Backscattering Cross Section in the H-Plane.  
 B = Bare Round-Backed Cone ( $\pi - \theta_0 = 10^\circ$ ), E = Plasma-Coated Cone, C = Conducting Cone-Sphere.

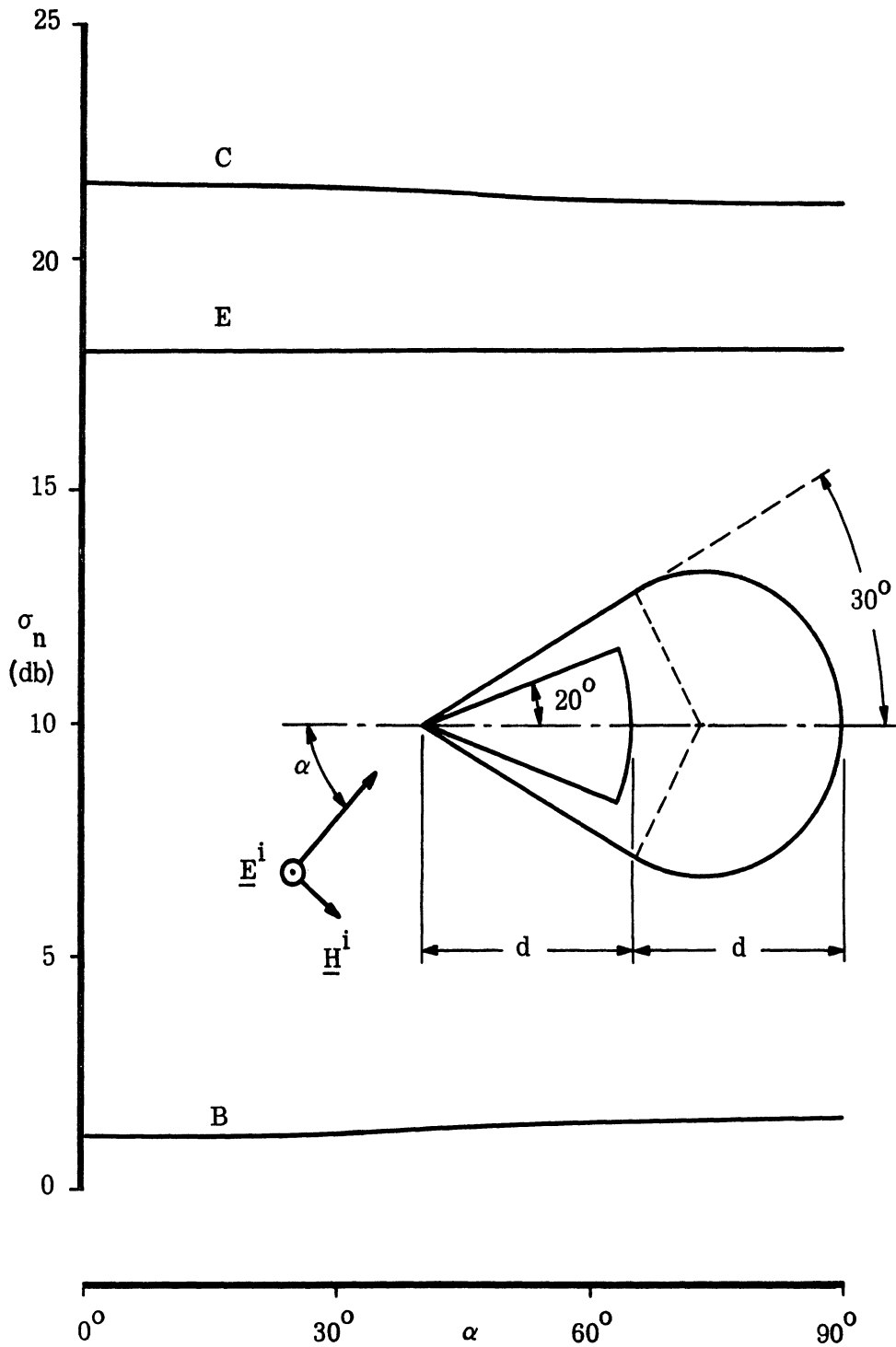


FIG. 5-2: Normalized Backscattering Cross Section in the H-Plane.  
 B = Bare Round-Backed Cone ( $\pi - \theta_0 = 20^\circ$ ), E = Plasma-Coated Cone, C = Conducting Cone-Sphere.



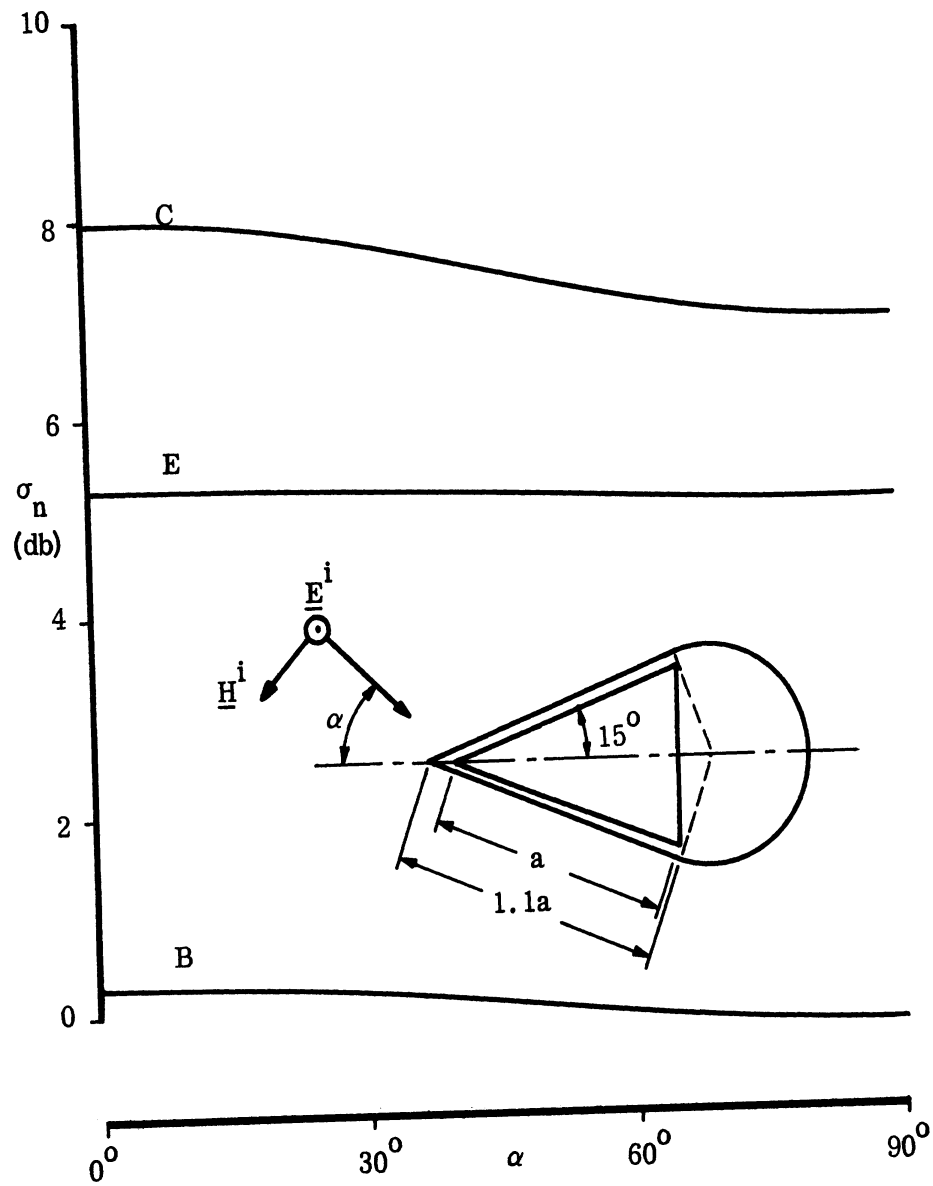


FIG. 5-3: Normalized Backscattering Cross Section in the H-Plane. B = Bare Flat-Base Cone, E = Plasma-Coated Cone, C = Conducting Cone-Sphere.

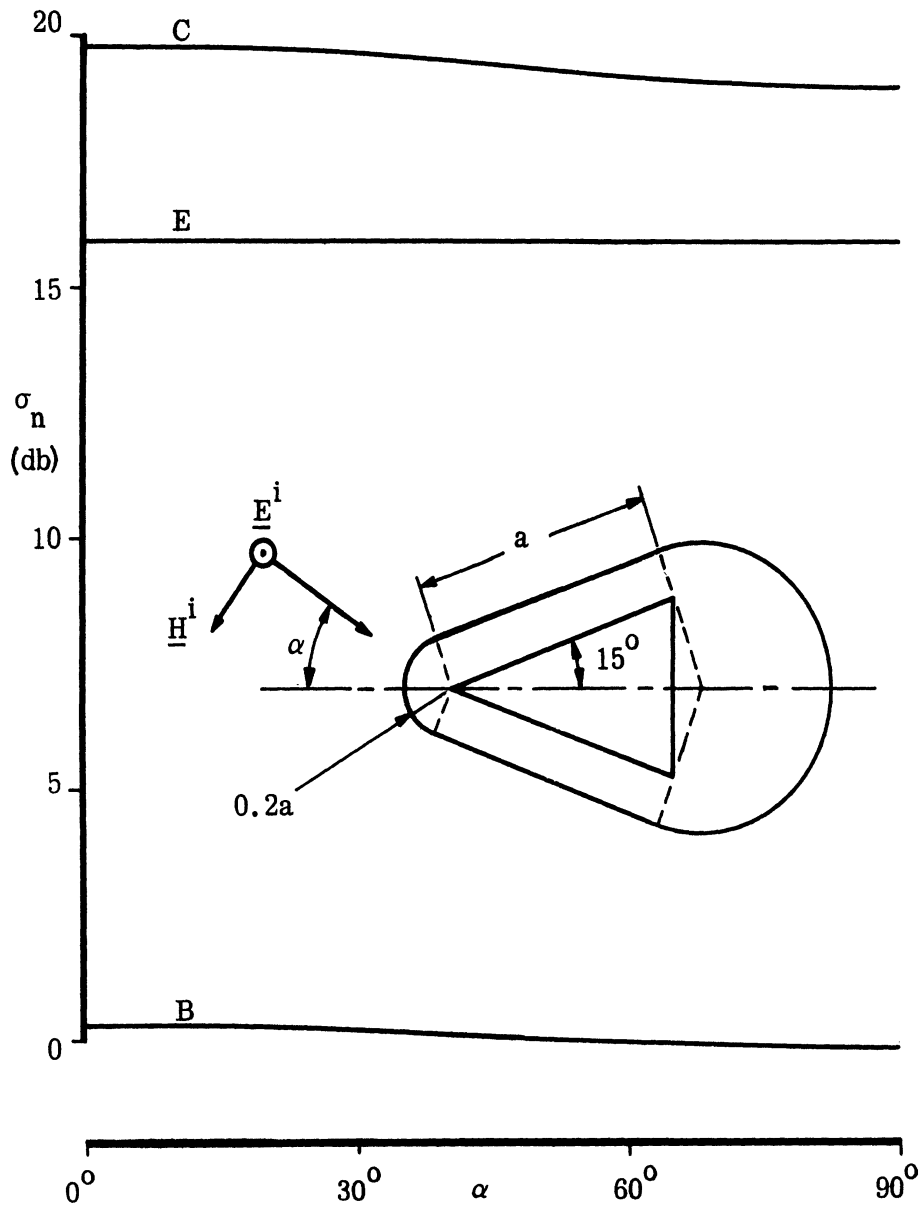


FIG. 5-4: Normalized Backscattering Cross Section in the H-Plane. B = Bare Flat-Base Cone, E = Plasma-Coated Cone, C = Conducting Sphere-Cone-Sphere.

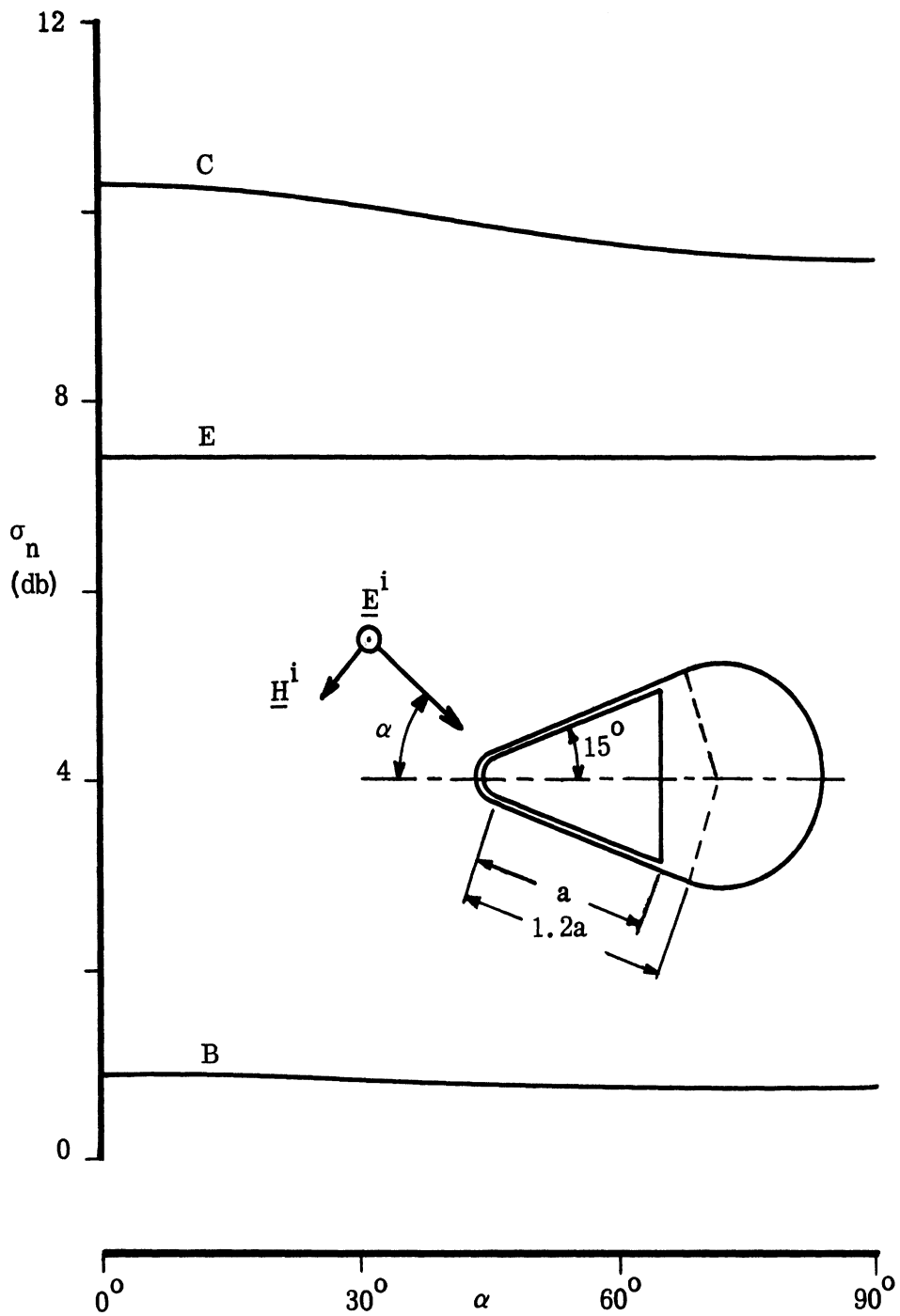


FIG. 5-5: Normalized Backscattering Cross Section in the H-Plane.  
 B = Bare Flat-Base Cone with Rounded Nose, E = Plasma-Coated Cone, C = Conducting Sphere-Cone-Sphere.

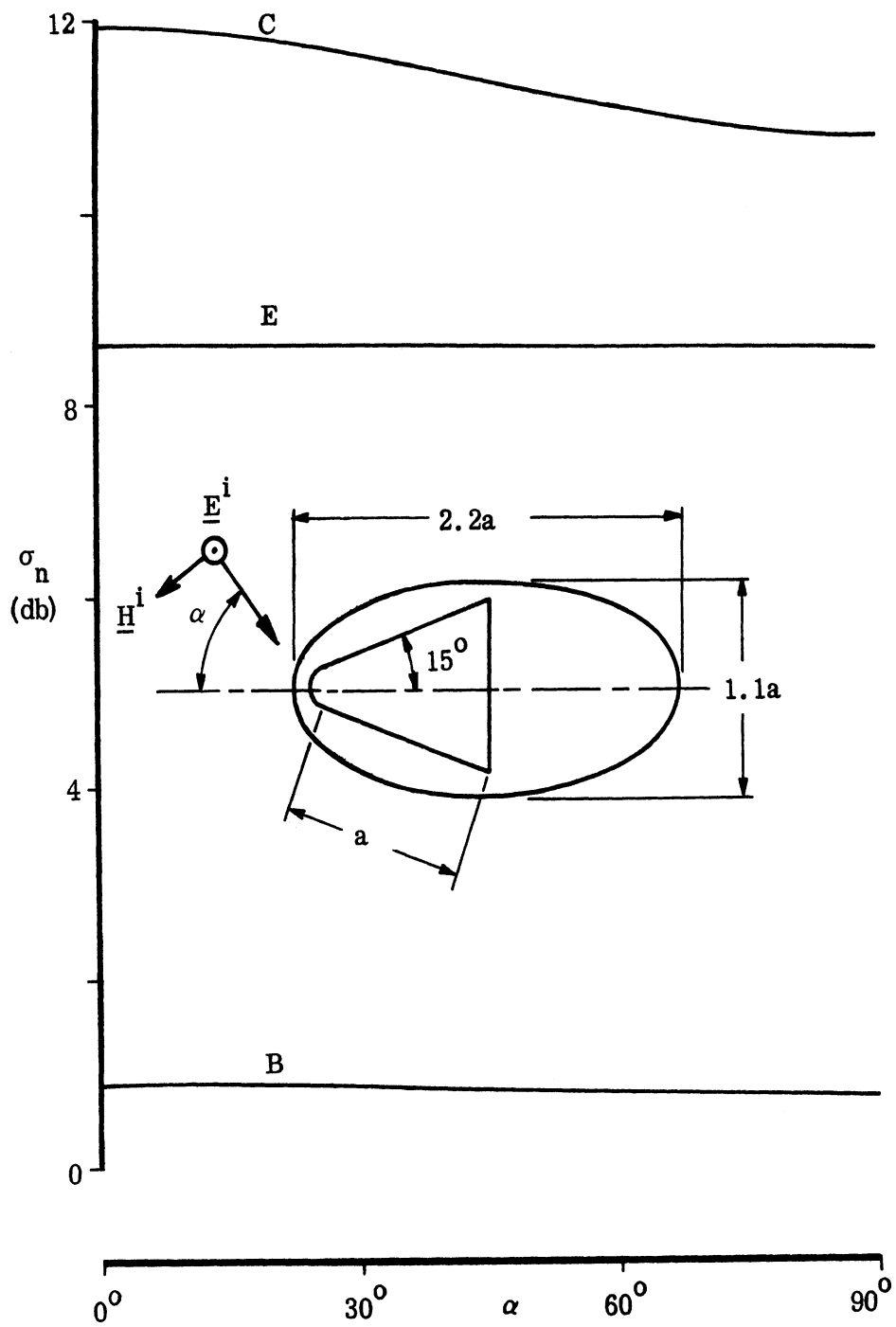


FIG. 5-6: Normalized Backscattering Cross Section in the H-Plane.  
 B = Bare Flat-Base Cone with Rounded Nose, E = Plasma-Coated Cone, C = Conducting Prolate Spheroid.

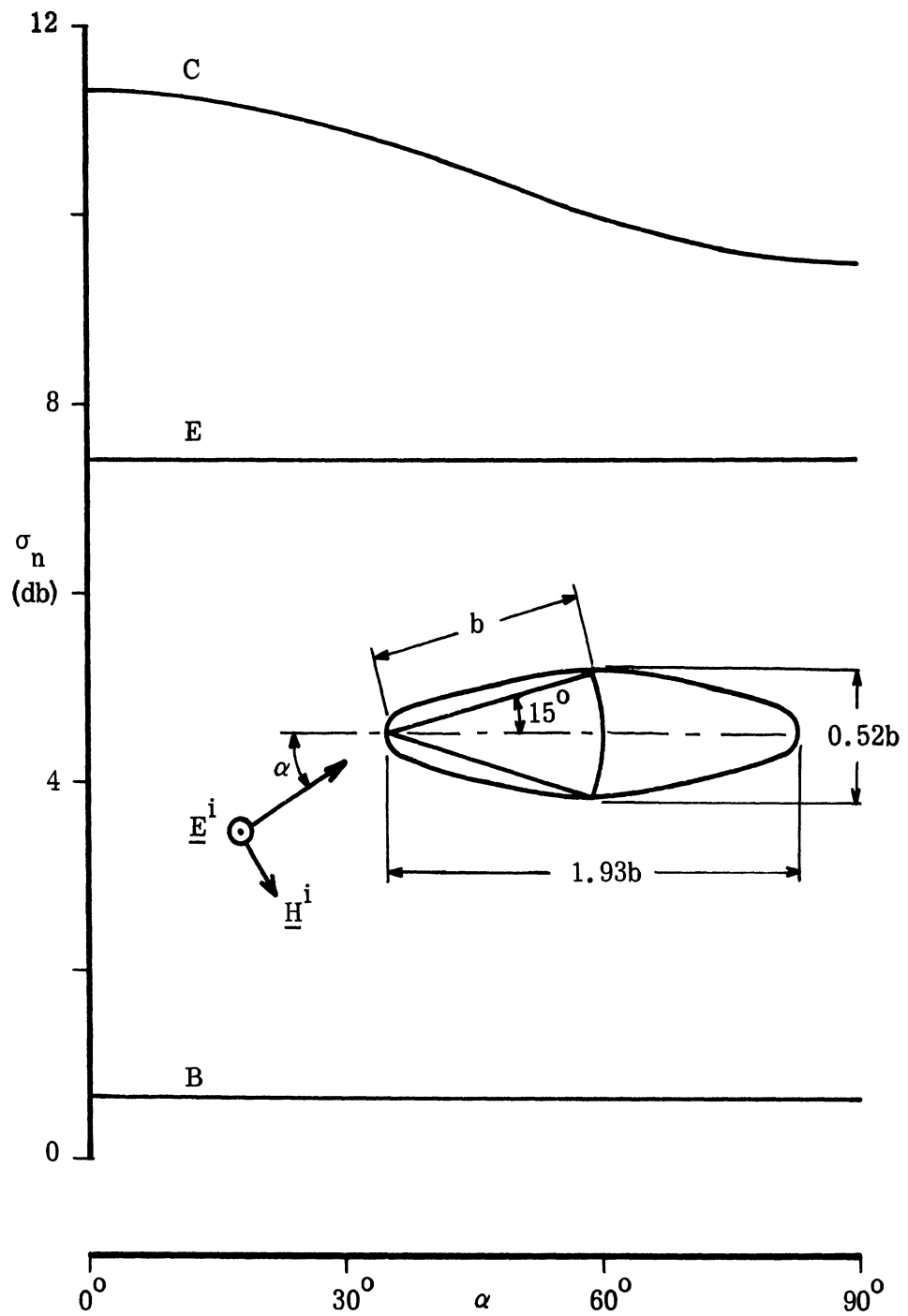


FIG. 5-7a: Normalized Backscattering Cross Section in the H-Plane. B = Bare Round-Backed Cone ( $\pi - \theta_0 = 15^\circ$ ), E = Plasma-Coated Cone, C = Conducting Prolate Spheroid.

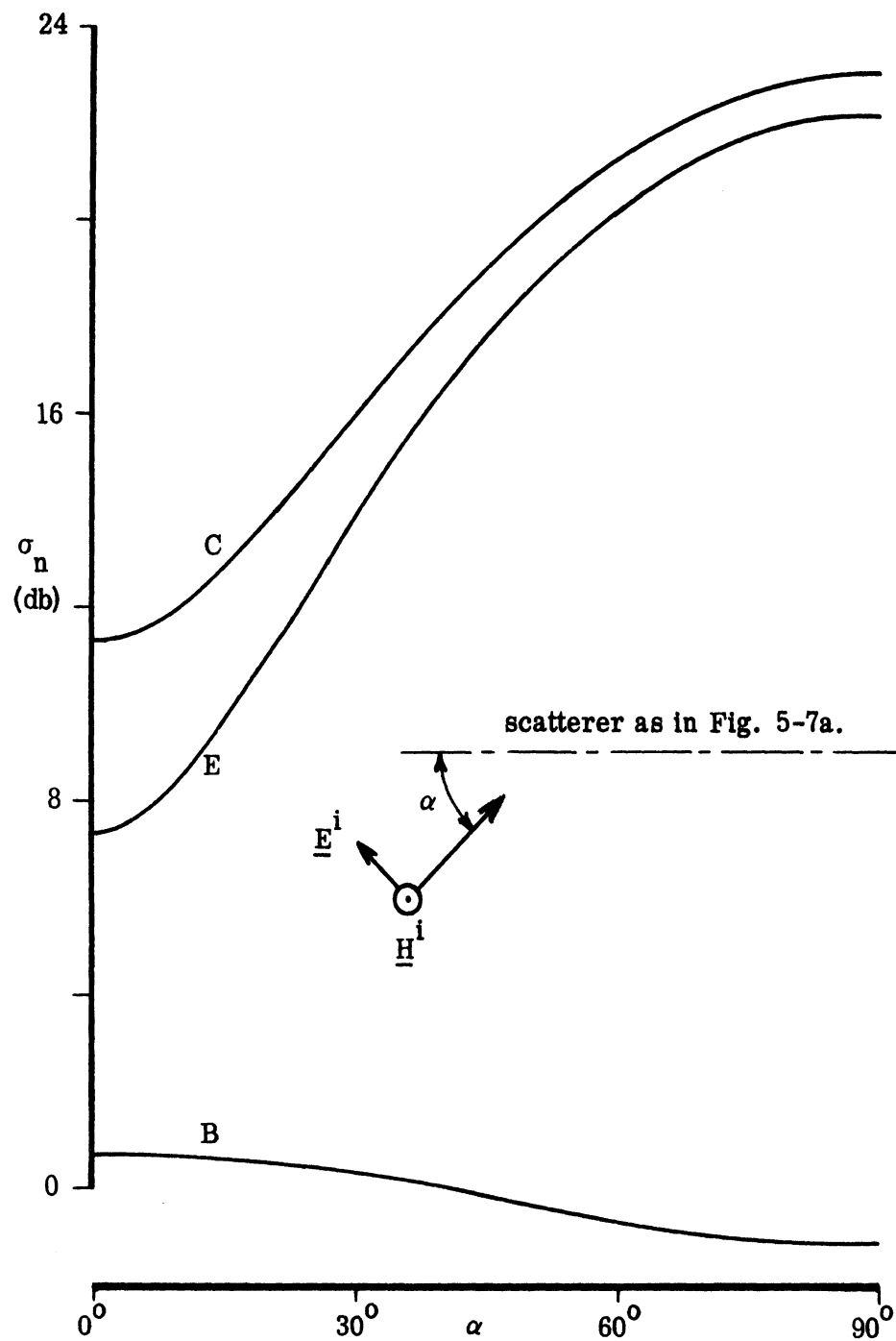


FIG. 5-7b: Normalized Backscattering Cross Section in the E-Plane. B = Bare Round-Backed Cone ( $\pi - \theta_0 = 15^\circ$ ), E = Plasma-Coated Cone, C = Conducting Prolate Spheroid.

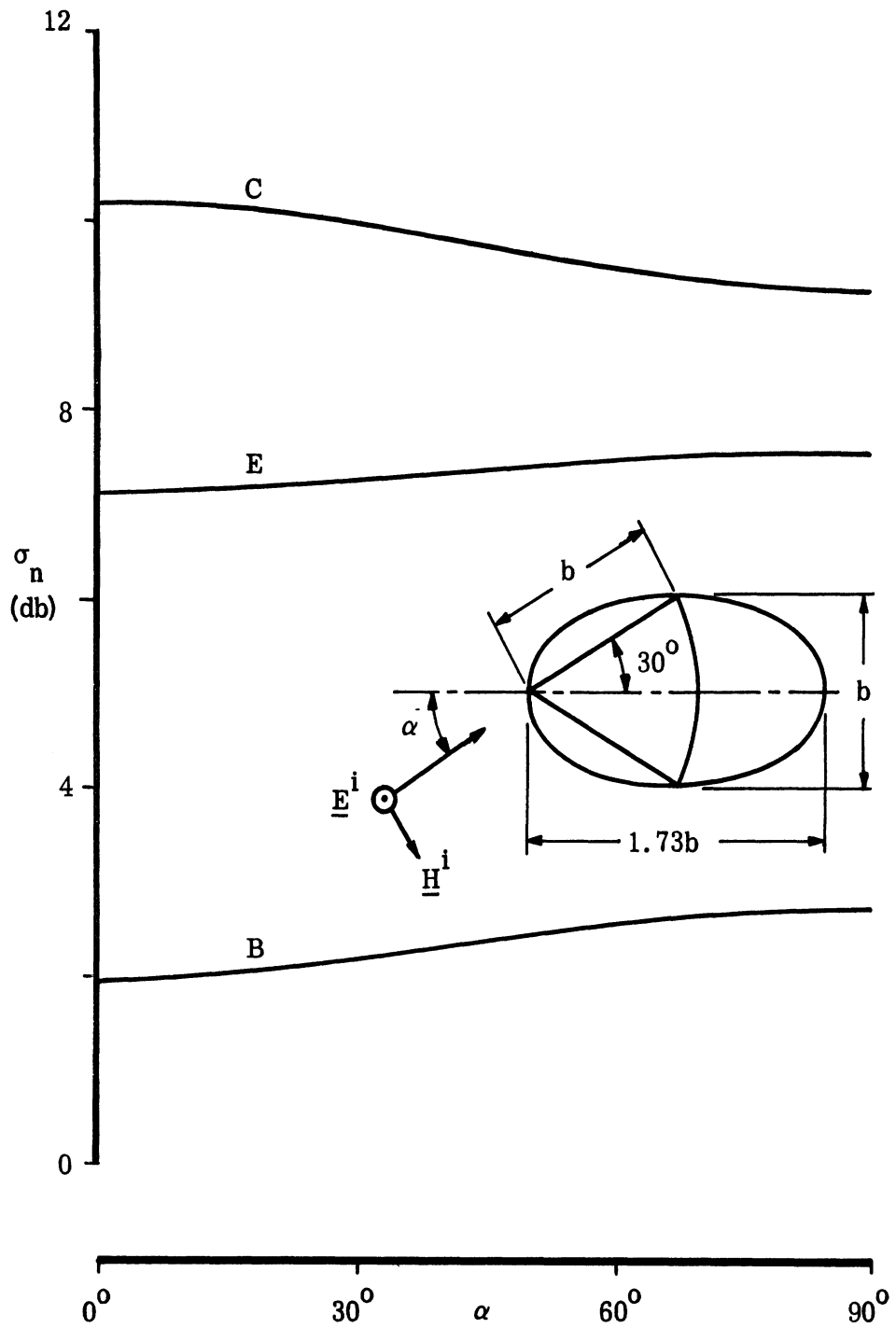


FIG. 5-8a: Normalized Backscattering Cross Section in the H-Plane. B = Bare Round-Backed Cone ( $\pi - \theta_0 = 30^\circ$ ), E = Plasma-Coated Cone, C = Conducting Prolate Spheroid.

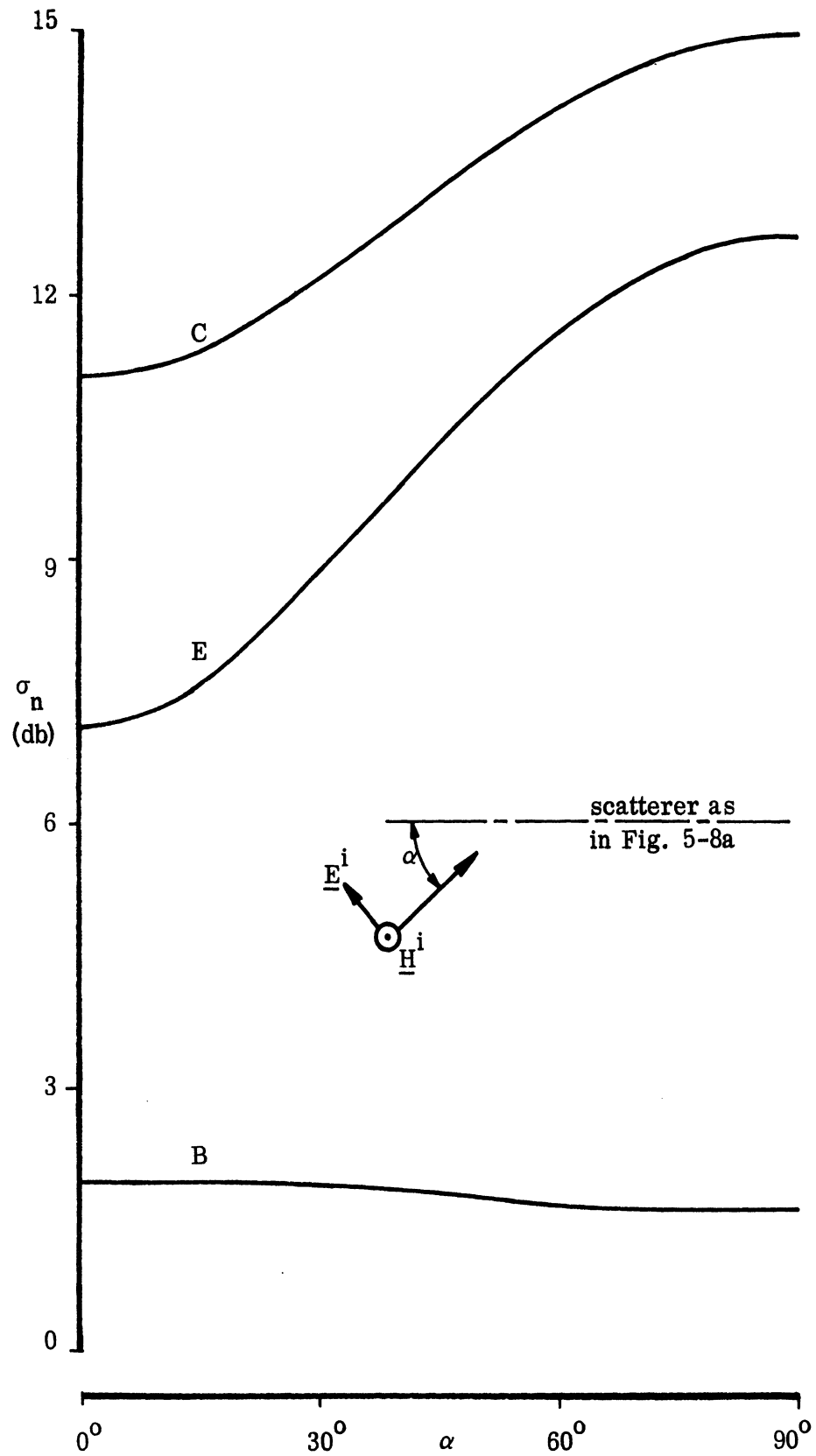


FIG. 5-8b: Normalized Backscattering Cross Section in the E-Plane. B = Bare Round-Backed Cone,  $(\pi - \theta_0 = 30^\circ)$ , E = Plasma-Coated Cone, C = Conducting Prolate Spheroid.



## CHAPTER VI

### CONCLUSIONS

#### 6.1 Summary of Results

The principal results which have herein been obtained in attempting to derive a reliable theoretical prediction for the radar cross section of a plasma coated, cone-like re-entry vehicle in the low frequency limit ( $k \rightarrow 0$ ) are listed in the following:

(1) The backscattered far field is a function of three electric dipole moment coefficients  $a_1^{(j)}$  and three magnetic dipole moment coefficients  $b_1^{(j)}$  ( $j = 1, 2, 3$ ), which are solely determined by the shape of the scatterer (assumed to be perfectly conducting). For a body of revolution about the z-axis, only the three coefficients  $a_1^{(1)} = a_1^{(2)} = -2b_1^{(3)}$ ,  $b_1^{(1)} = b_1^{(2)}$  and  $a_1^{(3)}$  are independent.

(2) A metallic body coated with a homogeneous isotropic plasma plasma sheath of collision frequency  $\nu_c$  has been considered. If  $\nu_c \gg \omega$ , the scattering phenomenon in the low-frequency limit has been reduced to two standard potential problems for perfect conductors. The  $b_1^{(j)}$ 's are those pertaining to the bare metal body (no plasma sheath), whereas the  $a_1^{(j)}$ 's are those that would obtain if the entire scatterer (vehicle plus plasma sheath) were metallic.

(3) All six coefficients  $a_1^{(j)}$  and  $b_1^{(j)}$  have been obtained for spheroids and round-backed cones. A computer program has been developed to calculate all coefficients except  $a_1^{(3)}$  for any body of revolution, and specific computations have been performed for flat-base cones and cone-spheres with either a sharp or a rounded nose. The computed coefficients are sufficient to determine the backscattering cross section in the entire H-plane.

(4) A variety of diagrams of the backscattering cross section for all angles of incidence and two different polarizations have been obtained, for a few shapes of the vehicle and of the outer surface of the plasma sheath. General conclusions drawn from these diagrams are to be found in section 5.4; here we only remark that our rigorous low-frequency analysis show that the predictions based on combining the results of Siegel (1959) and of Hiatt et al.(1960) can often be inaccurate.

(5) If  $\nu_c \ll \omega$ , and in particular if  $\nu_c = 0$  (lossless plasma), the scattering phenomenon has again been reduced to the solution of potential-type problems. However, the success of the method now depends on the existence of a continuous spectrum of non-trivial solutions for the boundary-value problem (3.13). The existence of such spectrum has been proven only in the case of a spherically symmetric scatterer.

During the above mentioned investigations, we have also obtained results which are of marginal interest to the main purpose of this report, but which have considerable importance per se and are therefore listed below:

a) It has been shown in section B.6 that the two hypotheses advanced by Siegel (1959) in deriving Eq. (2.1) are a consequence of the zeroth order approximation to the Neumann series solutions of two coupled integral equations for the components of the surface current. Unfortunately, the kernels of the equations are singular and therefore we do not know whether the Neumann series exist.

b) The new formula (4.37) for the low-frequency scattered far field  $\underline{E}^S$  has been derived. It expresses  $\underline{E}^S$  as the sum of three terms: the field that would be scattered by the

smallest sphere surrounding the body, plus two correction terms given by integrals over the volume exterior to the body but interior to the sphere.

c) A new integral equation, which generalizes a previous result by Barrar and Dolph, has been derived for the jump current at the surface of a thin overdense plasma sheath surrounding a conical metallic shell (see Appendix C).

## 6.2 Recommendations for Further Study

Further research along the general lines established in this report should, in our opinion, be based on the following points:

- (1) The existence of non-trivial solutions with a continuous spectrum for the boundary-value problem (3.13) ought to be proved in general, for all (sufficiently regular) shapes of the vehicle and of the plasma outer surface. Low-frequency cross sections, similar to the curves E plotted in Chapter V, should then be obtained for the case  $\nu_c \ll \omega$ .
- (2) The feasibility of low-frequency expansions which are uniformly valid for all values of  $\nu_c/\omega$  should be investigated. The results would be especially interesting when  $\nu_c \approx \omega$ , i. e. when the expansions for  $\nu_c \gg \omega$  or  $\nu_c \ll \omega$  cannot be used.
- (3) Extension of the previous results to the case of bistatic scattering. In particular, it may then be possible to prove that relation (4.5) is valid for all bodies of revolution, by invoking reciprocity relations.

(4) The results of this report as well as the suggestions of the above three points are based on the assumption that both the bare body and the plasma outer surface have characteristic dimensions which are small compared to the wavelength of the incident field. In practice, this is often true for the bare body but not for the plasma coating. We suggest two possible ways to overcome this difficulty: (i) determine the far field to higher orders (in particular, consider the contributions of the quadrupole moments); (ii) solve numerically the integral equation derived in Appendix C, and then obtain the far field by integration over the surface current.

Finally, we wish to emphasize two topics which are closely related to this research program and which could yield very interesting results:

- a) The possibility of using Neumann series solutions for the integral equations satisfied by the surface current components should be investigated (see point a) in section 6.1).
- b) The rigorous equation (4.37), previously mentioned at point b) of section 6.1, may lead to explicit low-frequency results for "fat" bodies, which would be analogous to Siegel's results for "thin" bodies.

## REFERENCES

- Ar, E. and R. E. Kleinman (1966), "The Exterior Neumann Problem for the Three-Dimensional Helmholtz Equation", *Arch. Rational Mech. Anal.* 23, 218-236.
- Asvestas, J. S. (1968), "Iterative Solutions of Maxwell's Equations", Radiation Laboratory Report No. 1363-2-T, (Contract No. F19628-68-C-0071), University of Michigan, Ann Arbor.
- Born, M. and E. Wolf (1959), Principles of Optics, Pergamon Press, New York
- Bowman, J. J., T. B. A. Senior and P. L. E. Uslenghi (1969), Electromagnetic and Acoustic Scattering by Simple Shapes, North-Holland Publishing Co., Amsterdam.
- Darling, D. A. (1960), "Some Relations Between Potential Theory and the Wave Equation", Radiation Laboratory Report No. 2871-5-T, University of Michigan, Ann Arbor.
- Darling, D. A. and T. B. A. Senior (1965), "Low Frequency Expansions for Scattering by Separable and Non-separable Bodies", *J. Acoust. Soc. Am.* 37, 228-234.
- Hiatt, R. E., K. M. Siegel and H. Weil (1960), "The Ineffectiveness of Absorbing Coatings on Conducting Objects Illuminated by Long Wavelength Radar", *Proc. IRE* 48, 1636-1642.
- Kleinman, R. E. (1965a), "The Rayleigh Region", *Proc. IEEE* 53, 848-856.
- Kleinman, R. E. (1965b), "The Dirichlet Problem for the Helmholtz Equation", *Arch. Rational Mech. Anal.* 18, 205-229.
- Kleinman, R. E. (1965c), "Low Frequency Solution of Electromagnetic Scattering Problems", presented at the URSI Symposium, Delft, The Netherlands; reprinted in: Electromagnetic Wave Theory, ed. J. Brown, 891-905, Pergamon Press, New York (1967).
- Kleinman, R. E. (1967), "Far-Field Scattering at Low Frequencies", *Appl. Sci. Res.* 18, 1-8.
- Noble, B. (1962), "Integral Equation Perturbation Methods in Low Frequency Diffraction", in: Electromagnetic Waves, ed. R. E. Langer, 323-360, The University of Wisconsin Press, Madison.

References, continued

- Senior, T. B. A. and E. F. Knott (1967), "Research on Resonant Region Radar Camouflage Techniques", Radiation Laboratory Report No. 8077-3-T, University of Michigan, Ann Arbor.
- Siegel, K. M. (1959), "Far Field Scattering from Bodies of Revolution", Appl. Sci. Res. B-7, 293-328.
- Siegel, K. M. (1963), "Low Frequency Radar Cross Section Computations", Proc. IEEE (Correspondence) 51, 232-233.
- Stevenson, A. F. (1953a), "Solution of Electromagnetic Scattering Problems as Power Series in the Ratio (Dimension of Scatterer)/Wavelength", J. Appl. Phys. 24, 1134-1142.
- Stevenson, A. F. (1953b), "Electromagnetic Scattering by an Ellipsoid in the Third Approximation", J. Appl. Phys. 24, 1143-1151.
- Strutt, J. W., Lord Rayleigh (1897), "On the Incidence of Aerial and Electric Waves upon Small Obstacles in the Form of Ellipsoids on Elliptic Cylinders, and on the Passage of Electric Waves through a Circular Aperture in a Conducting Screen," Phil. Mag. 44, 28-52.
- Twersky, V. (1964), "Rayleigh Scattering", Appl. Opt. 3, 1150-1162.
- Van Bladel, J. (1963), "Low Frequency Scattering by Cylindrical Bodies", Appl. Sci. Res. B10, 195-202.
- Van Bladel, J. (1964), Electromagnetic Fields, McGraw-Hill, New York, p. 287.
- Werner, P. (1963), "On the Exterior Boundary Value Problem of Perfect Reflection for Stationary Electromagnetic Wave Fields", J. Math. Anal. Appl. 7, 348-396.

## APPENDIX A

### DIPOLE MOMENTS FOR THE ROUND-BACKED CONE

#### A.1 Round-Backed Cone

The right circular cone backed by a spherical surface having center at the tip of the cone is the most convenient conical object for any analytical approach to the solution of the scattering problem. Schultz et al (1963, 1964) have used mode matching to produce a solution for an electromagnetic wave at axial incidence. The procedure leads to an infinite set of equations for the determination of the modal amplitudes, and hence, in principle, to the inversion of an infinite matrix. In practice the matrix must be truncated and because of the limited number of Legendre function zeros available and the maximum size of matrix that can be inverted, the numerical results obtained appear accurate only for  $kD \lesssim 4$ , where  $D$  is the base diameter of the cone. At low frequencies, however, the approach is certainly an effective one, and if attention is confined to the leading (Rayleigh) term in the low frequency expansion, the fact that the problem can be reduced to a potential problem provides a further simplification. We shall therefore seek the determination of the electric and magnetic dipole contributions using the simplified version of the above mode matching techniques that is appropriate to Rayleigh scattering, and do so not only for axial incidence on a  $15^\circ$  half-angle cone (as Schultz et al considered), but for all angles of incidence and a variety of cone angles.

As shown in Fig. A-1, the surface of the body is the intersection of a cone of (interior) half angle  $\pi - \theta_0$  with a sphere of radius  $d$  centered at the apex of the cone. The body is assumed perfectly conducting and in terms of the spherical polar coordinates  $(r, \theta, \phi)$  the boundary conditions on the total electric and magnetic fields at the surface are:

$$\begin{aligned} \hat{r} \cdot \underline{E} = \hat{\phi} \cdot \underline{E} = \hat{\theta} \cdot \underline{H} = 0 & \quad \text{for } \theta = \theta_0, 0 \leq r \leq d, 0 \leq \phi < 2\pi, \\ \hat{\theta} \cdot \underline{E} = \hat{\phi} \cdot \underline{E} = \hat{r} \cdot \underline{H} = 0 & \quad \text{for } r = d, \pi - \theta_0 \leq \theta \leq \pi, 0 \leq \phi < 2\pi. \end{aligned} \tag{A.1}$$

Although the conditions on the electric and magnetic fields are not, of course, independent, the decoupling of the fields that takes place at zero frequency makes it convenient to specify the conditions on  $\underline{H}$  as well as on  $\underline{E}$ .

In accordance with the procedure adopted in Section 4.3, we take the incident field to be a plane wave of arbitrary polarization incident in an arbitrary direction on the body, viz.

$$\begin{aligned}\underline{E}^i &= (\ell_1 \hat{x} + m_1 \hat{y} + n_1 \hat{z}) e^{ik(\ell x + my + nz)} \\ \underline{H}^i &= Y(\ell_2 \hat{x} + m_2 \hat{y} + n_2 \hat{z}) e^{ik(\ell x + my + nz)}\end{aligned}\tag{A.2}$$

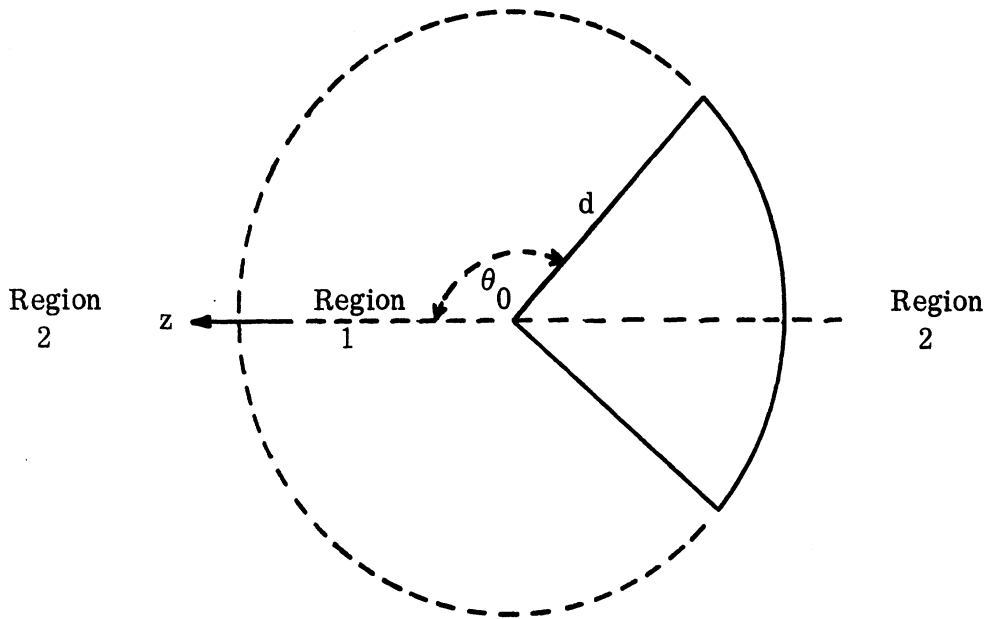


FIG. A-1: CONE GEOMETRY



where  $(x, y, z)$  is a rectangular Cartesian coordinate system such that

$$x = r \sin \theta \cos \phi, \quad y = r \sin \theta \sin \phi, \quad z = r \cos \theta,$$

and  $(\ell, m, n)$ ,  $(\ell_1, m_1, n_1)$  and  $(\ell_2, m_2, n_2)$  are sets of direction cosines for which

$$(\ell_1, m_1, n_1) = (\ell_2, m_2, n_2) \wedge (\ell, m, n),$$

$$(\ell_2, m_2, n_2) = (\ell, m, n) \wedge (\ell_1, m_1, n_1) .$$

$Y$  is the intrinsic admittance of free space and a time factor  $e^{-i\omega t}$  has been suppressed. To the first order at low frequencies

$$\underline{E}_0^i \sim \underline{E}_0^i = \ell_1 \hat{x} + m_1 \hat{y} + n_1 z$$

which can be written as

$$\underline{E}_0^i = \nabla (\ell_1 r \sin \theta \cos \phi + m_1 r \sin \theta \sin \phi + n_1 r \cos \theta). \quad (\text{A. 3})$$

Since this is independent of the direction cosines  $(\ell, m, n)$  and  $(\ell_2, m_2, n_2)$ ,  $\ell_1, m_1,$  and  $n_1$  can be chosen independently of one another. It follows that for the corresponding scattered electric vector we can write

$$\underline{E}_0^s = \nabla \Phi^s \quad (\text{A. 4})$$

with

$$\Phi^s = \sum_{n=1}^{\infty} r^{-n-1} \left\{ \ell_1 a_n^{(1)} P_n^1(\cos \theta) \cos \phi + m_1 a_n^{(2)} P_n^1(\cos \theta) \sin \phi + n_1 a_n^{(3)} P_n^0(\cos \theta) \right\}, \quad (\text{A. 5})$$

valid for  $r \geq d$ . The coefficients  $a_n^{(1)}$ ,  $a_n^{(2)}$  and  $a_n^{(3)}$  are independent of  $\ell_1, m_1,$  and  $n_1$ , and in general their determination requires the solution of three separate potential problems. For the particular case of a body of revolution, however, it has been pointed out earlier (and is at once evident

from Eqs. (A.3) through (A.5)) that  $a_n^{(2)} = a_n^{(1)}$ , which reduces the number of potential problems to two. In terms of the  $a_n^{(j)}$  the electric dipole moment is

$$\underline{P} = -4\pi\epsilon (\ell_1 a_1^{(1)} \hat{x} + m_1 a_1^{(2)} \hat{y} + n_1 a_1^{(3)} \hat{z}). \quad (\text{A.6})$$

Similarly for the magnetic field we have

$$\underline{H}^i \sim \underline{H}_0^i = Y \nabla (\ell_2 r \sin \theta \cos \phi + m_2 r \sin \theta \sin \phi + n_2 r \cos \theta) \quad (\text{A.7})$$

and the corresponding scattered magnetic field is

$$\underline{H}_0^s = Y \nabla \underline{\psi}^s \quad (\text{A.8})$$

with

$$\underline{\psi}^s = \sum_{n=1}^{\infty} r^{-n-1} \left\{ \ell_2 b_n^{(1)} P_n^{(1)}(\cos \theta) \cos \phi + n_2 b_n^{(2)} P_n^1(\cos \theta) \sin \phi + n_2 b_n^{(3)} P_n^0(\cos \theta) \right\}, \quad (\text{A.9})$$

valid for  $r > d$ . Here again there are in general three potential problems that must be solved to find the  $b_n^{(j)}$ , reducing to two for an axially symmetric body for which  $b_n^{(2)} = b_n^{(1)}$ . In terms of the  $b_n^{(j)}$  the magnetic dipole moment is

$$\underline{M} = -4\pi Y (\ell_2 b_1^{(1)} \hat{x} + m_2 b_1^{(2)} \hat{y} + n_2 b_1^{(3)} \hat{z}). \quad (\text{A.10})$$

We are now faced with four distinct potential problems that must be solved to compute the dipole moment coefficients  $a_1^{(1)} = a_1^{(2)}$ ,  $a_1^{(3)}$ ,  $b_1^{(1)} = b_1^{(2)}$  and  $b_1^{(3)}$  for the round-backed cone, and we shall treat these separately. Once these have been found, the scattered field at low frequencies can be determined from Eqs. (2.10) and (2.11) by inserting the expressions for  $\underline{P}$  and  $\underline{M}$ .

## A.2 Transverse Electric Dipole Moment

Consistent with Eq. (A.3) we here postulate an incident electric potential

$$\bar{\Phi}^i = r \sin \theta \cos \phi \quad (\text{A.11})$$

and assume that in region 2 (see Fig. A-1)

$$\bar{\Phi}^s = \sum_{n=1}^{\infty} r^{-n-1} a_n^{(1)} P_n^1(\cos \theta) \cos \phi \quad (\text{A.12})$$

The total potential in 2 is therefore

$$\bar{\Phi}_2 = \bar{\Phi}^i + \bar{\Phi}^s = \sum_{n=1}^{\infty} (r^{-n-1} a_n^{(1)} + r \delta_{1n}) P_n^1(\cos \theta) \cos \phi \quad (\text{A.13})$$

where  $\delta_{\alpha\beta}$  is the Kronecher delta (=1 if  $\alpha = \beta$ , 0 if  $\alpha \neq \beta$ ), but in region 1 we take the total potential to be

$$\bar{\Phi}_1 = \sum_{\nu} C_{\nu} r^{\nu} P_{\nu}^1(\cos \theta) \cos \phi \quad (\text{A.14})$$

For the Eqs. (A.1), the boundary conditions on the total potentials are

$$\frac{\partial \bar{\Phi}_1}{\partial r} = \frac{\partial \bar{\Phi}_2}{\partial r} = 0 \quad \text{for } \theta = \theta_0, \text{ all } \phi$$

$$\begin{aligned} \frac{\partial \bar{\Phi}_2}{\partial \phi} &= \frac{\partial \bar{\Phi}_1}{\partial \phi} && \text{for } r = d, 0 \leq \theta < \theta_0, \text{ all } \phi \\ &= 0 && \text{for } r = d, \theta_0 < \theta \leq \pi, \text{ all } \phi \end{aligned}$$

$$\begin{aligned} \frac{\partial \bar{\Phi}_2}{\partial \theta} &= \frac{\partial \bar{\Phi}_1}{\partial \theta} && \text{for } r = d, 0 \leq \theta < \theta_0, \text{ all } \phi \\ &= 0 && \text{for } r = d, \theta_0 < \theta \leq \pi, \text{ all } \phi \end{aligned}$$

$$\frac{\partial \Phi_2}{\partial r} = \frac{\partial \Phi_1}{\partial r} \quad \text{for } r = d, \quad 0 \leq \theta < \theta_0, \quad \text{all } \phi.$$

The first of these can be satisfied by choosing  $\nu$  such that

$$P_\nu^1(\cos \theta_0) = 0, \quad (\text{A.15})$$

with the summation extending over the zeros  $\nu = \nu_i$ ,  $i = 1, 2, 3, \dots$ , of the Legendre function of order unity. From the second and third boundary conditions, we obtain

$$\begin{aligned} \sum_{n=1}^{\infty} \left( d^{-n-1} a_n^{(1)} + d \delta_{1n} \right) P_n^1(\cos \theta) &= \sum_{\nu} c_{\nu} d^{\nu} P_{\nu}^1(\cos \theta), & 0 \leq \theta < \theta_0 \\ &= 0, & \theta_0 < \theta \leq \pi \end{aligned} \quad (\text{A.16})$$

and

$$\begin{aligned} \sum_{n=1}^{\infty} \left( d^{-n-1} a_n^{(1)} + d \delta_{1n} \right) \frac{\partial}{\partial \theta} P_n^1(\cos \theta) &= \sum_{\nu} c_{\nu} d^{\nu} \frac{\partial}{\partial \theta} P_{\nu}^1(\cos \theta), & 0 \leq \theta < \theta_0 \\ &= 0, & \theta_0 < \theta \leq \pi. \end{aligned} \quad (\text{A.17})$$

If Eq. (A.16) is multiplied by  $\frac{P_m^1(\cos \theta)}{\sin \theta}$ , Eq. (A.17) by  $\sin \theta \frac{\partial}{\partial \theta} P_m^1(\cos \theta)$ ,

and the results added, integration with respect to  $\theta$  from 0 to  $\pi$  gives

$$\frac{2m^2(m+1)^2}{2m+1} \left( d^{-m-1} a_m^{(1)} + d \delta_{1m} \right) = \sum_{\nu} c_{\nu} d^{\nu} \int_0^{\theta_0} \left( \sin \theta \frac{\partial P_{\nu}^1}{\partial \theta} \frac{\partial P_m^1}{\partial \theta} + \frac{P_{\nu}^1 P_m^1}{\sin \theta} \right) d\theta$$

from which we have

$$d^{-m-1} a_m^{(1)} + d \delta_{1m} = \frac{2m+1}{2m(m+1)} \sum_{\nu} c_{\nu} d^{\nu} X_{m\nu} \quad (\text{A.18})$$

where

$$X_{m\nu} = \frac{1}{m(m+1)} \int_0^{\theta_0} \left( \sin \theta \frac{\partial P_{\nu}^1}{\partial \theta} \frac{\partial P_m^1}{\partial \theta} + \frac{P_{\nu}^1 P_m^1}{\sin \theta} \right) d\theta . \quad (\text{A.19})$$

The fourth and last boundary condition yields

$$\sum_{n=1}^{\infty} (n+1) \left( d^{-n-2} a_n^{(1)} - \frac{1}{2} \delta_{1n} \right) P_n^1(\cos \theta) = - \sum_{\nu} \nu c_{\nu} d^{\nu-1} P_{\nu}^1(\cos \theta), \quad 0 \leq \theta < \theta_0 \quad (\text{A.20})$$

from which a further relation between the  $a_n^{(1)}$  and  $c_{\nu}$  can be found by invoking the orthogonality of the functions  $(\sin \theta)^{1/2} P_{\nu}^1(\cos \theta)$  over the range  $0 \leq \theta \leq \theta_0$ . If  $\alpha$  is any one of the zeros  $\nu_i$ , multiplication of Eq. (A.20) by  $\sin \theta P_{\alpha}^1(\cos \theta)$  and integration with respect to  $\theta$  from 0 to  $\theta_0$  gives

$$c_{\alpha} d^{\alpha} \Lambda_{\alpha} = - \sum_{n=1}^{\infty} (n+1) \left( d^{-n-1} a_n^{(1)} - \frac{1}{2} d \delta_{1n} \right) \int_0^{\theta_0} \sin \theta P_{\alpha}^1 P_n^1 d\theta$$

where

$$\Lambda_{\alpha} = \int_0^{\theta_0} \sin \theta \left( P_{\alpha}^1 \right)^2 d\theta . \quad (\text{A.21})$$

But

$$\int_0^{\theta_0} \sin \theta P_{\alpha}^1 P_n^1 d\theta = X_{n\alpha}$$

(see Eq. (A.71)), and hence

$$c_{\nu} d^{\nu} = - \frac{1}{\nu \Lambda_{\nu}} \sum_{n=1}^{\infty} (n+1) \left( d^{-n-1} a_n^{(1)} - \frac{1}{2} d \delta_{1n} \right) X_{n\nu} . \quad (\text{A.22})$$

If we now eliminate the coefficients  $c_\nu$  from Eqs. (A.18) and (A.22), we have

$$d^{-m-1} a_m^{(1)} + d \delta_{1m} = -\frac{2m+1}{2m(m+1)} \sum_{n=1}^{\infty} \sum_{\nu} (n+1) \left( d^{-n-1} a_n^{(1)} - \frac{1}{2} d \delta_{1n} \right) \frac{X_{m\nu} X_{n\nu}}{\nu \Lambda_\nu},$$

$m = 1, 2, 3, \dots$ , which can be written somewhat more compactly as

$$m A_m^{(1)} + \delta_{1m} = - \sum_{n=1}^{\infty} \left( n + \frac{1}{2} \right) A_n^{(1)} \sum_{\nu} \frac{X_{m\nu} X_{n\nu}}{\nu \Lambda_\nu} \quad (\text{A.23})$$

$m = 1, 2, 3, \dots$ , where

$$A_m^{(1)} = \frac{m+1}{2m+1} \left( d^{-m-2} a_m^{(1)} - \frac{1}{2} \delta_{1m} \right). \quad (\text{A.24})$$

The Eqs. (A.23) constitute an infinite set of simultaneous equations for the determination of the coefficients  $A_m^{(1)}$ . The particular coefficient of interest is  $A_1^{(1)}$  from which we have

$$a_1^{(1)} = \frac{d^3}{2} \left( 3A_1^{(1)} + 1 \right). \quad (\text{A.25})$$

### A.3 Transverse Magnetic Dipole Moment

The procedure is quite similar to that described above. The incident magnetic potential is now

$$\psi^i = r \sin \theta \cos \phi \quad (\text{A.26})$$

and in region 2 we therefore take the total magnetic potential to be

$$\psi_2 = \sum_{n=1}^{\infty} \left( r^{-n-1} b_n^{(1)} + r \delta_{1n} \right) P_n^1(\cos \theta) \cos \phi, \quad (\text{A.27})$$

whereas in region 1, the potential is

$$\psi_1 = \sum_{\mu} c_{\mu} r^{\mu} P_{\mu}^1(\cos \theta) \cos \phi. \quad (\text{A.28})$$

From the Eqs. (A.1), the boundary conditions on the total potentials are

$$\begin{aligned}
\frac{\partial \psi_1}{\partial \theta} &= 0 && \text{for } \theta = \theta_0, \text{ all } \phi \\
\frac{\partial \psi_2}{\partial r} &= \frac{\partial \psi_1}{\partial r} && \text{for } r = d, 0 \leq \theta < \theta_0, \text{ all } \phi \\
&= 0 && \text{for } r = d, \theta_0 < \theta \leq \pi, \text{ all } \phi \\
\frac{\partial \psi_2}{\partial \theta} &= \frac{\partial \psi_1}{\partial \theta} && \text{for } r = d, 0 \leq \theta < \theta_0, \text{ all } \phi \\
\frac{\partial \psi_2}{\partial \phi} &= \frac{\partial \psi_1}{\partial \phi} && \text{for } r = d, 0 \leq \theta < \theta_0, \text{ all } \phi .
\end{aligned}$$

The first of these is satisfied by choosing  $\mu$  such that

$$\left. \frac{\partial}{\partial \theta} P_{\mu}^1(\cos \theta) \right|_{\theta = \theta_0} = 0 \tag{A.29}$$

in which case the summation now extends over the zeros  $\mu = \mu_i$ ,  $i = 1, 2, 3, \dots$ , of the first derivative of the Legendre function of order unity. From the second boundary condition we have

$$\begin{aligned}
\sum_{n=1}^{\infty} (n+1) \left( d^{-n-2} b_n^{(1)} - \frac{1}{2} \delta_{1n} \right) P_n^1(\cos \theta) &= - \sum_{\mu} c_{\mu} d^{\mu-1} P_{\mu}^1(\cos \theta), 0 \leq \theta < \theta_0 \\
&= 0 && , \theta_0 < \theta \leq \pi
\end{aligned} \tag{A.30}$$

from which we obtain

$$d^{-m-1} b_m^{(1)} - \frac{1}{2} d \delta_{1m} = \frac{2}{2m(m+1)} \sum_{\mu} c_{\mu} d^{\mu} Y_{m\mu} \tag{A.31}$$

where

$$Y_{m\mu} = -\frac{\mu}{m+1} \int_0^{\theta_0} \sin \theta P_\mu^1 P_m^1 d\theta ; \quad (\text{A.32})$$

and from the third and fourth boundary conditions,

$$\sum_{n=1}^{\infty} \left( d^{-n-1} b_n^{(1)} + d\delta_{1n} \right) \frac{\partial}{\partial \theta} P_n^1(\cos \theta) = \sum_{\mu} c_{\mu} d^{\mu} \frac{\partial}{\partial \theta} P_{\mu}^1(\cos \theta), \quad 0 \leq \theta < \theta_0 \quad (\text{A.33})$$

$$\sum_{n=1}^{\infty} \left( d^{-n-1} b_n^{(1)} + d\delta_{1n} \right) P_n^1(\cos \theta) = \sum_{\mu} c_{\mu} d^{\mu} P_{\mu}^1(\cos \theta), \quad 0 \leq \theta < \theta_0 \quad (\text{A.34})$$

yielding

$$\beta(\beta+1) c_{\beta} d^{\beta} \Lambda_{\beta} = \sum_{n=1}^{\infty} \left( d^{-n-1} b_n^{(1)} + d\delta_{1n} \right) \int_0^{\theta_0} \left( \sin \theta \frac{\partial P_{\beta}^1}{\partial \theta} \frac{\partial P_n^1}{\partial \theta} + \frac{P_{\beta}^1 P_n^1}{\sin \theta} \right) d\theta$$

where  $\Lambda_{\beta}$  has the form shown in Eq. (A.21) and  $\beta$  is any one of the zeros  $\mu_i$ .

But

$$\int_0^{\theta_0} \left( \sin \theta \frac{\partial P_{\beta}^1}{\partial \theta} \frac{\partial P_n^1}{\partial \theta} + \frac{P_{\beta}^1 P_n^1}{\sin \theta} \right) d\theta = -(n+1)(\beta+1) Y_{n\beta} ; \quad (\text{A.35})$$

hence

$$c_{\mu} d^{\mu} = -\frac{1}{\mu \Lambda_{\mu}} \sum_{n=1}^{\infty} (n+1) \left( d^{-n-1} b_n^{(1)} + d\delta_{1n} \right) Y_{n\mu}, \quad (\text{A.36})$$

and by eliminating the coefficients  $c_{\mu}$  from Eqs. (A.31) and (A.36), we obtain



$$d^{-m-1} b_m^{(1)} - \frac{1}{2} d \delta_{1m} = - \frac{2m+1}{2m(m+1)} \sum_{n=1}^{\infty} \sum_{\mu} (n+1) \left( d^{-n-1} b_n^{(1)} + d \delta_{1n} \right) \frac{Y_{m\mu} Y_{n\mu}}{\mu \Lambda_{\mu}} \quad (\text{A. 37})$$

$m = 1, 2, 3, \dots$  If we now write

$$B_m^{(1)} = - \frac{m+1}{2m+1} \left( d^{-m-2} b_m^{(1)} + \delta_{1m} \right), \quad (\text{a. 38})$$

Eq. (A. 37) reduces to

$$m B_m^{(1)} + \delta_{1m} = - \sum_{n=1}^{\infty} \left( n + \frac{1}{2} \right) B_n^{(1)} \sum_{\mu} \frac{Y_{m\mu} Y_{n\mu}}{\mu \Lambda_{\mu}}, \quad (\text{A. 39})$$

$m = 1, 2, 3, \dots$ , the form of which is identical to that of Eq. (A. 23) for the coefficients  $A_m^{(1)}$ . The coefficient of interest is again the first one,  $B_1^{(1)}$ , in terms of which

$$b_1^{(1)} = - \frac{d^3}{2} \left( 3B_1^{(1)} + 2 \right), \quad (\text{A. 40})$$

cf Eq. (A. 25).

#### A. 4 Axial Magnetic Dipole Moment

It is convenient to treat this moment next because of the similarity of the analysis to that for the transverse electric case. For the incident magnetic potential we assume

$$\psi^i = r \cos \theta \quad (\text{A. 41})$$

and then write the total magnetic potential in region 2 as

$$\psi_2 = \sum_{n=1}^{\infty} \left( r^{-n-1} b_n^{(3)} + r \delta_{1n} \right) P_n^0(\cos \theta), \quad (\text{A. 42})$$

whereas in region 1,

$$\psi_1 = \sum_{\nu} c_{\nu} r^{\nu} P_{\nu}^0(\cos \theta). \quad (\text{A. 43})$$

We observe that there is no  $\phi$  dependence.

From the Eqs.(A. 1), the boundary conditions on the total potentials are

$$\begin{aligned} \frac{\partial \psi_1}{\partial \theta} &= 0 && \text{for } \theta = \theta_0, \\ \frac{\partial \psi_2}{\partial r} &= \frac{\partial \psi_1}{\partial r} && \text{for } r = d, \quad 0 \leq \theta < \theta_0, \\ &= 0 && \text{for } r = d, \quad \theta_0 < \theta \leq \pi, \\ \frac{\partial \psi_2}{\partial \theta} &= \frac{\partial \psi_1}{\partial \theta} && \text{for } r = d, \quad 0 \leq \theta < \theta_0. \end{aligned}$$

The first of these is satisfied if the  $\nu = \nu_i$ ,  $i = 1, 2, 3, \dots$ , are such that

$$\left. \frac{\partial}{\partial \theta} P_{\nu}^0(\cos \theta) \right|_{\theta = \theta_0} = 0, \quad (\text{A. 44})$$

and since

$$\frac{\partial}{\partial \theta} P_{\nu}^0(\cos \theta) \equiv -P_{\nu}^1(\cos \theta),$$

it follows that the  $\nu_i$  are identical to the zeros of the Legendre function of order unity that were employed in the analysis for the transverse electric dipole moment. From the second boundary condition we have,

$$\sum_{n=1}^{\infty} (n+1) \left( d^{-n-2} b_n^{(3)} - \frac{1}{2} \delta_{1n} \right) P_n^0(\cos \theta) = - \sum_{\nu} c_{\nu} d^{\nu-1} P_{\nu}^0(\cos \theta), \quad 0 \leq \theta < \theta_0$$

$$= 0 \quad \theta_0 < \theta \leq \pi$$

(A. 45)

from which we obtain

$$d^{-m-1} b_m^{(3)} - \frac{1}{2} d \delta_{1m} = - \frac{2m+1}{2(m+1)} \sum_{\nu} c_{\nu} d^{\nu} \frac{X_{m\nu}}{\nu+1} \quad (\text{A. 46})$$

where

$$X_{m\nu} = \nu(\nu+1) \int_0^{\theta_0} \sin \theta P_{\nu}^0 P_m^0 d\theta \quad (\text{A. 47})$$

which can be shown identical to the function defined in Eq. (A. 19). A further relation between the  $b_n^{(3)}$  and  $c_{\nu}$  is provided by the last boundary condition, which gives

$$\sum_{n=1}^{\infty} \left( d^{-n-1} b_n^{(3)} + d \delta_{1n} \right) \frac{\partial}{\partial \theta} P_n^0(\cos \theta) = \sum_{\nu} c_{\nu} d^{\nu} \frac{\partial}{\partial \theta} P_{\nu}^0(\cos \theta), \quad 0 \leq \theta < \theta_0.$$

Hence

$$c_{\alpha} d^{\alpha} \Lambda_{\alpha} = \sum_{n=1}^{\infty} \left( d^{-n-1} b_n^{(3)} + d \delta_{1n} \right) \int_0^{\theta_0} \sin \theta \frac{\partial P_{\beta}^0}{\partial \theta} \frac{\partial P_n^0}{\partial \theta} d\theta$$

where  $\alpha$  is any one of the set of zeros  $\nu_i$ ,  $i = 1, 2, 3, \dots$ , and

$$\Lambda_\alpha = \int_0^{\theta_0} \sin \theta \left( \frac{\partial P_\alpha^0}{\partial \theta} \right)^2 d\theta$$

is the quantity defined in Eq. (A.21). But

$$\int_0^{\theta_0} \sin \theta \frac{\partial P_\alpha^0}{\partial \theta} \frac{\partial P_n^0}{\partial \theta} d\theta = X_{n\alpha} ,$$

where  $X_{n\alpha}$  is defined in Eq. (A.19), and therefore

$$c_\nu d^\nu = \frac{1}{\Lambda_\nu} \sum_{n=1}^{\infty} \left( d^{-n-1} b_n^{(3)} + d\delta_{1n} \right) X_{n\nu} .$$

If we now eliminate the coefficients  $c_\nu$  from Eqs. (A.46) and (A.48), we obtain

$$d^{-m-1} b_m^{(3)} - \frac{1}{2} d\delta_{1m} = -\frac{2m+1}{2(m+1)} \sum_{n=1}^{\infty} \sum_{\nu} \left( d^{-n-1} b_n^{(3)} + d\delta_{1n} \right) \frac{X_{m\nu} X_{n\nu}}{(\nu+1)\Lambda_\nu} ,$$

$m = 1, 2, 3, \dots$ , which can be written more compactly as

$$(m+1) B_m^{(3)} + \delta_{1m} = - \sum_{n=1}^{\infty} \left( n + \frac{1}{2} \right) B_n^{(3)} \sum_{\nu} \frac{X_{m\nu} X_{n\nu}}{(\nu+1)\Lambda_\nu} \quad (\text{A.49})$$

$m = 1, 2, 3, \dots$ , where

$$B_m^{(3)} = - \frac{1}{2m+1} \left( d^{-m-2} b_m^{(3)} + \delta_{1m} \right). \quad (\text{A.50})$$

Equation (A.49) is very similar to that for the transverse electric dipole moment, and once again our main interest is confined to the leading coefficient  $B_1^{(3)}$ ,

in terms of which

$$b_1^{(3)} = -d^3 (3B_1^{(2)} + 1) . \quad (\text{A. 51})$$

#### A.5 Axial Electric Dipole Moment

This is the final moment to be considered, and because of the different Legendre function zeros involved, the analysis does not bear quite the same relation to the transverse magnetic dipole calculation as does the axial magnetic to the transverse electric.

The total electric potential is now

$$\Phi^i = r \cos \theta \quad (\text{A. 52})$$

and in region 2 we take the total electric potential to be

$$\Phi_2 = \sum_{n=1}^{\infty} (r^{-n-1} a_n^{(3)} + r \delta_{1n}) P_n^0(\cos \theta), \quad (\text{A. 53})$$

whereas in region 1 the potential is

$$\Phi_1 = \sum_{\mu} c_{\mu} r^{\mu} P_{\mu}^0(\cos \theta). \quad (\text{A. 54})$$

There is again no  $\phi$  dependence.

From the Eqs. (A.1) the boundary conditions on the total potentials are

$$\begin{aligned} \frac{\partial \Phi_1}{\partial r} &= 0 && \text{for } \theta = \theta_0 , \\ \frac{\partial \Phi_2}{\partial \theta} &= \frac{\partial \Phi_1}{\partial \theta} && \text{for } r = d, \quad 0 \leq \theta < \theta_0 , \\ &= 0 && \text{for } r = d, \quad \theta_0 < \theta \leq \pi , \\ \frac{\partial \Phi_2}{\partial r} &= \frac{\partial \Phi_1}{\partial r} && \text{for } r = d, \quad 0 \leq \theta < \theta_0 . \end{aligned}$$

The first of these is satisfied by choosing  $\mu$  such that

$$P_{\mu}^0(\cos \theta_0) = 0, \quad (\text{A.55})$$

implying that the summation extends over the zeros  $\mu = \mu_i$ ,  $i = 1, 2, 3, \dots$ , of the Legendre function of order zero. From the second boundary condition we have

$$\begin{aligned} \sum_{n=1}^{\infty} \left( d^{-n-1} a_n^{(3)} + d \delta_{1n} \right) \frac{\partial}{\partial \theta} P_n^0(\cos \theta) &= \sum_{\mu} c_{\mu} d^{\mu} \frac{\partial}{\partial \theta} P_{\mu}^0(\cos \theta), \quad 0 \leq \theta < \theta_0, \\ &= 0, \quad \theta_0 < \theta \leq \pi, \end{aligned} \quad (\text{A.56})$$

giving

$$d^{-m-1} a_m^{(3)} + d \delta_{1m} = -\frac{2m+1}{2} \sum_{\mu} c_{\mu} d^{\mu} \tilde{X}_{m\mu} \quad (\text{A.57})$$

where

$$\tilde{X}_{m\mu} = -\frac{1}{m(m+1)} \int_0^{\theta_0} \sin \theta \frac{\partial P_{\mu}^0}{\partial \theta} \frac{\partial P_m^0}{\partial \theta} d\theta. \quad (\text{A.58})$$

The third and last boundary condition yields

$$\sum_{n=1}^{\infty} (n+1) \left( d^{-n-1} a_n^{(3)} - \frac{1}{2} d \delta_{1n} \right) P_n^0(\cos \theta) = -\sum_{\mu} \mu c_{\mu} d^{\mu} P_{\mu}^0(\cos \theta), \quad 0 \leq \theta < \theta_0, \quad (\text{A.59})$$

from which we obtain

$$c_{\beta} d^{\beta} = -\frac{1}{\beta \tilde{\Lambda}_{\beta}} \sum_{n=1}^{\infty} (n+1) \left( d^{-n-1} a_n^{(3)} - \frac{1}{2} d \delta_{1n} \right) \int_0^{\theta_0} \sin \theta P_{\beta}^0 P_n^0 d\theta$$

where  $\beta$  is any one of the set of zeros  $\mu_i$ ,  $i = 1, 2, 3, \dots$ , and

$$\tilde{\Lambda}_\beta = \int_0^{\theta_0} \sin \theta \left( P_\beta^0 \right)^2 d\theta \quad (\text{A. 60})$$

But

$$\int_0^{\theta_0} \sin \theta P_\beta^0 P_n^0 d\theta = -\tilde{X}_{n\beta} ,$$

where  $\tilde{X}_{n\beta}$  is as defined in Eq. (A. 58), and hence

$$c_\mu d^\mu = \frac{1}{\mu \tilde{\Lambda}_\mu} \sum_{n=1}^{\infty} (n+1) \left( d^{-n-1} a_n^{(3)} - \frac{1}{2} d \delta_{1n} \right) \tilde{X}_{n\mu} . \quad (\text{A. 61})$$

Elimination of the coefficients  $c_\mu$  from Eqs. (A. 57) and (A. 61) gives

$$d^{-m-1} a_m^{(3)} + d \delta_{1m} = -\frac{2m+1}{2} \sum_{n=1}^{\infty} \sum_{\mu} (n+1) \left( d^{-n-1} a_n^{(3)} - \frac{1}{2} d \delta_{1n} \right) \frac{\tilde{X}_{m\mu} \tilde{X}_{n\mu}}{\mu \tilde{\Lambda}_\mu} ,$$

$m = 1, 2, 3, \dots$ , which can be written alternatively as

$$\frac{1}{m+1} \left( A_m^{(3)} + \delta_{1m} \right) = - \sum_{n=1}^{\infty} \left( n + \frac{1}{2} \right) A_n^{(3)} \sum_{\mu} \frac{\tilde{X}_{m\mu} \tilde{X}_{n\mu}}{\mu \tilde{\Lambda}_\mu} , \quad (\text{A. 62})$$

$m = 1, 2, 3, \dots$ , where

$$A_m^{(3)} = \frac{m+1}{2m+1} \left( d^{-m-2} a_m^{(3)} - \frac{1}{2} \delta_{1m} \right) . \quad (\text{A. 63})$$

The form of Eq. (A. 62) differs only slightly from that of the Eq. (A. 23) for the transverse magnetic dipole moment. Once again, only the first coefficient,  $A_1^{(3)}$ , is of direct interest to us, and in terms of this

$$a_1^{(3)} = \frac{d^3}{2} \left( 3 A_1^{(3)} + 1 \right) . \quad (\text{A. 64})$$

## A.6 Some Legendre Function Relations

Throughout the preceding analyses we have used the same symbols for a variety of Legendre function integrals which might, at first sight, appear quite distinct. For the sake of clarity and for the purposes of the subsequent computations it is therefore desirable to set down the orthogonality relations which we have invoked and to evaluate, where possible, the expressions for the  $X_{n\nu}$ ,  $Y_{n\mu}$ , etc. The derivations are rather similar to those in Appendix A of Schultz et al (1964).

For Legendre functions of order unity, the standard orthogonality relations are

$$\int_0^\pi \left\{ P_n^1 \frac{\partial P_m^1}{\partial \theta} + P_m^1 \frac{\partial P_n^1}{\partial \theta} \right\} d\theta = 0$$

$$\int_0^\pi \left\{ \sin \theta \frac{\partial P_n^1}{\partial \theta} \frac{\partial P_m^1}{\partial \theta} + \frac{P_n^1 P_m^1}{\sin \theta} \right\} d\theta = \frac{2m^2 (m+1)^2}{2m+1} \delta_{mn} \quad (\text{A. 65})$$

$$\int_0^\pi \sin \theta P_n^1 P_m^1 d\theta = \frac{2m(m+1)}{2m+1} \delta_{mn}$$

where  $m$  and  $n$  are integers. If  $\alpha$  and  $\beta$  belong to the same set of Legendre function zeros, either of the function itself, so that

$$P_\nu^1(\cos \theta_0) = 0, \quad \nu = \alpha, \beta$$

or of its first derivative, so that

$$\left. \frac{\partial}{\partial \theta} P_\mu^1(\cos \theta) \right|_{\theta = \theta_0} = 0, \quad \mu = \alpha, \beta$$



then

$$\int_0^{\theta_0} \left\{ \sin \theta \frac{\partial P_\alpha^1}{\partial \theta} \frac{\partial P_\beta^1}{\partial \theta} + \frac{P_\alpha^1 P_\beta^1}{\sin \theta} \right\} d\theta = \alpha(\alpha+1) \Lambda_\alpha \delta_{\alpha\beta} \quad (\text{A. 66})$$

$$\int_0^{\theta_0} \sin \theta P_\alpha^1 P_\beta^1 d\theta = \Lambda_\alpha \delta_{\alpha\beta} \quad (\text{A. 67})$$

with

$$\Lambda_\alpha = \int_0^{\theta_0} \sin \theta (P_\alpha^1)^2 d\theta . \quad (\text{A. 21})$$

It would not appear possible, in general, to evaluate analytically this expression for  $\Lambda_\alpha$ . With the above definitions of  $m$  and  $\alpha$ , we also have

$$\int_0^{\theta_0} \left\{ \sin \theta \frac{\partial P_m^1}{\partial \theta} \frac{\partial P_\alpha^1}{\partial \theta} + \frac{P_m^1 P_\alpha^1}{\sin \theta} \right\} d\theta = \frac{m(m+1)}{m(m+1) - \alpha(\alpha+1)} \left[ \sin \theta P_m^1 \frac{\partial P_\alpha^1}{\partial \theta} \right]_0^{\theta_0} - \frac{\alpha(\alpha+1)}{m(m+1) - \alpha(\alpha+1)} \left[ \sin \theta P_\alpha^1 \frac{\partial P_m^1}{\partial \theta} \right]_0^{\theta_0} , \quad (\text{A. 68})$$

$$\int_0^{\theta_0} \sin \theta P_m^1 P_\alpha^1 d\theta = \frac{1}{m(m+1) - \alpha(\alpha+1)} \left[ \sin \theta \left( P_m^1 \frac{\partial P_\alpha^1}{\partial \theta} - P_\alpha^1 \frac{\partial P_m^1}{\partial \theta} \right) \right]_0^{\theta_0} , \quad (\text{A. 69})$$

with the simplification that can be effected in the right hand sides of Eqs. (A. 68) and (A. 69) depending on whether  $\alpha$  is a zero of the Legendre function or its first derivative.

We are now in a position to detail the quantities appearing in the analyses of the transverse dipole moments. In the transverse electric case, where the required zeros are of the Legendre function itself,  $\alpha = \nu$  and

$$\int_0^{\theta_0} \left\{ \sin \theta \frac{\partial P_m^1}{\partial \theta} \frac{\partial P_\nu^1}{\partial \theta} + \frac{P_m^1 P_\nu^1}{\sin \theta} \right\} d\theta = \frac{m(m+1)}{m(m+1) - \nu(\nu+1)} \sin \theta_0 P_m^1(\cos \theta_0) \cdot \frac{\partial P_\nu^1}{\partial \theta} \Big|_{\theta = \theta_0}, \quad (\text{A. 70})$$

$$\int_0^{\theta_0} \sin \theta P_m^1 P_\nu^1 d\theta = \frac{1}{m(m+1) - \nu(\nu+1)} \sin \theta_0 P_m^1(\cos \theta_0) \frac{\partial P_\nu^1}{\partial \theta} \Big|_{\theta = \theta_0}. \quad (\text{A. 71})$$

Hence, the quantity  $X_{m\nu}$  defined in Eq. (A.19) is

$$X_{m\nu} = \frac{1}{m(m+1) - \nu(\nu+1)} \sin \theta_0 P_m^1(\cos \theta_0) \frac{\partial P_\nu^1}{\partial \theta} \Big|_{\theta = \theta_0}, \quad (\text{A. 72})$$

providing  $\nu \neq m$ . This, together with Eq. (A.21), completes the specification of the quantities appearing in the Eq. (A.23) for the  $A_m^{(1)}$ . In the case of the transverse magnetic dipole moment, the required zeros are of the derivative, so that  $\alpha = \mu$ , and

$$\int_0^{\theta_0} \left\{ \sin \theta \frac{\partial P_m^1}{\partial \theta} \frac{\partial P_\mu^1}{\partial \theta} + \frac{P_m^1 P_\mu^1}{\sin \theta} \right\} d\theta = -\frac{\mu(\mu+1)}{m(m+1) - \mu(\mu+1)} \sin \theta_0 P_\mu^1(\cos \theta_0) \cdot \frac{\partial P_m^1}{\partial \theta} \Big|_{\theta = \theta_0}, \quad (\text{A. 73})$$

$$\int_0^{\theta_0} \sin \theta P_m^1 P_\mu^1 d\theta = - \frac{1}{m(m+1) - \mu(\mu+1)} \sin \theta_0 P_\mu^1 (\cos \theta_0) \frac{\partial P_m^1}{\partial \theta} \Big|_{\theta = \theta_0} . \quad (\text{A.74})$$

Hence, the quantity  $Y_{m\mu}$  defined in Eq. (A.32) is

$$Y_{m\mu} = \frac{\mu / (m+1)}{m(m+1) - \mu(\mu+1)} \sin \theta_0 P_\mu^1 (\cos \theta_0) \frac{\partial P_m^1}{\partial \theta} \Big|_{\theta = \theta_0} , \quad (\text{A.75})$$

providing  $\mu \neq m$ . This, together with Eq. (A.21), completes the specification of the quantities appearing in the Eq. (A.39) for the  $B_m^{(1)}$ .

The results for the Legendre functions of order zero are quite comparable to the above, and we shall again present only those relations which are required in the analysis of the dipole moments.

The standard orthogonality relations are

$$\int_0^\pi \sin \theta \frac{\partial P_m^0}{\partial \theta} \frac{\partial P_n^0}{\partial \theta} d\theta = \frac{2m(m+1)}{2m+1} \delta_{mn} , \quad (\text{A.76})$$

$$\int_0^\pi \sin \theta P_m^0 P_n^0 d\theta = \frac{2}{2m+1} \delta_{mn} ,$$

where  $m$  and  $n$  are integers. If  $\alpha$  and  $\beta$  belong to the same set of zeros of the Legendre function of order zero, or of its first derivative, then

$$\int_0^{\theta_0} \sin \theta \frac{\partial P_\alpha^0}{\partial \theta} \frac{\partial P_\beta^0}{\partial \theta} d\theta = \Lambda_\alpha \delta_{\alpha\beta} \quad (\text{A.77})$$

$$\int_0^{\theta_0} \sin \theta P_\alpha^0 P_\beta^0 d\theta = \frac{\Lambda_\alpha}{\alpha(\alpha+1)} \delta_{\alpha\beta} \quad (\text{A. 78})$$

where

$$\begin{aligned} \Lambda_\alpha &= \int_0^{\theta_0} \sin \theta \left( \frac{\partial P_\alpha^0}{\partial \theta} \right)^2 d\theta \\ &= \int_0^{\theta_0} \sin \theta (P_\alpha^1)^2 d\theta \end{aligned} \quad (\text{A. 79})$$

and is identical to the quantity shown in Eq. (A.21). Moreover, with the above definitions of  $m$  and  $\alpha$ ,

$$\begin{aligned} \int_0^{\theta_0} \sin \theta \frac{\partial P_m^0}{\partial \theta} \frac{\partial P_\alpha^0}{\partial \theta} d\theta &= \frac{m(m+1)}{m(m+1) - \alpha(\alpha+1)} \left[ \sin \theta P_m^0 \frac{\partial P_\alpha^0}{\partial \theta} \right]_0^{\theta_0} - \\ &\quad - \frac{\alpha(\alpha+1)}{m(m+1) - \alpha(\alpha+1)} \left[ \sin \theta P_\alpha^0 \frac{\partial P_m^0}{\partial \theta} \right]_0^{\theta_0}, \end{aligned} \quad (\text{A. 80})$$

$$\int_0^{\theta_0} \sin \theta P_m^0 P_\alpha^0 d\theta = \frac{1}{m(m+1) - \alpha(\alpha+1)} \left[ \sin \theta \left( P_m^0 \frac{\partial P_\alpha^0}{\partial \theta} - P_\alpha^0 \frac{\partial P_m^0}{\partial \theta} \right) \right]_0^{\theta_0}, \quad (\text{A. 81})$$

with the simplifications that can be effected in the right hand sides depending on whether  $\alpha$  is a zero of the Legendre function or its first derivative.

Thus, in the case of the axial magnetic dipole moment where the required zeros are of the derivative,

$$\int_0^{\theta_0} \sin \theta \frac{\partial P_m^0}{\partial \theta} \frac{\partial P_\alpha^0}{\partial \theta} d\theta = - \frac{\alpha(\alpha+1)}{m(m+1) - \alpha(\alpha+1)} \sin \theta_0 P_\alpha^0(\cos \theta_0) \frac{\partial P_m^0}{\partial \theta} \Big|_{\theta = \theta_0},$$

(A. 82)

$$\int_0^{\theta_0} \sin \theta P_m^0 P_\alpha^0 d\theta = - \frac{1}{m(m+1) - \alpha(\alpha+1)} \sin \theta_0 P_\alpha^0(\cos \theta_0) \frac{\partial P_m^0}{\partial \theta} \Big|_{\theta = \theta_0}.$$

(A. 83)

But  $\frac{\partial P_m^0}{\partial \theta} = -P_m^1$  and with the definition of  $\alpha$ ,

$$P_\alpha^0(\cos \theta_0) = \frac{1}{\alpha(\alpha+1)} \frac{\partial P_\alpha^1}{\partial \theta} \Big|_{\theta = \theta_0}.$$

(A. 84)

Hence, the quantity  $X_{m\nu}$  defined in Eq. (A. 47) is indeed identical to that given in Eq. (A. 72). Together with Eq. (A. 21), this completes the specification of the quantities appearing in the Eq. (A. 49) for the  $B_m^{(3)}$ . The case of the axial electric dipole is, however, somewhat different. The required zeros are those of the Legendre function of order zero, and if  $\mu$  is such a zero, the quantity  $\tilde{\Lambda}_\mu$  is simply

$$\tilde{\Lambda}_\mu = \frac{\Lambda_\mu}{\mu(\mu+1)}$$

(A. 85)

but cannot otherwise be simplified. Also

$$\int_0^{\theta_0} \sin \theta \frac{\partial P_m^0}{\partial \theta} \frac{\partial P_\mu^0}{\partial \theta} d\theta = \frac{m(m+1)}{m(m+1) - \mu(\mu+1)} \sin \theta_0 P_m^0(\cos \theta_0) \frac{\partial P_\mu^0}{\partial \theta} \Big|_{\theta = \theta_0},$$

(A. 86)

$$\int_0^{\theta_0} \sin \theta P_m^0 P_\mu^0 d\theta = \frac{1}{m(m+1) - \mu(\mu+1)} \sin \theta_0 P_m^0(\cos \theta) \left. \frac{\partial P_\mu^0}{\partial \theta} \right|_{\theta = \theta_0} \quad (\text{A. 87})$$

and hence the quantity  $\tilde{X}_{m\mu}$  defined in Eq. (A. 58) is

$$\tilde{X}_{m\mu} = - \frac{1}{m(m+1) - \mu(\mu+1)} \sin \theta_0 P_m^0(\cos \theta) \left. \frac{\partial P_\mu^0}{\partial \theta} \right|_{\theta = \theta_0} \quad (\text{A. 88})$$

This completes the specification of the quantities appearing in Eq. (A. 68) for the  $A_m^{(3)}$ .

#### A. 7 The Hemisphere

When  $\theta_0 = \pi/2$  the round-backed cone is, in fact, a hemisphere, and though our main interest is in small cone angles (and the computations will be confined to values of  $\pi - \theta_0$  less than  $\pi/2$ ), a few comments about this limiting case would appear to be in order.

Formally at least the approach that we have adopted is valid for all values of  $\theta_0$ , including those less than or equal to  $\pi/2$ , but when  $\theta_0 = \pi/2$ , some of the expressions for the  $X_{m\nu}$ ,  $\Lambda_\alpha$ , etc given in the previous section are no longer applicable, and still others are capable of simpler forms. These changes are bound up with the Legendre function zeros. As is well known (see, for example, Senior and Wilcox, 1967), for  $\theta_0 = \pi/2$  the zeros of the Legendre function of order unity are even integers. Thus, from Eq. (A. 15),

$$\nu = 2k, \quad k = 1, 2, 3, \dots \quad (\text{A. 89})$$

and these are also the zeros of the first derivative of the Legendre function of order zero. Similarly, for the first derivative of the function of order unity, and for the function of order zero, the zeros are the odd integers.

Thus, from Eq. (A.54) as well as from Eq. (A.29),

$$\mu = 2k - 1, \quad k = 1, 2, 3, \dots \quad (\text{A.90})$$

To illustrate the changes and/or simplifications to the general analysis that are appropriate when  $\theta_0 = \pi/2$ , it is sufficient to consider the case of the transverse electric dipole moment. The zeros  $\nu$  are then given by Eq. (A.89), and since

$$m(m+1) - \nu(\nu+1) = (m-\nu)(m+\nu+1),$$

it is at once evident that the evaluation of the expression for  $X_{m\nu}$  given in Eq. (A.72) is no longer applicable if  $m$  is even. From Eq. (A.19), however, with  $\theta_0 = \pi/2$  and  $\nu$  an even integer, we observe that if  $m$  is even

$$\begin{aligned} X_{m\nu} &= \frac{1}{2m(m+1)} \int_0^\pi \left( \sin \theta \frac{\partial P_\nu^1}{\partial \theta} \frac{\partial P_m^1}{\partial \theta} + \frac{P_\nu^1 P_m^1}{\sin \theta} \right) d\theta \\ &= \frac{m(m+1)}{2m+1} \delta_{m\nu} \end{aligned} \quad (\text{A.91})$$

and similarly

$$\Lambda_\nu = \frac{\nu(\nu+1)}{2\nu+1} \quad (\text{A.92})$$

If, on the other hand,  $m$  is odd, Eq. (A.72) remains applicable, but can be "simplified" by observing that ( $\nu$  even)

$$\left. \frac{\partial P_\nu^1}{\partial \theta} \right|_{\theta = \pi/2} = -(\nu+1) P_{\nu-1}^1(0);$$

since

$$\begin{aligned} P_m^1(0) &= -\frac{m}{m-1} P_{m-2}^1(0) \\ &= (-1)^{1/2(m-1)} \frac{\left(\frac{m}{2}\right)!}{\frac{1}{2}! \left(\frac{m-1}{2}\right)!} , \end{aligned}$$

it follows that for  $m$  odd

$$X_{m\nu} = \frac{8}{\pi} (-1)^{1/2(m+\nu-1)} \frac{1}{(m-\nu)(m+\nu+1)} \frac{\left(\frac{m}{2}\right)! \left(\frac{\nu+1}{2}\right)!}{\left(\frac{m-1}{2}\right)! \left(\frac{\nu-1}{2}\right)!} . \quad (\text{A. 93})$$

Turning now to the Eq. (A. 23) for the coefficients  $A_m^{(1)}$ , for purposes of digital solution it seems preferable to leave this in the form shown and to treat the case  $\theta_0 = \pi/2$  like any other value of  $\theta_0$  with the sole distinction that for  $m$  and  $n$  even Eq. (A. 91) is used in place of Eq. (A. 72). If so desired, Eq. (A. 92) can also be used to obviate the need for the numerical integration that Eq. (A. 21) would otherwise entail. It is, however, interesting to note that as a result of Eq. (A. 91) each coefficient  $A_m^{(1)}$  with even subscript is expressible as a sum over the coefficients with odd subscripts, viz.

$$A_m^{(1)} = -\frac{1}{m(3m+1)} \sum_{n=1,3,\dots}^{\infty} (2n+1) A_n^{(1)} X_{mn} , \quad m \text{ even}, \quad (\text{A. 94})$$

and this enables us to reduce the set of equations represented by (A. 23) to a set involving only the coefficients  $A_m^{(1)}$  with odd subscripts, viz.

$$mA_m^{(1)} + \delta_{1m} = - \sum_{n=1,3,\dots} (2n+1) A_n^{(1)} \sum_{\nu} \frac{2\nu+1}{\nu(\nu+1)(3\nu+1)} X_{m\nu} X_{n\nu} , \quad (\text{A. 95})$$



$m = 1, 3, 5, \dots$ . It is not obvious that this is other than of academic interest, and though it would appear that the relatively simple geometry of the hemisphere should permit a more straightforward derivation of the dipole moments, no such analysis has been found, nor are we aware of any treatment of this shape in the technical literature.

### A.8 Numerical Solution

In order to determine the dipole moments  $a_1^{(1)}$ ,  $a_1^{(3)}$ ,  $b_1^{(1)}$  and  $b_1^{(3)}$ , it is necessary to solve the four infinite sets of equations shown in (A.23), (A.39), (A.49) and (A.62) respectively, and we wish to do so for a variety of  $\theta_0$  in the range  $\frac{\pi}{2}$  to  $\pi$ .

For a given value of  $\theta_0$  there are three main computational tasks associated with the solution of each equation set: (i) the calculation of an adequate number of Legendre function zeros; (ii) the evaluation of the various factors involved, including the numerical integration of the expression for  $\Lambda_\alpha$ ; and (iii) the matrix inversion. Only the first of these is other than straightforward, and even here we were fortunate in having available a computational technique that had been devised (Wilcox, 1968) in connection with the scattering of an electromagnetic wave by a semi-infinite cone (Senior and Wilcox, 1967). Taking, for example, the problem of the transverse electric dipole moment for which the required zeros are those of the Legendre function of order unity, we write

$$P_\nu^1(\cos \theta_0) = -\frac{1}{\sqrt{\pi} \sin \theta_0} \frac{(\nu+1)!}{\left(\nu+\frac{1}{2}\right)!} S_\nu(\theta_0), \quad (\text{A.96})$$

where

$$S_\nu(\theta_0) = \sum_{k=0}^{\infty} \frac{\left(-\frac{1}{2}\right)_k \binom{\nu}{k}}{k! \left(\nu+\frac{3}{2}\right)_k} \sin\left\{(\nu+2k)\theta_0\right\} \quad (\text{A.97})$$

valid for  $0 < \theta_0 < 180$ . The series does converge, albeit slowly, at a rate which is independent of  $\theta_0$ , and the zeros can be found by an iterative method. Similarly, for the zeros of the Legendre function derivative we use the recurrence relations to write

$$\frac{\partial}{\partial \theta_0} P_{\mu}^1(\cos \theta_0) = -\frac{\mu}{\sqrt{\pi} \sin^2 \theta_0} \frac{(\mu+1)!}{(\mu+\frac{1}{2})!} \left\{ \cos \theta_0 S_{\mu}(\theta_0) - \left(1 + \frac{1}{2\mu}\right) S_{\mu-1}(\theta_0) \right\}, \quad (\text{A. 98})$$

and again resort to an iterative method. Inasmuch as a computer program was already available to calculate any number of these zeros for any given value of  $\theta_0$  and, in addition, to compute the first derivative (or function itself) at each zero, task (i) for the transverse moments required only the updating of this program (including rewriting in Fortran IV). Data were obtained for 20 zeros of each type at each of about 20 values of  $\theta_0$ .

Of the axial dipole moments, only the electric involves Legendre function zeros differing from the above, namely, those of the function of order zero. A new program was written to compute these and in order to use to the utmost the procedures developed for the first order function, the recurrence relations were employed to give

$$P_{\mu}^0(\cos \theta_0) = \frac{1}{\mu(\mu+1)} \left\{ \frac{\partial P_{\mu}^1}{\partial \theta_0} + \cos \theta_0 P_{\mu}^1 \right\}. \quad (\text{A. 99})$$

With the aid of Eq. (A.96), the right hand side can be expressed in terms of the same function  $S_{\mu}(\theta_0)$  previously computed, and the zeros again found by iteration.

The remaining tasks (ii) and (iii) associated with the solution of the equation sets for the dipole moments were straightforward and require no comment. Because of the form of the original program for the computation of the zeros of  $P_\nu^1(\cos \theta)$  and  $\frac{\partial}{\partial \theta} P_\mu^1(\cos \theta)$ , it was found convenient to treat the solution of Eqs. (A.23) and (A.39) together in the same program. A slight modification then yielded the solution of Eq. (A.50), and a somewhat greater change provided the solution of Eq. (A.62). In each instance, only the leading coefficient, e.g.  $A_1^{(1)}$ , was printed out. The programs were run for  $\theta_0 = 95^\circ$  ( $5^\circ$ )  $150^\circ$  ( $2-1/2^\circ$ )  $177-1/2^\circ$ ; the results are shown in Table A-1, along with the deduced values of the dipole moments, and the latter are plotted as functions of  $\theta_0$  in Fig. A-2. Examination of the first and second differences of the computed dipole moments suggests that the results are accurate to only about 3 significant figures. This somewhat limited accuracy is a consequence of the several stops and tolerance criteria inserted into the program to reduce the computation time involved. Though it would be a straightforward task to improve the accuracy at the expense of an increase in the running time of the program, such an improvement was not felt to be necessary for the purposes of this study.

TABLE A-1: Computed Dipole Moments

$\theta_0^o$	$A_1^{(1)}$	$B_1^{(1)}$	$B_1^{(3)}$	$A_1^{(3)}$	$a_1^{(1)}/d^3$	$b_1^{(1)}/d^3$	$b_1^{(3)}/d^3$	$a_1^{(3)}/d^3$
95	-0.7882	-0.8024	-0.4471	-0.5444	-0.6823	0.2036	0.3412	-0.3165
100	-0.7498	-0.7879	-0.4375	-0.5165	-0.6247	0.1819	0.3124	-0.2747
105	-0.7091	-0.7743	-0.4273	-0.4919	-0.5637	0.1614	0.2819	-0.2379
110	-0.6675	-0.7615	-0.4169	-0.4720	-0.5012	0.1423	0.2507	-0.2080
115	-0.6253	-0.7497	-0.4063	-0.4539	-0.4379	0.1245	0.2190	-0.1808
120	-0.5836	-0.7378	-0.3959	-0.4384	-0.3753	0.1066	0.1877	-0.1577
125	-0.5433	-0.7276	-0.3859	-0.4252	-0.3150	0.0914	0.1576	-0.1377
130	-0.5050	-0.7182	-0.3763	-0.4151	-0.2576	0.0773	0.1288	-0.1226
135	-0.4700	-0.7092	-0.3675	-0.4059	-0.2051	0.0638	0.1026	-0.1089
140	-0.4383	-0.7017	-0.3596	-0.3973	-0.1574	0.0525	0.0787	-0.0960
145	-0.4108	-0.6942	-0.3527	-0.3902	-0.1163	0.0412	0.0582	-0.0853
150	-0.3876	-0.6871	-0.3469	-0.3836	-0.0814	0.0306	0.0407	-0.0754
152.2	-0.3777	-0.6842	-0.3444	-0.3805	-0.0666	0.0263	0.0333	-0.0708
155	-0.3688	-0.6815	-0.3422	-0.3766	-0.0533	0.0223	0.0266	-0.0650
157.5	-0.3611	-0.6781	-0.3403	-0.3732	-0.0416	0.0171	0.0208	-0.0597
160	-0.3545	-0.6760	-0.3386	-0.3696	-0.0318	0.0139	0.0159	-0.0545
162.5	-0.3489	-0.6741	-0.3372	-0.3661	-0.0234	0.0111	0.0117	-0.0491
165	-0.3442	-0.6723	-0.3361	-0.3625	-0.0163	0.0084	0.0082	-0.0438
167.5	-0.3406	-0.6708	-0.3352	-0.3588	-0.0108	0.0062	0.0054	-0.0383
170	-0.3378	-0.6694	-0.3345	-0.3555	-0.0066	0.0041	0.0033	-0.0332
172.5	-0.3357	-0.6683	-0.3339	-0.3516	-0.0035	0.0025	0.0017	-0.0274
175	-0.3343	-0.6674	-0.3336	-0.3473	-0.0014	0.0011	0.0007	-0.0210
177.5	-0.3335	-0.6669	-0.3334	-0.3430	-0.0003	0.0003	0.0001	-0.0144

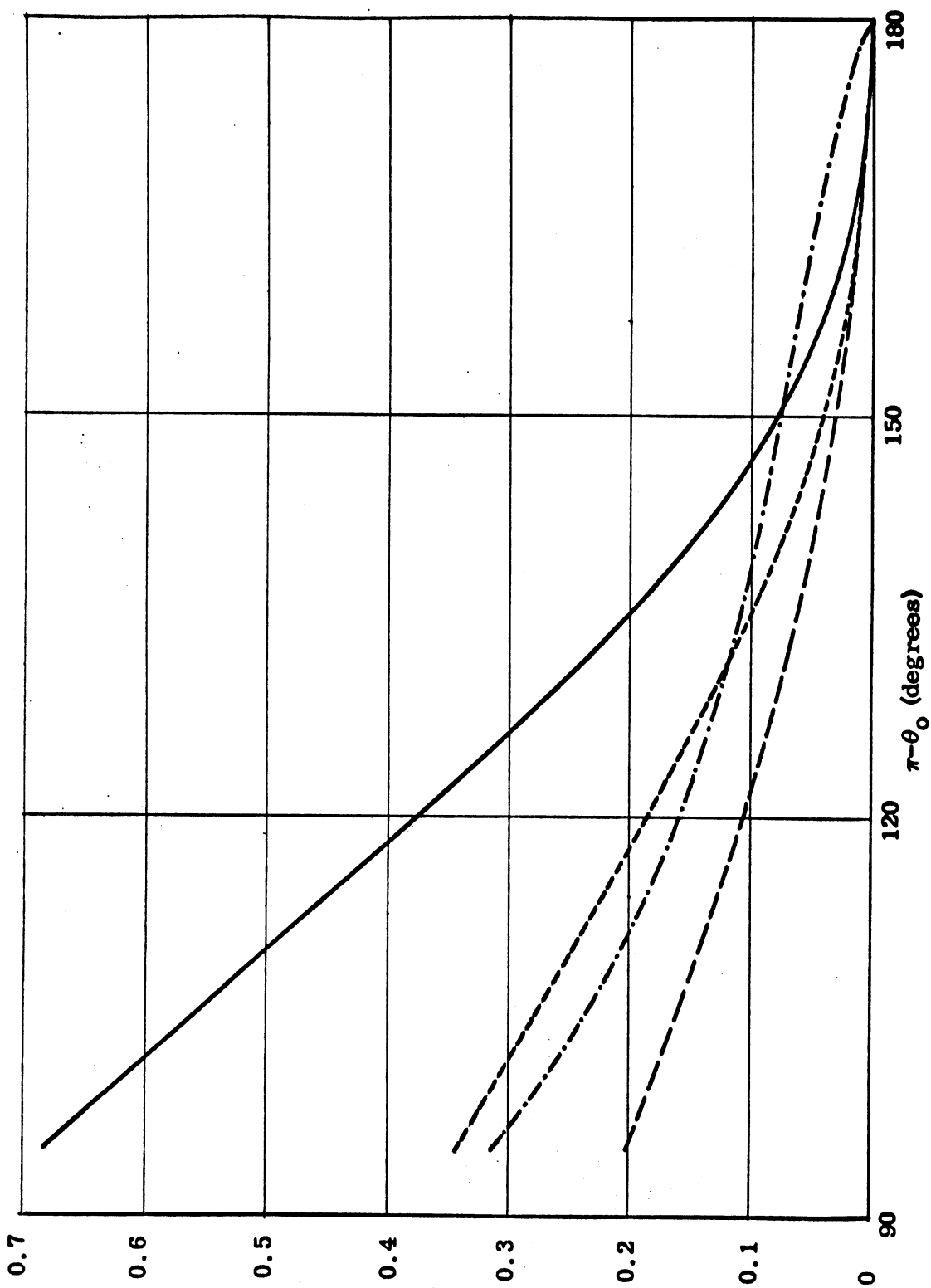


FIG. A-2: Computed Dipole Moments:  $-a_1^{(1)}/d^3$ , —;  $-a_1^{(3)}/d^3$ , - - -;  $b_1^{(1)}/d^3$ , - · - · -; and  $b_1^{(3)}/d^3$ , · · · · ·.

## A.9 References

- Rogers, C. C., J.K. Schindler and F. V. Schultz (1963), "The Scattering of a Plane Electromagnetic Wave by a Finite Cone," Electromagnetic Theory and Antennas, Pergamon Press, New York, Part 1, pp. 67-80.
- Schultz, F. V., G. M. Ruckgaber, S. Richter and J. K. Schindler (1964), The Theoretical and Numerical Determination of the Radar Cross Section of a Finite Cone, Purdue University Report No. TR-EE64-14.
- Senior, T. B. A., and P. H. Wilcox (1967), Traveling Waves in Relation to the Surface Fields on a Semi-Infinite Cone, Radio Science, 2, 479-487.
- Wilcox, P. H. (1968), The Zeros of  $P_{\nu}^1(\cos \theta)$  and  $\frac{\partial}{\partial \theta} P_{\mu}^1(\cos \theta)$ , Math. Comp. 22, 205-208.

## APPENDIX B

### NUMERICAL DETERMINATION OF SURFACE CURRENTS AND FAR FIELDS FOR BODIES OF REVOLUTION

#### B.1 Introduction

In this Appendix we examine the backscattered field produced by the plane electromagnetic wave

$$\underline{E}^i = \hat{x} e^{ikz}, \quad \underline{H}^i = \hat{y} Y e^{ikz} \quad (\text{B.1})$$

when it impinges axially on a perfectly conducting body of revolution. Numerical computations of surface currents and far fields have been previously developed by Andreasen (1965) and by Harrington and Mautz (1969a, b), among others. The method given here permits the determination of the various multipole (in particular, dipole) contributions to the far field.

In section B.2, the surface current is studied by means of the integral equation of Maue (1949). The longitudinal and circumferential components of the current are solutions of two coupled one-dimensional integral equations of Fredholm's type; these equations become uncoupled only for a conical surface. Low-frequency approximations to these equations are discussed in section B.3.

In section B.4, the general expansion of the scattered far field in terms of the TM and TE modes is reviewed; the coefficients of the expansion are given by integrals over the electric current in the scattering volume (much of this material may also be found distributed through the book by Panofsky and Phillips (1962)). In particular, the dipole contributions to the backscattered field are examined in section B.5, and a comparison with the well known formula by Siegel (1959) is given in section B.6.

Finally, a numerical evaluation of the low-frequency backscattered field is performed for various bodies of revolution, in section B.7. This result is

achieved in two steps. Firstly, the coupled integral equations for the surface current components are replaced by a system of linear algebraic equations, by dividing the body profile into a number of cells, over each of which the current is assumed to be constant. It is well known that at high frequencies this procedure entails considerable difficulties when the field point and the integration point belong to the same cell or to neighboring cells (Goodrich and Stenger, 1969); however, it is shown here that the difficulties can be avoided if the scatterer is not large compared to the wavelength. Secondly, an integration of the surface currents over the body surface yields the dipole contributions to the far back-scattered field. The computer program is printed in section B.8.

## B.2 Surface Currents

Consider the perfectly conducting body of revolution shown in Fig. B-1. Maue's integral equation for the surface current density  $\underline{I}(\underline{r})$  at the point P ( $\underline{r}$ ) is:

$$\underline{I}(\underline{r}) + \frac{1}{2\pi} \iint_S K(R) \hat{n} \wedge \left\{ (\underline{r}' - \underline{r}) \wedge \underline{I}(\underline{r}') \right\} dS' = 2 \hat{n} \wedge \underline{H}^i(\underline{r}), \quad (\text{B.2})$$

where  $\hat{n}$  is the outward unit normal,  $\underline{r}'$  is the integration point on the surface S of the scatterer,  $\underline{H}^i$  is the incident magnetic field which we choose according to (B.1), and

$$K(R) = R^{-2} (ik - R^{-1}) e^{ikR}, \quad R = \left| \underline{r}' - \underline{r} \right|. \quad (\text{B.3})$$

Set:

$$\underline{I}(\underline{r}) = I_t(\underline{r}) \hat{t} + I_\phi(\underline{r}) \hat{\phi}. \quad (\text{B.4})$$

With reference to Fig. B-2, observe that

$$\hat{t} = \cos \beta \hat{r} - \sin \beta \hat{\theta}, \quad \hat{n} = \cos \beta \hat{\theta} + \sin \beta \hat{r} \quad (\text{B.5})$$



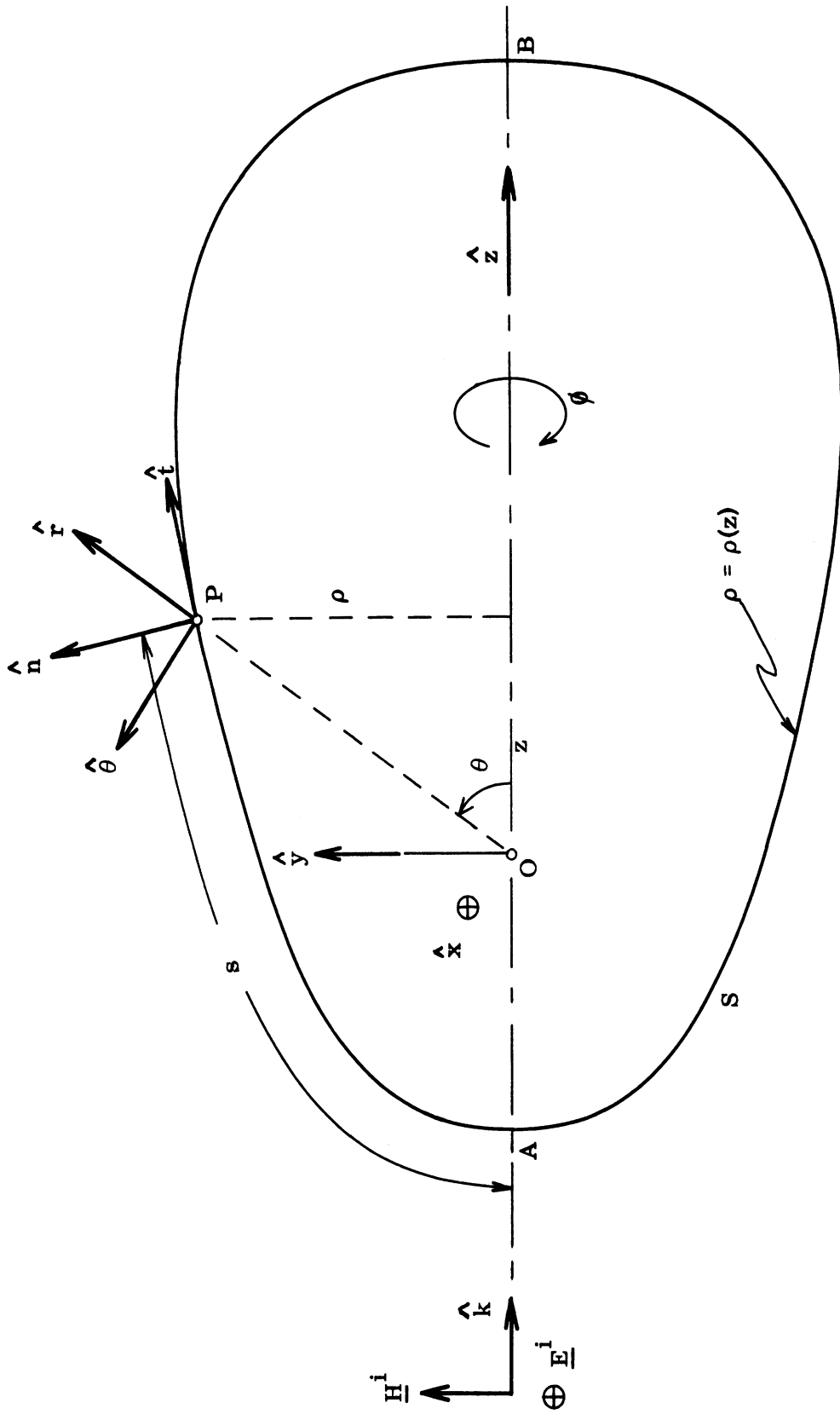


FIG. B-1: Geometry for Body of Revolution.

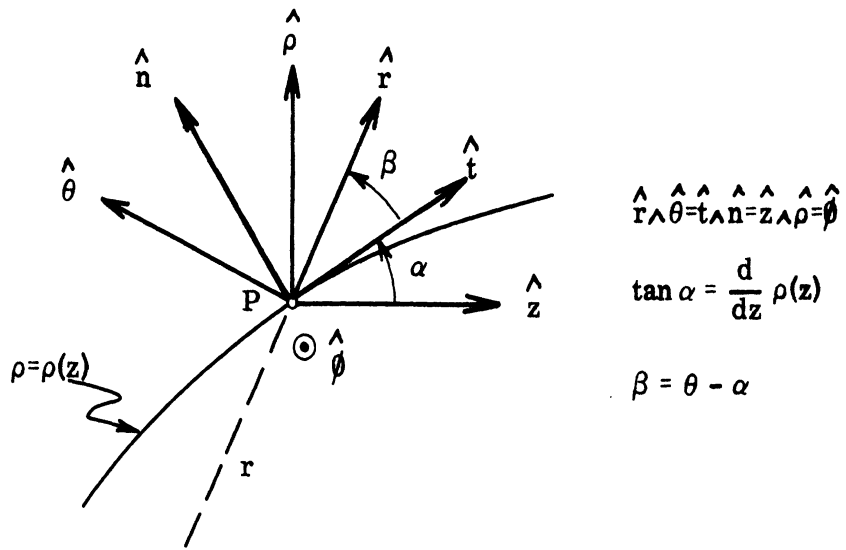


FIG. B-2: Unit Vectors at the Point P.

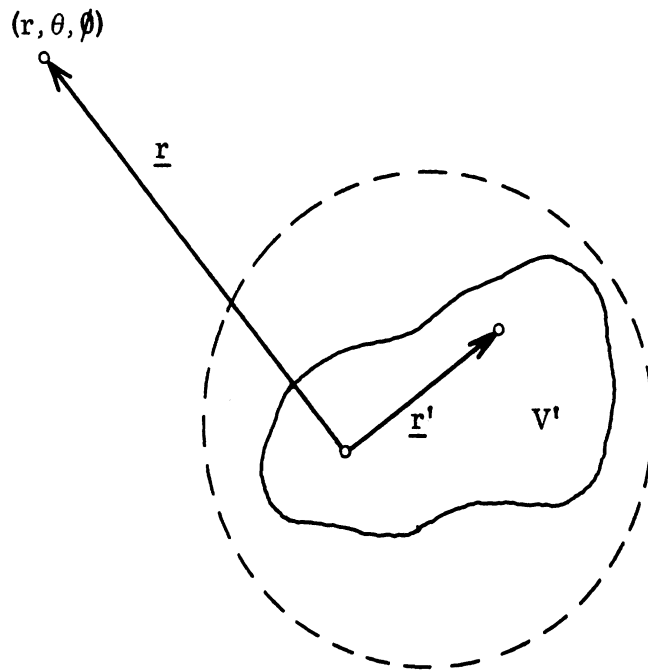


FIG. B-3: Geometry for the Far-field Expansion.

and therefore:

$$\begin{aligned}
\hat{n} \wedge (\hat{r}' \wedge \hat{t}') &= -\sin \beta' \cos \gamma \hat{t} - \sin \beta' \sin \alpha \sin \gamma \hat{\phi} , \\
\hat{n} \wedge (\hat{r}' \wedge \hat{\phi}') &= -\cos \theta' \sin \gamma \hat{t} + (\cos \theta' \sin \alpha \cos \gamma - \sin \theta' \cos \alpha) \hat{\phi} , \\
\hat{n} \wedge (\hat{r}' \wedge \hat{t}') &= (\cos \theta \sin \alpha' \cos \gamma - \sin \theta \cos \alpha') \hat{t} - \sin \beta \sin \gamma \sin \alpha' \hat{\phi} , \\
\hat{n} \wedge (\hat{r}' \wedge \hat{\phi}') &= -\cos \theta \sin \gamma \hat{t} - \sin \beta \cos \gamma \hat{\phi} ,
\end{aligned}$$

(B.6)

where  $\beta' = \theta' - \alpha'$ , and

$$\gamma = \phi' - \phi . \quad (B.7)$$

Now we make the Ansatz:

$$I_{\underline{t}}(\underline{r}) = Y f(s) \cos \phi e^{ikz} , \quad I_{\underline{\phi}}(\underline{r}) = Y g(s) \sin \phi e^{ikz} , \quad (B.8)$$

and we observe that since

$$\begin{aligned}
R &= \sqrt{r^2 + r'^2 - 2 r r' (\cos \theta \cos \theta' + \sin \theta \sin \theta' \cos \gamma)} = \\
&= \sqrt{(\rho - \rho')^2 + (z - z')^2 + 2 \rho \rho' (1 - \cos \gamma)}
\end{aligned}$$

(B.9)

is an even periodic function of  $\gamma$  with period  $2\pi$ , and is symmetric with respect to  $\gamma = \pi$ , then so is  $K(R)$ .

Therefore:

$$\int_0^{2\pi} d\phi' K \cos \phi' = 2 \Delta_0 \cos \phi , \quad \int_0^{2\pi} d\phi' K \cos \phi' \cos \gamma = 2 \Delta_2 \cos \phi ,$$

$$\int_0^{2\pi} d\phi' K \sin \phi' \sin \gamma = 2 \Delta_1 \cos \phi, \quad \int_0^{2\pi} d\phi' K \cos \phi' \sin \gamma = -2 \Delta_1 \sin \phi, \quad (\text{B.10})$$

$$\int_0^{2\pi} d\phi' K \sin \phi' \cos \gamma = 2 \Delta_2 \sin \phi, \quad \int_0^{2\pi} d\phi' K \sin \phi' = 2 \Delta_0 \sin \phi,$$

where

$$\Delta_0 = \int_0^\pi d\gamma K(R) \cos \gamma, \quad \Delta_1 = \int_0^\pi d\gamma K \sin^2 \gamma, \quad \Delta_2 = \int_0^\pi d\gamma K \cos^2 \gamma. \quad (\text{B.11})$$

When equations (B.4) - (B.11) are substituted into (B.2) the  $\phi$  - dependence drops out (the Ansatz (B.8) is thus justified), and one finds that

$$f(s) = 2 - \frac{1}{\pi} \int_A^B ds' \rho' e^{ik(z'-z)} \left\{ f(s') \left[ \Delta_0 \rho \cos \alpha' - \Delta_2 \left\{ \rho' \cos \alpha' + (z-z') \sin \alpha' \right\} \right] + \right. \\ \left. + g(s') \Delta_1 (z - z') \right\}, \quad (\text{B.12})$$

$$g(s) = -2 \sin \alpha + \frac{1}{\pi} \int_A^B ds' \rho' e^{ik(z'-z)} \cdot \\ \cdot \left\{ g(s') \left[ \Delta_0 \rho' \cos \alpha - \Delta_2 \left\{ \rho \cos \alpha + (z'-z) \sin \alpha \right\} \right] + \right. \\ \left. + f(s') \Delta_1 \left[ \rho \sin \alpha' \cos \alpha - \rho' \sin \alpha \cos \alpha' - (z-z') \sin \alpha \sin \alpha' \right] \right\}, \quad (\text{B.13})$$

where  $s$  is the arclength from  $A$  to  $P$  shown in Fig. B-1, and  $\int_A^B$  means that the integration is along one half of the whole contour, i. e. in the semi-plane ( $x = 0, y > 0$ ).

The fundamental equations (B. 12) and (B. 13) are two coupled one-dimensional integral equations of Fredholm's type. They become uncoupled only for a conical surface.

### B. 3 Low-Frequency Approximation

Equations (B. 12) and (B. 13) are exact. If low-frequency approximations are desired and if  $d$  is a characteristic dimension of the scatterer, then

$$\delta = kd \ll 1 \quad (\text{B. 14})$$

is the parameter of smallness. Let us normalize all lengths to  $d$ , and let us "bar" the normalized quantities, e. g.

$$\bar{R} = R/d, \quad \bar{s} = s/d, \quad \text{etc. ;}$$

$$\bar{K} = \left[ \frac{i\delta}{\bar{R}^2} - \frac{1}{\bar{R}^3} \right] e^{i\bar{R}\delta} = K(R) d^3. \quad (\text{B. 15})$$

Now observe that

$$\bar{K} = \bar{R}^{-3} \left[ -1 + \sum_{n=2}^{\infty} \frac{n-1}{n!} (i\bar{R}\delta)^n \right], \quad (\text{B. 16})$$

and assume that

$$f(\bar{s}) = \sum_{n=0}^{\infty} f_n(\bar{s}) (i\delta)^n, \quad g(\bar{s}) = \sum_{n=0}^{\infty} g_n(\bar{s}) (i\delta)^n, \quad (\text{B. 17})$$

where  $f_n$  and  $g_n$  are independent of  $\delta$ . Substitution of (B.14) - (B.17) into (B.12) and (B.13) yields the following set of coupled integral equations, all independent of  $\delta$ . The zeroth-order approximation is:

$$f_0(\bar{s}) = 2 + \frac{1}{\pi} \int_A^B d\bar{s}' \bar{\rho}' \int_0^\pi \frac{d\gamma}{\bar{R}^3} \left\{ f_0(\bar{s}') \left[ \bar{\rho} \cos \alpha' \cos \gamma - \right. \right. \\ \left. \left. - (\bar{\rho}' \cos \alpha' + (\bar{z} - \bar{z}') \sin \alpha') \cos^2 \gamma \right] + g_0(\bar{s}') (\bar{z} - \bar{z}') \sin^2 \gamma \right\}, \quad (\text{B.18})$$

$$g_0(\bar{s}) = -2 \sin \alpha - \frac{1}{\pi} \int_A^B d\bar{s}' \bar{\rho}' \int_0^\pi \frac{d\gamma}{\bar{R}^3} \left\{ g_0(\bar{s}') \left[ \bar{\rho}' \cos \alpha \cos \gamma - \right. \right. \\ \left. \left. - (\bar{\rho} \cos \alpha + (\bar{z}' - \bar{z}) \sin \alpha) \cos^2 \gamma \right] + f_0(\bar{s}') \left[ \bar{\rho} \sin \alpha' \cos \alpha - \right. \right. \\ \left. \left. - \bar{\rho}' \sin \alpha \cos \alpha' - (\bar{z} - \bar{z}') \sin \alpha \sin \alpha' \right] \sin^2 \gamma \right\}. \quad (\text{B.19})$$

The higher-order approximations are obtained by putting  $n = 1, 2, 3, \dots$  in the following coupled equations:

$$f_n(\bar{s}) = -\frac{1}{\pi} \sum_{\ell=0}^n \int_A^B d\bar{s}' \bar{\rho}' \int_0^\pi \frac{d\gamma}{\bar{R}^3} \left[ \frac{(n-\ell)\bar{R}}{\bar{R} + \bar{z}' - \bar{z}} - 1 \right] \frac{(\bar{R} + \bar{z}' - \bar{z})^{n-\ell}}{(n-\ell)!} \chi \\ \chi \left\{ f_\ell(\bar{s}') \left[ \bar{\rho} \cos \alpha' \cos \gamma - (\bar{\rho}' \cos \alpha' + (\bar{z} - \bar{z}') \sin \alpha') \cos^2 \gamma \right] + \right. \\ \left. + g_\ell(\bar{s}') (\bar{z} - \bar{z}') \sin^2 \gamma \right\}, \quad (\text{B.20})$$

$$\begin{aligned}
g_n(\bar{s}) = & \frac{1}{\pi} \sum_{\ell=0}^n \oint_A^B d\bar{s}' \bar{\rho}' \int_0^\pi \frac{d\gamma}{\bar{R}^3} \left[ \frac{(n-\ell)\bar{R}}{\bar{R} + \bar{z}' - \bar{z}} - 1 \right] \frac{(\bar{R} + \bar{z}' - \bar{z})^{n-\ell}}{(n-\ell)!} \chi \\
& \chi \left\{ g_\ell(\bar{s}') \left[ \bar{\rho}' \cos \alpha \cos \gamma - (\bar{\rho} \cos \alpha + (\bar{z}' - \bar{z}) \sin \alpha) \cos^2 \gamma \right] + \right. \\
& \left. + f_\ell(\bar{s}') \left[ \bar{\rho} \sin \alpha' \cos \alpha - \bar{\rho}' \sin \alpha \cos \alpha' + (\bar{z}' - \bar{z}) \sin \alpha \sin \alpha' \right] \sin^2 \gamma \right\}.
\end{aligned} \tag{B.21}$$

It will be shown later that both  $f_0, g_0$  and  $f_1, g_1$  are needed to obtain the first-order term in the low frequency expansion of the far field. From a numerical viewpoint, it is thus apparent that it is simpler to deal directly with the system (B.12) - (B.13), rather than with the two systems (B.18) - (B.19) and (B.20) - (B.21).

#### B.4 Far-Field Expansion

Let us suppose that the scattering body (or bodies) occupies the finite volume  $V'$  of Fig. B-3, so that the secondary sources are confined within a sphere of finite radius. The scattered electric field at a point  $(r, \theta, \phi)$  in the far zone is:

$$\underline{E}^s = \sum_{\ell} \sum_m (a_\ell^m \underline{E}_E^s + b_\ell^m \underline{E}_M^s), \tag{B.22}$$

where the subscripts E and M correspond respectively to the TM and TE modes,

$$\begin{aligned}
\underline{E}_E^s &= (-i)^\ell e^{ikr} \nabla Y_\ell^m(\theta, \phi) = \\
&= (-i)^\ell \frac{e^{ikr}}{r} \left\{ \frac{\partial Y_\ell^m(\theta, \phi)}{\partial \theta} \hat{\theta} + \frac{im}{\sin \theta} Y_\ell^m(\theta, \phi) \hat{\phi} \right\}, \tag{B.23}
\end{aligned}$$

$$\begin{aligned}
\underline{E}_M^s &= -(-i)^\ell e^{ikr} \hat{r} \wedge \nabla Y_\ell^m(\theta, \phi) = \\
&= -(-i)^\ell \frac{e^{ikr}}{r} \left\{ \frac{\partial Y_\ell^m(\theta, \phi)}{\partial \theta} \hat{\phi} - \frac{im}{\sin \theta} Y_\ell^m(\theta, \phi) \hat{\theta} \right\}, \tag{B.24}
\end{aligned}$$

with

$$Y_\ell^m(\theta, \phi) = \left[ (2\ell + 1) \frac{(\ell - m)!}{(\ell + m)!} \right]^{1/2} P_\ell^m(\cos \theta) e^{im\phi}, \tag{B.25}$$

$$Y_\ell^{-m}(\theta, \phi) = (-1)^m Y_\ell^{m*}(\theta, \phi), \tag{B.26}$$

$$\begin{aligned}
P_\ell^{-m}(\cos \theta) &= 0, \quad \text{for } \ell < m, \\
&= (-1)^m \frac{(\ell - m)!}{(\ell + m)!} P_\ell^m(\cos \theta), \quad \text{for } \ell \geq m. \tag{B.27}
\end{aligned}$$

The coefficients  $a_\ell^m$  and  $b_\ell^m$  are given by:

$$a_\ell^m = \frac{Z}{4\pi} \int_{V'} \underline{J} \cdot \nabla' \wedge \left\{ \nabla' \wedge \left[ \underline{r}' \pi_\ell^{-m}(\underline{r}') \right] \right\} dV', \tag{B.28}$$

$$b_\ell^m = \frac{ikZ}{4\pi} \int_{V'} \underline{J} \cdot \nabla' \wedge \left[ \underline{r}' \pi_\ell^{-m}(\underline{r}') \right] dV', \tag{B.29}$$



where  $\underline{J}$  is the true volume current density, i. e.

$$\nabla \wedge \underline{H} = \underline{J} - i\omega \epsilon_0 \underline{E}, \quad \nabla \wedge \underline{E} = i\omega \mu_0 \underline{H}, \quad \nabla \cdot \underline{J} - i\omega \rho = 0, \quad (\text{B. 30})$$

and

$$\pi_{\ell}^{-m}(\underline{r}) = j_{\ell}(kr) Y_{\ell}^{-m}(\theta, \phi), \quad j_{\ell}(kr) = \sqrt{\frac{\pi}{2kr}} J_{\ell + \frac{1}{2}}(kr). \quad (\text{B. 31})$$

The above results are exact. If  $kr' \ll 1$  in  $V'$ , then the multipole description of the scattered far field becomes useful; by replacing  $j_{\ell}(kr')$  with its first term in the expansion for small argument in  $a_{\ell}^m$  ( $b_{\ell}^m$ ), one obtains the contribution of the electric (magnetic) multipole of order  $2^{\ell}$ . In particular,  $a_{\ell}^m$  and  $b_{\ell}^m$  vanish for  $\ell = 0$  (no radiating monopoles); thus, the leading term is due to the electric and magnetic dipoles.

Finally, we remark that in (B. 28) and (B. 29):

$$\nabla' \wedge \left[ \underline{r}' \pi_{\ell}^{-m}(\underline{r}') \right] = -j_{\ell}(kr') \left\{ \hat{\theta}' \frac{i m}{\sin \theta'} + \hat{\phi}' \frac{\partial}{\partial \theta'} \right\} Y_{\ell}^{-m}(\theta', \phi'), \quad (\text{B. 32})$$

$$\begin{aligned} \nabla' \wedge \left\{ \nabla' \wedge \left[ \underline{r}' \pi_{\ell}^{-m}(\underline{r}') \right] \right\} &= \hat{r}' \ell(\ell+1) \frac{j_{\ell}(kr')}{r'} Y_{\ell}^{-m}(\theta', \phi') + \\ &+ \frac{1}{r'} \frac{\partial}{\partial r'} \left[ r' j_{\ell}(kr') \right] \left\{ \hat{\theta}' \frac{\partial}{\partial \theta'} - \frac{i m}{\sin \theta'} \hat{\phi}' \right\} Y_{\ell}^{-m}(\theta', \phi'). \end{aligned} \quad (\text{B. 33})$$

The above formulas are useful if higher-order approximations (such as quadrupole contributions) are desired in the low-frequency expansion of the far-field. The leading contribution is due to the electric and magnetic dipoles, and is considered in detail in the following section.

### B.5 Dipole Contributions to the Backscattered Field

The radiation field due to the electric dipole  $\underline{P}$  is:

$$\begin{aligned}\underline{E}^s &= -\frac{k^3}{4\pi\epsilon_0} \frac{e^{ikr}}{kr} \left[ (\underline{P} \wedge \hat{\underline{r}}) \wedge \hat{\underline{r}} \right], \\ \underline{H}^s &= -\frac{k^3}{4\pi\epsilon_0} \frac{e^{ikr}}{kr} (\underline{P} \wedge \hat{\underline{r}}),\end{aligned}\tag{B.34}$$

where

$$\underline{P} = \frac{i}{\omega} \int_{V'} \underline{J} dV', \quad (\omega = k/\sqrt{\epsilon_0 \mu_0}).\tag{B.35}$$

The radiation field due to the magnetic dipole  $\underline{M}$  is:

$$\begin{aligned}\underline{H}^s &= -\frac{k^3}{4\pi} \frac{e^{ikr}}{kr} \left[ (\underline{M} \wedge \hat{\underline{r}}) \wedge \hat{\underline{r}} \right], \\ \underline{E}^s &= \frac{k^3}{4\pi} \frac{e^{ikr}}{kr} (\underline{M} \wedge \hat{\underline{r}}),\end{aligned}\tag{B.36}$$

where

$$\underline{M} = \frac{1}{2} \int_{V'} (\underline{r}' \wedge \underline{J}) dV' .\tag{B.37}$$

By using the results of section B.2, it is found that

$$\underline{P} = \frac{i\epsilon_0}{k} \int_A^B ds' \int_0^{2\pi} d\phi' \rho' e^{ikz'} \left\{ f(s') \cos \phi' \hat{\underline{t}}' + g(s') \sin \phi' \hat{\underline{\phi}}' \right\},\tag{B.38}$$

and since

$$\begin{aligned}\hat{\underline{t}}' &= \sin \alpha' \cos \phi' \hat{\underline{x}} + \sin \alpha' \sin \phi' \hat{\underline{y}} + \cos \alpha' \hat{\underline{z}}, \\ \hat{\underline{\phi}}' &= -\sin \phi' \hat{\underline{x}} + \cos \phi' \hat{\underline{y}}.\end{aligned}\tag{B.39}$$

it follows that

$$\underline{P} = P_x \hat{x} = \hat{x} \frac{i\pi\epsilon_0}{k} \int_A^B ds' \rho' e^{ikz'} \left\{ f(s') \sin \alpha' - g(s') \right\}. \quad (\text{B. 40})$$

Similarly, it can be proven that

$$\underline{M} = M_y \hat{y} = \hat{y} \left(-\frac{\pi}{2} Y\right) \int_A^B ds' \rho' e^{ikz'} \left\{ f(s') (\rho' \cos \alpha' - z' \sin \alpha') + g(s') z' \right\}. \quad (\text{B. 41})$$

The far backscattered field due to the electric and magnetic dipoles is:

$$\underline{E}^{\text{b. s.}} = \frac{e^{ikr}}{kr} F \hat{x}, \quad F = F_e + F_m, \quad (\text{B. 42})$$

where  $F_e$  and  $F_m$  are the electric and magnetic dipole far field coefficients:

$$F_e = \frac{k^3}{4\pi\epsilon_0} P_x = \frac{i}{4} k^2 \int_A^B ds' \rho' e^{ikz'} \left\{ f(s') \sin \alpha' - g(s') \right\}, \quad (\text{B. 43})$$

$$F_m = -\frac{k^3 Z}{4\pi} M_y = \frac{k^3}{8} \int_A^B ds' \rho' e^{ikz'} \left\{ f(s') (\rho' \cos \alpha' - z' \sin \alpha') + g(s') z' \right\}. \quad (\text{B. 44})$$

Let us now consider the low-frequency approximations to Eqs. (B. 43) and (B. 44). By using (B. 17) and expanding the factor  $e^{ikz'}$  in powers of  $kz'$ , it is found that

$$\begin{aligned} F_e &= \frac{i}{4} \delta^2 \int_A^B d\bar{s}' \bar{\rho}' \left[ f_0(\bar{s}') \sin \alpha' - g_0(\bar{s}') \right] - \\ &- \frac{\delta^3}{4} \int_A^B d\bar{s}' \bar{\rho}' \left\{ \bar{z}' \left[ f_0(\bar{s}') \sin \alpha' - g_0(\bar{s}') \right] + f_1(\bar{s}') \sin \alpha' - g_1(\bar{s}') \right\} + O(\delta^4), \end{aligned} \quad (\text{B. 45})$$

$$F_m = \frac{\delta^3}{8} \int_A^B d\bar{s}' \bar{\rho}' \left\{ f_0(\bar{s}') \left[ \bar{\rho}' \cos \alpha' - \bar{z}' \sin \alpha' \right] + g_0(\bar{s}') \bar{z}' \right\} + O(\delta^4). \quad (\text{B. 46})$$

It can be proven that the integral in the term  $O(\delta^2)$  in  $F_e$  is always equal to zero, so that both  $F_e$  and  $F_m$  are  $O(\delta^3)$ . The solutions  $f_0, g_0$  of the system (B. 18) - (B. 19) determine  $F_m$ , whereas both  $f_0, g_0$  and  $f_1, g_1$  are needed to find  $F_e$ ; thus, four near-field quantities determine only two far-field quantities. A reduction in the number of needed near-field functions can be achieved only by recognizing that both electric and magnetic fields are gradients of potential functions, in the static ( $k \rightarrow 0$ ) limit. This is done in other methods, such as Stevenson's; the present approach is specially suitable for numerical evaluation of surface currents and far-field dipole contributions, not for low-frequency expansions in powers of  $\delta$ .

#### B.6 Comparison With Siegel's Formula

In this section, a comparison of our results (B. 43) and (B. 44) with those of Siegel (1959) is performed. On the basis of physical intuition, Siegel assumes that for elongated bodies:

$$f(s) = 2, \quad (\text{B. 47})$$

$$F_e = F_m. \quad (\text{B. 48})$$

Hypothesis (B. 47) corresponds to the zeroth-order approximating

$$f(s) = 2, \quad g(s) = -2 \sin \alpha \quad (\text{B. 49})$$

to the solution of the system (B. 12)-(B. 13). Now set  $e^{ikz'} \approx 1$  in Eq. (B. 44) and  $e^{ikz'} \approx 1 + ikz'$  in Eq. (B. 43), observe that  $ds' \sin \alpha' = d\rho'$ , and that,

obviously

$$\int_A^B ds' \rho' \sin \alpha' = \int_A^B \rho' d\rho' = 0 . \quad (\text{B. 50})$$

Thus, within the approximations (B. 49),

$$F_e = -k^3 \int_A^B ds' \rho' z' \sin \alpha' = -k^3 \int_A^B dz' \rho' z' \tan \alpha' , \quad (\text{B. 51})$$

$$F_m = \frac{F_e}{2} + \frac{k^3}{4} \int_A^B dz' \rho'^2 . \quad (\text{B. 52})$$

Now,

$$\int_A^B dz' \rho'^2 = \frac{V}{\pi} , \quad (\text{B. 53})$$

where  $V$  is the volume of the scatterer, hence:

$$F_m = \frac{F_e}{2} + \frac{k^3}{4\pi} V . \quad (\text{B. 54})$$

Therefore hypothesis (B. 48) implies that

$$F_e = F_m = \frac{k^3}{2\pi} V , \quad (\text{B. 55})$$

so that the backscattering cross section assumes the familiar form:

$$\sigma = \frac{4}{\pi} k^4 V^2 . \quad (\text{B. 56})$$



### B.7 Numerical Formulation

In order to solve numerically the system (B.12) - (B.13), we replace the two integral equations with a system of  $2N$  linear algebraic equations obtained by dividing the profile AB into  $N$  arcs over each of which  $f(s)$  and  $g(s)$  are assumed to be constant (see Fig. B-4).

We indicate with  $\Delta s_\ell$  the length of the  $\ell$ -th arc ( $1 \leq \ell \leq N$ ), with  $f_\ell$  and  $g_\ell$  the constant values of  $f(s)$  and  $g(s)$  over  $\Delta s_\ell$ , and with  $\rho_\ell, z_\ell, \alpha_\ell$  the values of  $\rho, z, \alpha$  corresponding to the midpoint of the  $\ell$ -th arc. Also, the quantities  $\Delta_0, \Delta_1, \Delta_2$  of Eqs. (B.11) are evaluated in correspondence of these midpoints; for example,  $\Delta_0 = \Delta_0$  means that the first of the integrals

$$\int_{\ell, n}^{\rho, z} \int_{n, \ell}^{\rho', z'}$$

(B.11) is to be evaluated with  $\rho = \rho_n, z = z_n, \rho' = \rho_\ell, z' = z_\ell$  in the

expression (B.9) for  $R$ . The integrals  $\int_A^B$  in (B.12) and (B.13) are thus

replaced by summations over the  $N$  arcs.

A difficulty arises when the fixed point  $n$  and the running point  $\ell$  in the summations belong to the same arc (i.e.,  $\ell = n$ ). This difficulty is due to the singularity in the kernels of the integral equations, and complicates the problem considerably at high frequencies (Goodrich and Stenger, 1969). At low frequencies, however, the difficulty can be avoided in the following manner: we divide the  $n$ -th arc in two equal parts and take  $f = f_n$ , and  $g = g_n$  on both, but choose the summation points  $n_-$  and  $n_+$  at distances  $\frac{\Delta s_n}{8}$  from the midpoint  $n$  (see Fig. B-4). The system (B.12) - (B.13) is thus replaced by the following system of  $2N$  linear algebraic equations in the  $2N$  unknowns  $f_n$  and  $g_n$  ( $1 \leq n \leq N$ ):

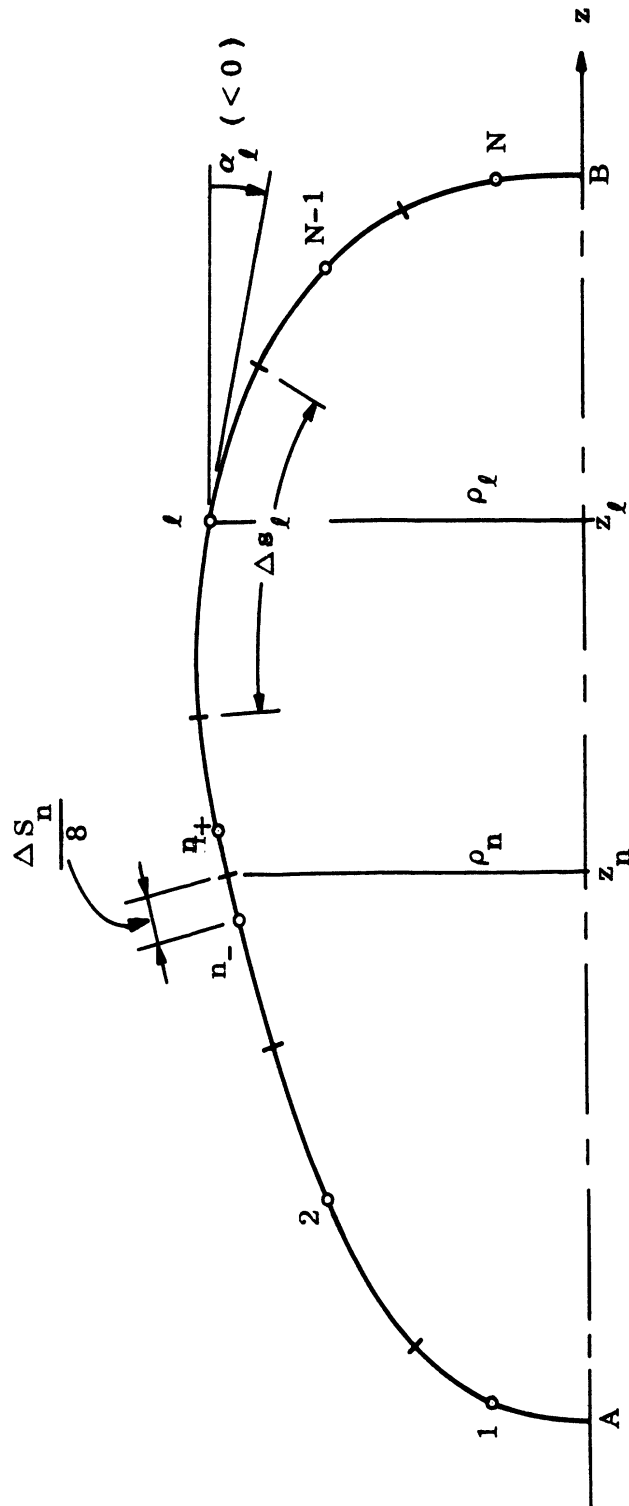


FIG. B-4: Geometry for Numerical Computations.



$$\begin{aligned}
f_n = & 2 - \frac{1}{\pi} \sum_{\ell=1}^N \rho_{\ell} \Delta s_{\ell} e^{ik(z_{\ell} - z_n)} \left\{ f_{\ell} \left[ \Delta_0 \rho_n \cos \alpha_{\ell} - \right. \right. \\
& \left. \left. - \Delta_2 \left( \rho_{\ell} \cos \alpha_{\ell} + (z_n - z_{\ell}) \sin \alpha_{\ell} \right) \right] + g_{\ell} \Delta_1 \left( z_n - z_{\ell} \right) \right\} - \\
& - \frac{\Delta s_n}{2\pi} \rho_{n-} e^{ik(z_{n-} - z_n)} \left\{ f_n \left[ \Delta_0 \rho_n \cos \alpha_{n-} - \right. \right. \\
& \left. \left. - \Delta_2 \left( \rho_{n-} \cos \alpha_{n-} + (z_n - z_{n-}) \sin \alpha_{n-} \right) \right] + g_n \Delta_1 \left( z_n - z_{n-} \right) \right\} - \\
& - \frac{\Delta s_n}{2\pi} \rho_{n+} e^{ik(z_{n+} - z_n)} \left\{ f_n \left[ \Delta_0 \rho_n \cos \alpha_{n+} - \right. \right. \\
& \left. \left. - \Delta_2 \left( \rho_{n+} \cos \alpha_{n+} + (z_n - z_{n+}) \sin \alpha_{n+} \right) \right] + g_n \Delta_1 \left( z_n - z_{n+} \right) \right\} ,
\end{aligned}$$

(1 ≤ n ≤ N) ,

(B. 59)

$$\begin{aligned}
g_n = & -2 \sin \alpha_n + \frac{1}{\pi} \sum_{\ell=1}^N \rho_\ell \Delta s_\ell e^{ik(z_\ell - z_n)} \left\{ g_\ell \left[ \Delta_{\ell,n} \rho_\ell \cos \alpha_n - \right. \right. \\
& - \Delta_{\ell,n} \left( \rho_n \cos \alpha_n + (z_\ell - z_n) \sin \alpha_n \right) \left. \right] + f_{\ell,n} \Delta_{\ell,n} \left[ \rho_n \cos \alpha_n \sin \alpha_\ell - \right. \\
& \left. \left. - \rho_\ell \cos \alpha_\ell \sin \alpha_n + (z_\ell - z_n) \sin \alpha_n \sin \alpha_\ell \right] \right\} + \\
& + \frac{\Delta s_n}{2\pi} \rho_{n-} e^{ik(z_{n-} - z_n)} \left\{ g_n \left[ \Delta_{n-,n} \rho_{n-} \cos \alpha_n - \Delta_{n-,n} \left( \rho_n \cos \alpha_n + \right. \right. \right. \\
& \left. \left. \left. + (z_{n-} - z_n) \sin \alpha_n \right) \right] + f_{n-,n} \Delta_{n-,n} \left[ \rho_n \cos \alpha_n \sin \alpha_{n-} - \rho_{n-} \cos \alpha_{n-} \sin \alpha_n + \right. \right. \\
& \left. \left. \left. + (z_{n-} - z_n) \sin \alpha_n \sin \alpha_{n-} \right] \right\} + \\
& + \frac{\Delta s_n}{2\pi} \rho_{n+} e^{ik(z_{n+} - z_n)} \left\{ g_n \left[ \Delta_{n+,n} \rho_{n+} \cos \alpha_n - \Delta_{n+,n} \left( \rho_n \cos \alpha_n + \right. \right. \right. \\
& \left. \left. \left. + (z_{n+} - z_n) \sin \alpha_n \right) \right] + f_{n+,n} \Delta_{n+,n} \left[ \rho_n \cos \alpha_n \sin \alpha_{n+} - \rho_{n+} \cos \alpha_{n+} \sin \alpha_n + \right. \right. \\
& \left. \left. \left. + (z_{n+} - z_n) \sin \alpha_n \sin \alpha_{n+} \right] \right\} \quad (1 \leq n \leq N) , \tag{B.60}
\end{aligned}$$

where the prime attached to the summation sign  $\sum$  means that the term  $l = n$  must be excluded from the sum.

The distance of  $n_+$  and  $n_-$  from  $n$  must be less than  $\frac{\Delta s_n}{4}$ , because

$\Delta_0$ ,  $\Delta_1$  and  $\Delta_2$  become infinite at  $n$ . The choice  $\frac{\Delta s_n}{8}$  is arbitrary, but we have verified numerically in a variety of cases that other choices produce very small variations (of the order of one per cent) in the surface current components.

The correctness of (B. 59) - (B. 60) and of the related computer program has been checked by calculating the surface currents on a sphere of radius  $a$  with  $ka = 0.1$  and by comparing these results with the numerical tables of Ducmanis and Liepa (1965), which were based on the Mie series solution to the scattering problem. The excellent agreement between these two different approaches is exhibited in Fig. B-5.

Once the surface current components are known, it is an easy matter to derive the electric and magnetic dipole far-field coefficients  $F_e$  and  $F_m$ . From (B. 43) and (B. 44) :

$$F_e = \frac{i}{4} k^2 \sum_{n=1}^N \rho_n \Delta s_n e^{ikz_n} (f_n \sin \alpha_n - g_n) , \quad (\text{B. 61})$$

$$F_m = \frac{k^3}{8} \sum_{n=1}^N \rho_n \Delta s_n e^{ikz_n} [f_n (\rho_n \cos \alpha_n - z_n \sin \alpha_n) + g_n z_n] . \quad (\text{B. 62})$$

For a sphere with  $ka = 0.1$ , it is found that  $F_e = 1.008 \times 10^{-3} + i 7 \times 10^{-7}$  and  $F_m = 0.497 \times 10^{-3} - i 1.6 \times 10^{-7}$ ; the exact values are  $F_e = 10^{-3}$  and  $F_m = 0.5 \times 10^{-3}$ .

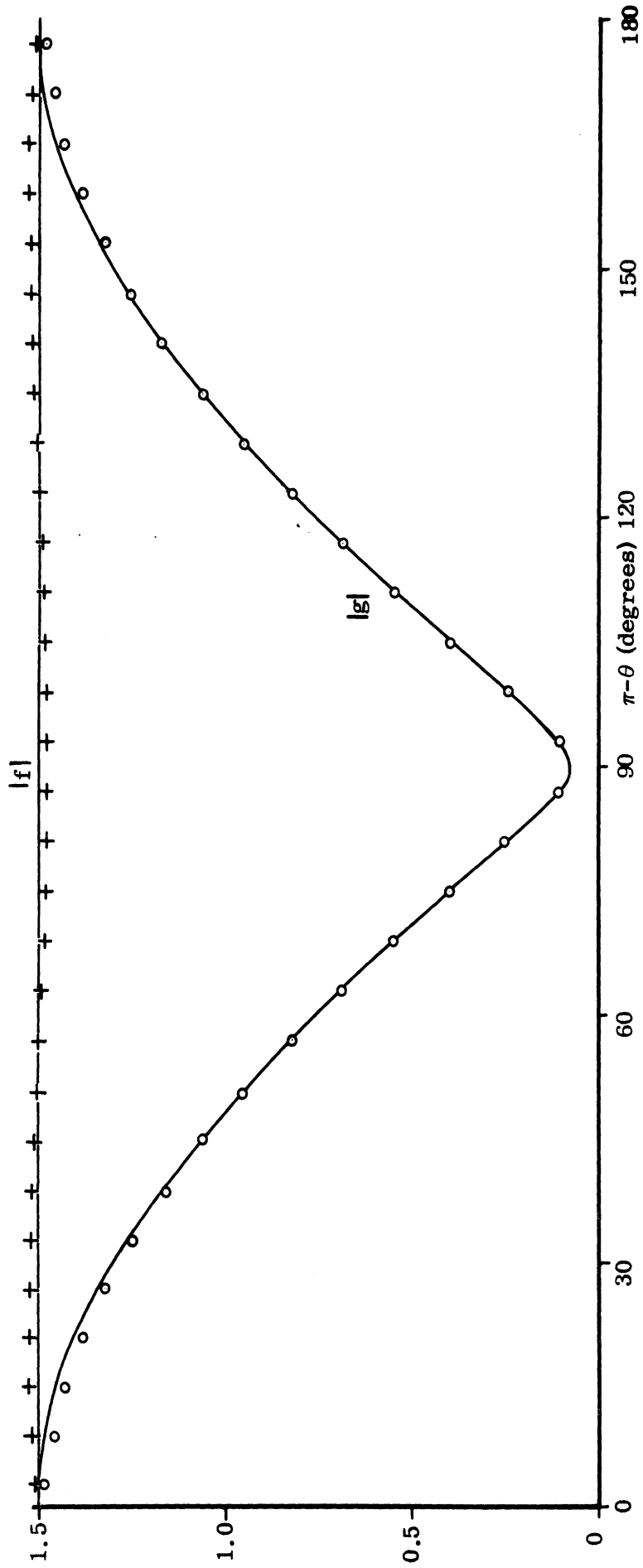


FIG. B-5: Amplitude of Surface Currents on a Sphere with  $ka = 0.1$ . Comparison Between our Numerical Results with  $N=30$  (++++  $|f|$ ; o o o  $|g|$ ) and the Exact Results (Ducmanis and Liepa, 1965).

The computer program based on Eqs. (B.59) - (B.63) has been applied to a variety of scattering shapes. The results obtained are presented in Chapter 4. Among these shapes is a round-backed cone, whose far-field coefficients agree very well with the values obtained by another method in Appendix A.

#### B.8 Computer Program \*

The main program and the various subroutines for the solution of the system (B.59) - (B.60) and for the determination of  $F_e$  and  $F_m$  are printed in the following, with a few obvious changes of symbols. We only remark that the total number of subdivisions of the arc AB is indicated by  $M = MA + MB + MC$ , instead of N. The most general profile AB that can thus be dealt with is made of three parts, with subdivisions MA, MB and MC; the length of the subdivisions is a constant within each part. The contour part with MA subdivisions always begins at A and is either a straight line (such as for a cone-sphere) or an arc of a circle whose tangent is perpendicular to the symmetry axis at A; thus  $MA \neq 0$  always.

The contour part with MB subdivisions is a straight line joining the first and third parts of AB (such as the conical part of a sphere-cone-sphere), or a straight line ending at B (such as for a flat-base cone), or an arc of a circle ending at B with a tangent perpendicular to the symmetry axis (such as for a cone-sphere). The contour part with MC subdivisions is either a straight line ending at B (such as the base of a flat-base cone with a rounded nose), or an arc of a circle perpendicular to the z-axis at B (such as for a sphere-cone-sphere). If the contour AB has two parts only, such as for a cone-sphere or a flat-base cone, then  $MC = 0$ ; if AB has one part only, such as for a sphere, then  $MB=MC=0$ . If the contour AB is more complicated than those considered in the present report and must be broken into four or more parts, the computer program can still be used as it stands, the only needed modifications being the appropriate additions to the data subroutine.

---

\* This program was written by Mr. Wei Cheng Yang.

LIST OF THE MAIN PROGRAM

```

FORTRAN IV G COMPILER      MAIN
0001      C CMPLX DELTA0,DELTA1,DELTA2,W,MATRIX(60,64),X(60),
1 FE,FM,FEM,EXPIKZ
0002      REAL K,S(32),C(32),RHO(32,3),Z(32,3),ALF(30,3),ARC(32,3),V(60)
0003      COMMON M2,PI,K,ZZPRM/DEL/DELTA0,DELTA1,DELTA2/SOL/MATRIX,IPS(60),
1 V,X/DAI/RHO,Z,ALF,ARC,A,RA,H,THEIA
0004      PI=3.1415927
0005      9 READ(5,60) M,MA,MB,MC,IA,IB,IC,A,RA,K,H,DEGREE
0006      WRITE(6,70)M,MA,MB,MC,A,RA,K,H,DEGREE
0007      WRITE(6,10)
0008      M2=M*2
0009      MM=M+1
0010      MP=M+2
0011      MO=M2+3
0012      MJ=M2+4
0013      THETA=DEGREE*PI/180.0
C
C      *** CALL SUBROUTINE TO GET RHO, Z, ALF AND ARC.
C
0014      CALL DATA(IA,0,MA)
0015      IF(MA.EQ.M) GOTO 102
0016      CALL DATA(IB,MA,MA+MB)
0017      IF(MA+MB.EQ.M) GO TO 102
0018      CALL DATA(IC,MA+MB,M)
0019      102 DO 103 I=1,M
0020      S(I)=SIN(ALF(I,1))
0021      103 C(I)=CCS(ALF(I,1))
C
C      *** FORM A MATRIX LINEAR SYSTEM BY COUPLE OF INTEGRAL EQUATIONS.
C

```

```

0022      DO 2 N=1,M
0023      NA=2*N-1
0024      NB=2*N
0025      NC=N+MP
0026      DO 104 I=1,2
0027      RHO(M+I,1)=RHC(N,I+1)
0028      Z(M+I,1)=Z(N,I+1)
0029      ARC(M+I,1)=ARC(N,I+1)
0030      S(M+I)=SIN(ALF(N,I+1))
0031      104 C(M+I)=CCS(ALF(N,I+1))
0032      DO 5 L=1,MP
0033      LA=L+MP
0034      IF(L.EQ.N) GO TO 5
0035      ZZPRM=Z(L,1)-Z(N,1)
0036      W=RHO(L,1)*ARC(L,1)*CEXP((0.0,1.0)*K*ZZPRM)/PI
0037      CALL DELTA(RHO(N,1),RHO(L,1))
0038      MATRIX(NA,L)=W*(DFLTAO*RHC(N,1)*C(L)-DELTA2*(RHO(L,1)*C(L)-ZZPRM*
1 S(L)))
0039      MATRIX(NA,LA)=W*DELTA1*(-ZZPRM)
0040      MATRIX(NB,L)=W*DELTA1*(RHC(N,1)*S(L)*C(N)-RHO(L,1)*S(N)*C(L)+ZZPRM
1*S(N)*S(L))
0041      MATRIX(NB,LA)=W*(DELTAO*RHO(L,1)*C(N)-DELTA2*(RHO(N,1)*C(N)+ZZPRM*
1 S(N)))
0042      5 CONTINUE
0043      MATRIX(NA,N)=(MATRIX(NA,MM)+MATRIX(NA,MP))/2.0+1.0
0044      MATRIX(NA,NC)=(MATRIX(NA,MO)+MATRIX(NA,MJ))/2.0
0045      MATRIX(NB,N)=(MATRIX(NB,MM)+MATRIX(NB,MP))/2.0
0046      MATRIX(NB,NC)=(MATRIX(NB,MO)+MATRIX(NB,MJ))/2.0-1.0
0047      DO 6 I=1,M2
0048      DO 6 J=MM,M2
0049      6 MATRIX(I,J)=MATRIX(I,J+2)
0050      DO 7 I=2,M2,2
0051      V(I-1)=2.0
0052      7 V(I)=2.0*S(I/2)
C
C
C      *** CALL SUBROUTINES TO SOLVE THE MATRIX SYSTEM.

```

```

0053 CALL DECCMP
0054 CALL SOLVE
0055 DO 8 I=1,M2
0056 ABSVAL=CABS(X(I))
0057 PHASE=ATAN(AIMAG(X(I))/REAL(X(I)))
0058 IF(I.GT.M) GO TO 4
0059 WRITE(6,20)I,X(I),ABSVAL,PHASE
0060 GO TO 8
0061 4 J=I-M
0062 WRITE(6,50)J,X(I),ABSVAL,PHASE
0063 8 CONTINUE
C
C
C *** CALCULATE FE AND FM.
0064 FE=(0.0,0.0)
0065 FM=FE
0066 DO 101 I=1,M
0067 EXPKZ=CEXP((0.0,1.0)*K*Z(I,1))
0068 FE=FE+RHO(I,1)*ARC(I,1)*EXPKZ*(X(I)*S(I)-X(I+M))
0069 FM=FM+RHO(I,1)*EXPKZ*(X(I)*(RHO(I,1)*C(I))-Z(I,1)*S(I))+X(I+M)*
1 Z(I,1)*ARC(I,1)
0070 101 CONTINUE
0071 FE=FE*(0.0,1.0)*K*K/4.0
0072 FM=FM*K*K/8.0
0073 FEM=FE+FM
0074 ABSFEM=CABS(FEM)
0075 PHSFEM=ATAN(AIMAG(FEM)/REAL(FEM))
0076 WRITE(6,80) FE,FM,FEM,ABSFEM,PHSFEM
0077 GO TO 9
0078 10 FORMAT(14X,'REAL PART',11X,'IMAG. PART',10X,'ARS. VALUE',10X,
1 'PHASE')
0079 20 FORMAT(' F(',I2,')',4E20.8)
0080 50 FORMAT(' G(',I2,')',4E20.8)
0081 60 FORMAT(7I3,5F4.1)
0082 70 FORMAT('OM =',I3,' MA =',I3,' MB =',I3,' MC =',I3/'OA =',F4.1,
1 ' RA =',F4.1,' K =',F4.1,' H =',F4.1,' DEGREE =',F5.1)
0083 80 FORMAT('OFE =',2E18.8/'OFM =',2E18.8/'OFM =',2E18.8/'O(FE+FM) =',2E18.8/
1 'OARS. VALUE OF (FE+FM) =',E18.8/'OPHASE OF (FE+FM) =',E18.8)
0084 CALL SYSTEM
0085 END

```



LIST OF SUBROUTINE FOR DATA

FORTRAN	IV G COMPILER	DATA
0001		SUBROUTINE DATA(IN,MY,MZ)
0002		REAL MR(3),RHO(32,3),Z(32,3),ALF(30,3),ARC(32,3)
0003		COMMON M2,PI/DAT/RHC,Z,ALF,ARC,A,RA,H,THETA
0004		RT=PI/2.0
0005		MX=MY+1
0006		SI=SIN(THETA)
0007		CI=CCS(THETA)
	C	
	C	*** CALCULATE ALL VALUES OF RHO, Z, ALF AND ARC.
	C	
0008		GO TO (1,2,3,4,5),IN
0009	1	BETA=RT-THETA
0010		R=RA
0011		AA=RA/ST
0012		GC TO 10
0013	2	BETA=RT+THETA
0014		R=RA+A*ST/CT
0015		AA=RA/ST+A/CT
0016		GO TO 10
0017	3	BETA=THETA
0018		IF(THETA.LT.RT) GC TO 17
0019		R=A
0020		GO TO 18
0021	17	R=A+RA*CI/ST
0022	18	AA=0.0
0023	10	BETA=BETA/(2*(MZ-MY))
0024		WA=BETA/H
0025		DO 11 I=MX,MZ
0026		GO TO (12,13,13),IN
0027	12	WB=PI-FETA*(2*(I-MY)-1)
0028		GO TO 14
0029	13	WB=BETA*(2*(MZ-I)+1)

```

0030      14 ALF(I,1)=WD-RT
0031      ALF(I,2)=ALF(I,1)+B*G
0032      ALF(I,3)=ALF(I,1)-V*G
0033      DO 11 J=1,3
0034      WR=PT+ALF(I,J)
0035      RHO(I,J)=R*SIN(WR)
0036      Z(I,J)=R*CCS(WR)+AA
0037      11 ARC(I,J)=BETA*PI*2.0
0038      RETURN
0039      4  BETA=A/(M7-MY)
0040      WR=BETA/2.0
0041      WA=WR/H
0042      DO 15 I=NX,M7
0043      WD(1)=(I-MY)*BETA-VR+PA*CT/ST
0044      WD(2)=WD(1)-WA
0045      WD(3)=WD(1)+WA
0046      DO 15 J=1,3
0047      RHO(I,J)=WD(J)*ST
0048      Z(I,J)=WD(J)*CT
0049      ARC(I,J)=BETA
0050      15 ALF(I,J)=THETA
0051      RETURN
0052      5  BETA=(A*ST+PA*CT)/(M7-MY)
0053      WR=BETA/2.0
0054      WA=WR/H
0055      AA=(A+PA*CT/ST)*CT
0056      DO 16 I=MX,MZ
0057      WD(1)=(MZ-I)*BETA+WR
0058      WD(2)=WD(1)+WA
0059      WD(3)=WD(1)-WA
0060      DO 16 J=1,3
0061      RHO(I,J)=WD(J)
0062      Z(I,J)=AA
0063      ALF(I,J)=-PT
0064      16 ARC(I,J)=BETA
0065      RETURN
0066      END

```

LIST OF SUBROUTINE FOR  $\Delta_0, \Delta_1, \Delta_2$

```

FORTRAN IV G COMPILER      DELTA
0001      SUBROUTINE DELTA(RHC,RHOPRM)
0002      COMPLEX K(101),KO(101),K1(101),K2(101),DELTA0,DELTA1,DELTA2
0003      REAL GAMMA(101),KOREAL(101),KOIMAG(101),KIREAL(101),R(101),
1      KIIMAG(101),K2REAL(101),K2IMAG(101)
0004      COMMON M2,PI,C,ZZPRM/DEL/DELTA0,DELTA1,DELTA2
C
C      *** CALCULATE DELTA0, DELTA1 AND DELTA2.
C
0005      N=100
0006      H=0.01
0007      N1=N+1
0008      GAMMA(1)=0.0
0009      DO 3 I=2,N1
0010      3 GAMMA(I)=GAMMA(1)+(I-1)*H
0011      B=2.0*RHC*RHOPRM
0012      A=ZZPRM**2+RHC**2+RHOPRM**2
0013      DO 1 I=1,N1,1
0014      R(I)= SQRT(A-B*COS(PI*GAMMA(I)))
0015      IF( ABS(R(I)).LE.1.0E-4) GO TO 4
0016      K(I)=((0.0,1.0)*C-1.0/R(I))*CEXP((0.0,1.0)*C*R(I))/R(I)**2
0017      KO(I)=K(I)*COS(PI*GAMMA(I))
0018      K1(I)=K(I)*SIN(PI*GAMMA(I))**2
0019      K2(I)=K(I)*COS(PI*GAMMA(I))**2
0020      KOREAL(I)=REAL(KO(I))
0021      KOIMAG(I)=AIMAG(KO(I))
0022      KIREAL(I)=REAL(K1(I))
0023      KIIMAG(I)=AIMAG(K1(I))
0024      K2REAL(I)=REAL(K2(I))
0025      1 K2IMAG(I)=AIMAG(K2(I))
0026      DELREL=SIMPSPM(KOREAL,N,H)
0027      DELIMG=SIMPSPM(KOIMAG,N,H)
0028      DELTA0=CMPLX(DELREL,DELIMG)*PI
0029      DELREL=SIMPSPM(KIREAL,N,H)

```

```
0030 DELIMG=SIMPXM(K1IMAG,N,H)
0031 DELTA1=CMPLX(DELREL,DELIMG)*PI
0032 DELREL=SIMPXM(K2REAL,N,H)
0033 DELIMG=SIMPXM(K2IMAG,N,H)
0034 DELTA2=CMPLX(DELREL,DELIMG)*PI
0035 GO TO 5
0036 4 WRITE (6,30) RHO,RHOPRM,ZZPRM
0037 5 CONTINUE
0038 30 FORMAT(3F6.2,4X,'INTEGRAL FUNCTION IS DISCONTINUOUS')
0039 RETURN
0040 END
```

LIST OF SUBROUTINE FOR INTEGRATION BY SIMPSON'S RULE

```

FORTRAN IV G COMPILER      SIMPSM
-----
0001      REAL FUNCTION SIMPSM(Q,N,H)
0002      DIMENSION Q(101)
          C
          C      *** INTEGRATION BY SIMPSON'S RULE.
          C
0003      SIMPSM=Q(1)+4.0*Q(2)+Q(N+1)
0004      DO 1 I=4,N,2
0005      1 SIMPSM=SIMPSM+2.0*Q(I-1)+4.0*Q(I)
0006      SIMPSM=SIMPSM*H/3.0
0007      RETURN
0008      END

```

LIST OF SUBROUTINES TO SOLVE THE MATRIX SYSTEM  
 1- Subroutine DECOMP.

```

FORTRAN IV G_COMPILER      DECOMP
0001      SUBROUTINE DECOMP
0002      COMPLEX UL(60,64),PIVOT,EM
0003      REAL SCALES(60)
0004      COMMON N/SOL/UL,IPS(60)
C
C      *** DECOMPOSE THE MATRIX TO TWO TRIANGULAR FORM U AND L.
C
0005      DO 5 I=1,N
0006      IPS(I)=I
0007      RCWNRN=0.0
0008      DO 2 J=1,N
0009      W=CABS(UL(I,J))
0010      IF(ROWNRN-W) 1,2,2
0011      1 ROWNRN=W
0012      2 CONTINUE
0013      IF(ROWNRN) 3,4,3
0014      3 SCALES(I)=1.0/ROWNRN
0015      GO TO 5
0016      4 CALL SING(I)
0017      SCALES(I)=0.0
0018      5 CONTINUE
C
C      *** GAUSSIAN ELIMINATION WITH PARTIAL PIVOTING.
C
0019      NM1=N-1
0020      DO 16 K=1,NM1
0021      BIG=0.0
0022      DO 11 I=K,N
0023      IP=IPS(I)
0024      SIZE=CARS(UL(IP,K))*SCALES(IP)
0025      IF(SIZE-BIG) 11,11,10
0026      10 BIG=SIZE
0027      11 IDXPIV=I

```

0028	11 CONTINUE
0029	IF(BIG) 13,12,13
0030	12 CALL SING(2)
0031	GO TO 16
0032	13 IF(IDXPIV-K) 14,15,14
0033	14 J=IPS(K)
0034	IPS(K)=IPS(IDXPIV)
0035	IPS(IDXPIV)=J
0036	15 KP=IPS(K)
0037	PIVOT=UL(KP,K)
0038	KP1=K+1
0039	DO 16 I=KP1,N
0040	IP=IPS(I)
0041	EM=-UL(IP,K)/PIVOT
0042	UL(IP,K)=-EM
0043	DO 16 J=KP1,N
0044	UL(IP,J)=UL(IP,J)+EM*UL(KP,J)
0045	16 CONTINUE
0046	KP=IPS(N)
0047	IF(CABS(UL(KP,N))) 19,18,19
0048	18 CALL SING(2)
0049	19 RETURN
0050	END

LIST OF SUBROUTINES TO SOLVE THE MATRIX SYSTEM

2 - Subroutine SOLVE

```

FORTRAN IV G COMPILER      SOLVE
0001      SUBROUTINE SOLVE
0002      COMPLEX UL(60,64),X(60),SUM
0003      COMMON N/SOL/UL,IPS(60),B(60),X
C
C      *** BACK SUBSTITUTION TO SOLVE MAIRIX UL.
C
0004      NPI=N+1
0005      IP=IPS(1)
0006      X(1)=B(IP)
0007      DO 2 I=2,N
0008      IP=IPS(I)
0009      IM1=I-1
0010      SUM=(0.0,0.0)
0011      DO 1 J=1,IM1
0012      1 SUM=SUM+UL(IP,J)*X(J)
0013      2 X(I)=B(IP)-SUM
0014      IP=IPS(N)
0015      X(N)=X(N)/UL(IP,N)
0016      DO 4 IBACK=2,N
0017      I=NPI-IBACK
0018      IP=IPS(I)
0019      IP1=I+1
0020      SUM=(0.0,0.0)
0021      DO 3 J=IP1,N
0022      3 SUM=SUM+UL(IP,J)*X(J)
0023      4 X(I)=(X(I)-SUM)/UL(IP,I)
0024      RETURN
0025      END

```



LIST OF SUBROUTINES TO SOLVE THE MATRIX SYSTEM

3 - Subroutine SING

```

FORTRAN IV G COMPILER      SING
-----
0001      SUBROUTINE SING(IWHY)
0002      NOUT=6
          C
          C      *** MATRIX IS SINGULAR. NO SOLUTION.
          C
0003      GO TO (1,2),IWHY
0004      1 WRITE(NOUT,11)
0005      GC TO 10
0006      2 WRITE(NOUT,12)
0007      11 FORMAT(' MATRIX WITH ZERO ROW IN DECOMPOSE.')
0008      12 FORMAT(' SINGULAR MATRIX IN DECOMPOSE. ZERO DIVIDE IN SOLVE. ')
0009      10 RETURN
0010      END
    
```

## B.9 References

- Andreasen, M.G. (1965), "Scattering from Bodies of Revolution", IEEE Trans. AP-13, pp. 303-310.
- Ducmanis, J.A. and V.V. Liepa (1965), "Surface Field Components for a Perfectly Conducting Sphere", Radiation Laboratory Report No. 5548-3-T (Contract AF 19(628)-2374), The University of Michigan.
- Goodrich, R.F., and F. Stenger (1969), "Movable Singularities and Quadrature", Math. Comp. (to be published).
- Harrington, R.F., and J.R. Mautz (1969a), "Radiation and Scattering From Bodies of Revolution", Report AFCRL-69-0305 (Contract No. F-19628-67-C-0233), Syracuse University.
- Harrington, R.F., and J.R. Mautz (1969b), "Radiation and Scattering From Bodies of Revolution", App. Sci. Res. 20, pp. 405-435.
- Maue, A.W. (1949), "On the Formulation of a General Diffraction Problem Through an Integral Equation", Zeit. f. Phys. 126, pp. 601-618, (in German).
- Panofsky, W.K.H. and M. Phillips (1962), Classical Electricity and Magnetism, 2nd Edition, Addison-Wesley, Reading, Mass.
- Siegel, K.M. (1959), "Far Field Scattering from Bodies of Revolution", Appl. Sci. Res. B7, pp. 293-328.

## APPENDIX C

### INTEGRAL EQUATION FORMULATION OF LOW-FREQUENCY SCATTERING FROM A SLENDER CONE SURROUNDED BY A PENETRABLE OVERDENSE PLASMA SHEATH\*

#### C.1 The Fundamental Integral Equation

We shall consider a conical metallic shell coated with a thin overdense plasma sheath extending well beyond the rear of the shell (see Fig. C-1). The metallic shell should be a good approximation to a slender finite cone for frequencies in the Rayleigh region.

At a point  $\underline{x}_0$  exterior to both coating and shell, the total electric field intensity can be expressed in terms of the field components on the outer surface of the plasma sheath (denoted by  $S_2$ ) and on the inner portion of the conical shell (denoted by  $S_1^-$ ) by means of the relation:

$$\begin{aligned} \underline{E}(\underline{x}_0) = \underline{E}^0(\underline{x}_0) + \frac{1}{4\pi} \int_{S_2} \left\{ i\omega \mu_0 \hat{n} \wedge \underline{H} \Phi + (\hat{n} \wedge \underline{E}) \wedge \nabla \Phi + (\hat{n} \cdot \underline{E}^e) \nabla \Phi \right\} dS + \\ + \frac{1}{4\pi} \int_{S_1^-} \left\{ i\omega \mu_0 \hat{n} \wedge \underline{H} \Phi + (\hat{n} \cdot \underline{E}^e) \nabla \Phi \right\} dS, \end{aligned} \quad (C.1)$$

where  $\underline{E}^0$  is the incident electric field,

$$\Phi = \frac{e^{ikR}}{R}, \quad (C.2)$$

---

\* This formulation is due to Dr. Vaughan H. Weston.

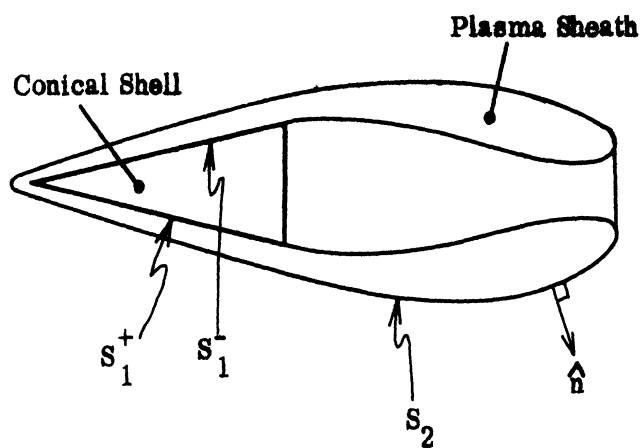


FIG. C-1: Geometry of the Problem.

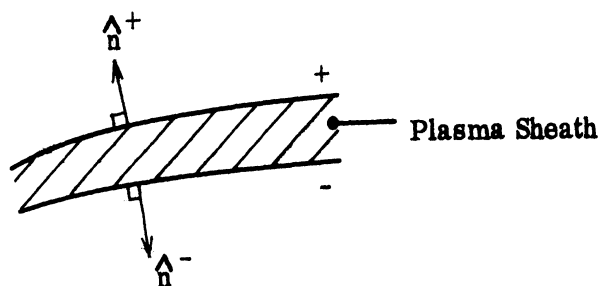


FIG. C-2: Convention for Unit Normals.

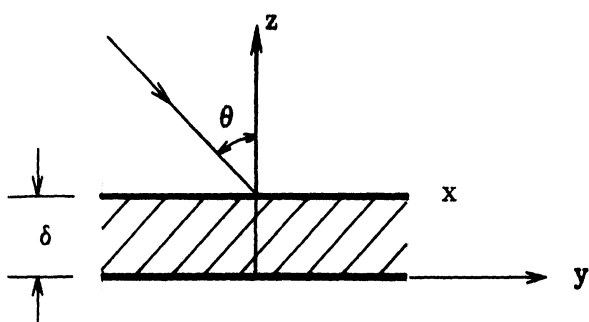


FIG. C-3: Geometry for Jump Condition.

and  $R = |\underline{x} - \underline{x}_0|$  is the distance between the integration point  $\underline{x}$  and the observation point  $\underline{x}_0$ ; the unit normal  $\hat{n}$  is directed from the shell or plasma into the surrounding free space (Fig. C-1). The superscript e on  $\hat{n} \cdot \underline{E}^e$  denotes the exterior value of the normal component. If  $\hat{n} \cdot \underline{E}^i$  represents the interior value, then on the plasma boundary  $S_2$ , we have the continuity conditions

$$\hat{n} \cdot \underline{E}^e = N^2 \hat{n} \cdot \underline{E}^i, \quad (C.3)$$

where  $N$  is the local index of refraction of the plasma sheath.

If  $S$  is the complete surface enclosing the plasma, i. e.  $S = S_2 + S_1^-$  where  $S_1^-$  is the concave portion of the conical surface, and  $V$  is the volume enclosed by  $S$ , it can be shown that for  $\underline{x}_0$  not in  $V$ ,

$$\int_V (k_1^2 - k^2) \underline{E} \Phi dV = \int_S \left\{ i \omega \mu_0 \hat{n} \wedge \underline{H} \Phi + (\hat{n} \wedge \underline{E}) \wedge \nabla \Phi + (\hat{n} \cdot \underline{E}^i) \nabla \Phi \right\} dS$$

where  $k_1^2 = N^2 k^2$ . Employing this relation, Eq. (C.1) can be placed in the form

$$\begin{aligned} \underline{E}(\underline{x}_0) = \underline{E}^0(\underline{x}_0) + \frac{1}{4\pi} \int_V (k_1^2 - k^2) \underline{E} \Phi dV + \frac{1}{4\pi} \int_{S_2} \hat{n} \cdot \underline{E}^e (1 - N^{-2}) \nabla \Phi dS + \\ + \frac{1}{4\pi} \int_{S_1} \left\{ i \omega \mu_0 \hat{n} \wedge (\underline{H}^- - \underline{H}^+) \Phi + \hat{n} \cdot (\underline{E}^- - \underline{E}^+) \nabla \Phi \right\} dS, \end{aligned} \quad (C.4)$$

where use has been made of relation (C.3). The notation  $\underline{H}^-$  and  $\underline{H}^+$  refers to the values of  $\underline{H}$  on the concave and convex portions of  $S_1$ , respectively. It can be shown that Eq. (C.4) is valid also for  $\underline{x}_0$  in  $V$ . As a check, it is seen that when  $S_1$  vanishes, i. e. only the conical sheath is present, Eq. (C.4) reduces to the integral equation of Barrar and Dolph (1954).

By taking the curl of Eq. (C.4), it can be deduced that

$$\underline{H}(\underline{x}_0) = \underline{H}^0(\underline{x}_0) - \frac{i}{4\pi\omega\mu_0} \int_V (k_1^2 - k^2) \nabla_0 \Phi \wedge \underline{E} dV + \frac{1}{4\pi} \int_{S_1} \nabla_0 \Phi \wedge [\hat{n} \wedge (\underline{H}^- - \underline{H}^+)] dS, \quad (C.5)$$

where  $\nabla_0$  operates on  $\underline{x}_0$ .

We shall consider the case of an overdense penetrable sheath, i. e.

$|N| \gg 1$ , but  $|k\delta N| \ll 1$  where  $\delta$  is the thickness of the sheath. The process shall be accomplished by taking the limits  $k\delta \rightarrow 0$ ,  $N \rightarrow \infty$ , such that the factor

$$\eta = N^2 k\delta \quad (C.6)$$

remains constant. For such a situation, it is shown in section C.2 that for the portion of the plasma sheath not bounded by the conductor  $S_1$ , jump conditions upon the tangential magnetic field will prevail, namely

$$Z \left[ \hat{n}^+ \wedge \underline{H}^+ + \hat{n}^- \wedge \underline{H}^- \right] = -\frac{i\eta}{2} \left[ \underline{E}_{\tan}^+ + \underline{E}_{\tan}^- \right], \quad (C.7)$$

where  $\hat{n}^+$  and  $\hat{n}^-$  are the normal unit vectors directed out of the plasma sheath (see Fig. C-2). In addition, there is little change in the tangential component of the electric field intensity, i. e.

$$\underline{E}_{\tan}^+ \sim \underline{E}_{\tan}^- \quad (C.8)$$

When the sheath is bounded on one side by a perfect conductor, the tangential fields on the free side can be expressed in terms of an impedance boundary condition. Since the permeability is the same as in free space, the tangential fields approximate those for a perfect conductor, i. e.  $\underline{E}_{\tan} \sim 0$ .

By employing Eqs. (C.4) and (C.8), or Eqs. (C.1) and (C.7) for the unbounded portion of the sheath, it can be shown that

$$\begin{aligned} \underline{\underline{E}}(\underline{\underline{x}}_0) = \underline{\underline{E}}^0(\underline{\underline{x}}_0) + \frac{i\omega\mu_0}{4\pi} \int_{S_1} \hat{\underline{\underline{n}}} \wedge [\underline{\underline{H}}^- - \underline{\underline{H}}^+] \Phi \, dS + \frac{k}{4\pi} \int_{S_2} \eta \underline{\underline{E}}_{\tan} \Phi \, dS + \\ + \frac{1}{4\pi} \int_{S_2+S_1} \hat{\underline{\underline{n}}} \cdot [\underline{\underline{E}}^- - \underline{\underline{E}}^+] \nabla \Phi \, dS . \end{aligned} \quad (\text{C.9})$$

The representation for the magnetic field becomes

$$\underline{\underline{H}}(\underline{\underline{x}}_0) = \underline{\underline{H}}^0(\underline{\underline{x}}_0) + \frac{1}{4\pi} \int_{S_1} \nabla_0 \Phi \wedge \left\{ \hat{\underline{\underline{n}}} \wedge (\underline{\underline{H}}^- - \underline{\underline{H}}^+) \right\} dS - \frac{iY}{4\pi} \int_{S_2} \eta k \nabla_0 \Phi \wedge \underline{\underline{E}}_{\tan} \, dS . \quad (\text{C.10})$$

To develop the integral equation we first set

$$\underline{\underline{J}} = \hat{\underline{\underline{n}}} \wedge [\underline{\underline{H}}^- - \underline{\underline{H}}^+] . \quad (\text{C.11})$$

It can be shown that

$$i\omega\epsilon_0 \hat{\underline{\underline{n}}} \cdot [\underline{\underline{E}}^- - \underline{\underline{E}}^+] = \hat{\underline{\underline{n}}} \cdot [\nabla \wedge \underline{\underline{H}}^- - \nabla \wedge \underline{\underline{H}}^+] = \nabla \cdot [\hat{\underline{\underline{n}}} \wedge \underline{\underline{H}}^- - \hat{\underline{\underline{n}}} \wedge \underline{\underline{H}}^+] = -\nabla \cdot \underline{\underline{J}} . \quad (*)$$

(\*) Note. For a curvilinear surface formed by the coordinate  $u_3 = \text{constant}$  of an orthogonal coordinate system  $(u_1, u_2, u_3)$ , the relation should be

$$\hat{\underline{\underline{n}}} \cdot [\nabla \wedge \underline{\underline{H}}^- - \nabla \wedge \underline{\underline{H}}^+] = -\nabla \cdot \underline{\underline{J}} + \frac{\nabla h_3 \cdot \underline{\underline{J}}}{h_3} ,$$

where  $h_3$  is the metric coefficient normal to the surface.

Equation (C.9) then reduces to the form

$$\underline{E}(\underline{x}_o) = \underline{E}^o(\underline{x}_o) + \frac{i\omega\mu_o}{4\pi} \int_S \underline{J} \bar{\Phi} dS - \frac{i}{4\pi\omega\epsilon_o} \int_S (\nabla \cdot \underline{J}) \nabla \bar{\Phi} dS$$

where  $S = S_1 + S_2$ . Let the point  $\underline{x}_o$  approach the surface  $S$ . We then obtain the following integral equation

$$\hat{n}_p \wedge \underline{E}(\underline{x}_p) = \hat{n}_p \wedge \underline{E}^o(\underline{x}_p) + \frac{i\omega\mu_o}{4\pi} \int_S (\hat{n}_p \wedge \underline{J}) \bar{\Phi} dS - \frac{i}{4\pi\omega\epsilon_o} \int_S (\nabla \cdot \underline{J}) \hat{n}_p \wedge \nabla \bar{\Phi} dS, \quad (C.12)$$

where

$$\begin{aligned} \hat{n}_p \wedge \underline{E}(\underline{x}_p) &= 0, & \text{for } \underline{x}_p \text{ on } S_1, \\ &= \frac{iZ}{\eta} \hat{n}_p \wedge \underline{J}, & \text{for } \underline{x}_p \text{ on } S_2. \end{aligned} \quad (C.13)$$

Equation (C.12) is thus the fundamental integral equation. For Rayleigh scattering, this equation can be simplified by replacing  $\bar{\Phi}$  with  $1/R$ .

## C.2 The Jump Condition

We shall derive the jump conditions associated with the magnetic field for a plane wave incident upon an overdense plasma slab whose thickness is less than the skin depth, i.e. a penetrable slab.

The geometry is given in Fig. C-3 with the plane of incidence being the  $y$ - $z$  plane. The angle of incidence is given by  $\theta$ , the thickness of the slab by  $\delta$ , and the index of refraction by  $N$ . The two cases of polarization will be treated separately.



### 1) Polarization Perpendicular to the Plane of Incidence

In this case we have

$$\underline{E} = \hat{x} u(z) e^{iky \sin \theta},$$

$$i\omega\mu_0 H_y = \frac{\partial u}{\partial z} e^{iky \sin \theta}$$

where  $u(z)$  will have the following form

$$\begin{aligned} u &= T e^{-i\alpha_0 z}, & \text{for } z < 0, \\ &= T \left[ \cos \alpha_p z - ip \sin \alpha_p z \right], & \text{for } 0 \leq z \leq \delta, \\ &= e^{-i\alpha_0(z-\delta)} + R e^{i\alpha_0(z-\delta)}, & \text{for } z \geq \delta. \end{aligned}$$

The parameters  $\alpha_0$ ,  $p$ , and  $\alpha_p$  are defined as follows

$$\begin{aligned} \alpha_0^2 &= k^2 \cos^2 \theta, \\ \alpha_p^2 &= (N^2 - \sin^2 \theta) k^2, \\ p &= \alpha_0 / \alpha_p. \end{aligned}$$

The transmission coefficient  $T$  is given by the relation

$$T = \left[ \cos \phi - \frac{i}{2} \left( \frac{1}{p} + p \right) \sin \phi \right]^{-1},$$

where  $\phi = \alpha_p \delta$ , and the reflection coefficient  $R$  satisfies the relations

$$\begin{aligned} 1 + R &= T \left[ \cos \phi - ip \sin \phi \right], \\ R - 1 &= \frac{T}{p} \left[ i \sin \phi - p \cos \phi \right]. \end{aligned}$$

By omitting the factor  $e^{iky \sin \theta}$ , we have

$$\begin{aligned} Z \left[ H_y(\delta) - H_y(0) \right] &= -\frac{i}{k} \left[ \left( \frac{\partial u}{\partial z} \right)_\delta - \left( \frac{\partial u}{\partial z} \right)_0 \right] \\ &= -\frac{i}{k} \left[ i\alpha_o (R-1) + iT\alpha_o \right] = (R+T-1) \cos \theta = T \cos \theta \left[ 1 + \frac{i \sin \phi}{p} - \cos \phi \right] \\ &\sim T \left[ i\phi \sqrt{N^2 - \sin^2 \theta} + O(\phi^2 \cos \theta) \right], \end{aligned}$$

$$\frac{1}{2} \left[ E_x(\delta) + E_x(0) \right] = \frac{1}{2} [1+R+T] = \frac{T}{2} [1 + \cos \phi - i p \sin \phi] \sim T [1 + O(p\phi) + O(\phi^2)].$$

From these two relations we have the jump condition for  $|Nk\delta| \ll 1$  :

$$Z \left[ H_y^+ - H_y^- \right] \sim \frac{i}{2} N^2 k \delta \left[ E_x^+ + E_x^- \right] \quad (C.14)$$

In addition we have

$$E_x^+ - E_x^- = 1 + R - T \sim T \left[ \cos \phi - i p \sin \phi - 1 \right] \sim T \left[ -\frac{\phi^2}{2} - i p \phi \right] \sim -i p \phi \rightarrow 0. \quad (C.15)$$

## 2) Polarization in the Plane of Incidence

Here we have

$$Z \underline{H} = \hat{x} u(z) e^{iky \sin \theta},$$

and

$$E_y = \frac{iZ}{N^2 k} \frac{\partial H_x}{\partial z}.$$

The function  $u(z)$  has the form

$$\begin{aligned}
 u &= T e^{-i\alpha_0 z}, & \text{for } z < 0, \\
 &= T \left[ \cos(\alpha_p z) - iq \sin(\alpha_p z) \right], & \text{for } 0 \leq z \leq \delta, \\
 &= e^{-i\alpha_0(z-\delta)} + R e^{i\alpha_0(z-\delta)}, & \text{for } \delta < z,
 \end{aligned}$$

where

$$q = N_p^2 \nu N \cos \theta.$$

The transmission coefficient  $T$  is given by

$$T = \left[ \cos \theta - \frac{i}{2} \left( q + \frac{1}{q} \right) \sin \theta \right]^{-1}$$

and the reflection coefficient  $R$  satisfies the relations

$$1 + R = T \left[ \cos \theta - iq \sin \theta \right],$$

$$R - 1 = \frac{T}{q} \left[ i \sin \theta - q \cos \theta \right].$$

By omitting the factor  $e^{ik_y \sin \theta}$ , we have

$$Z \left[ H_x^+ - H_x^- \right] = 1 + R - T = T \left[ \cos \theta - iq \sin \theta - 1 \right] = T \left[ -iq \sin \theta - (\cos^2 \theta) \right]$$

and

$$\begin{aligned}
 \frac{1}{2} \left[ E_y^+ + E_y^- \right] &= \frac{i}{2k} \left[ +i\alpha_0(-1+R) - i\alpha_0 T \right] = \frac{\cos \theta}{2} (T+1-R) \\
 &= \frac{1}{2} \cos \theta T \left[ 1 - \frac{i \sin \theta}{q} + \cos \theta \right] \nu T \left[ \cos \theta - \frac{i}{2} k\delta \right].
 \end{aligned}$$

Thus we have

$$Z \left[ \underline{H}_x^+ - \underline{H}_x^- \right] = -\frac{i}{2} N^2 k \delta \left[ \underline{E}_y^+ + \underline{E}_y^- \right] . \quad (C.16)$$

In addition, it can be shown that

$$\begin{aligned} \underline{E}_x^+ - \underline{E}_x^- \sim \cos \theta (-T+1-R) &= T \cos \theta \left[ -1 - \frac{i \sin \phi}{q} + \cos \phi \right] \\ &\sim T \cos \theta \left[ -\frac{\phi^2}{2} - \frac{i\phi}{q} \right] \sim -\frac{i\phi}{q} \cos \theta \left[ 1 + \frac{i\phi}{2} q \right] T \sim O(k\delta) . \end{aligned} \quad (C.17)$$

By using (C.14) and (C.16), we see that the jump condition can be expressed in the vector form:

$$Z \left[ \hat{n} \wedge \underline{H} \right]_{-}^{+} = -\frac{i}{2} N^2 k \delta \left[ \underline{E}_{\tan}^+ + \underline{E}_{\tan}^- \right] ,$$

which is relation (C.7). Furthermore, it follows from (C.15) and (C.17) that  $\underline{E}_{\tan}$  is continuous, i.e.

$$\underline{E}_{\tan}^+ \sim \underline{E}_{\tan}^- ,$$

which is relation (C.8).

### C.3 Reference

Barrar, R. B. and C. L. Dolph, (1954), "On a Three Dimensional Transmission Problem of Electromagnetic Theory," J. Rational Mech. Anal. (now J. Math. Mech.) 3, pp. 725-743.

## DOCUMENT CONTROL DATA - R &amp; D

(Security classification of title, body of abstract and indexing annotation must be entered when the overall report is classified)

1. ORIGINATING ACTIVITY (Corporate author) The University of Michigan Radiation Laboratory, Dept. of Electrical Engineering, 201 Catherine Street, Ann Arbor, Michigan 48108		2a. REPORT SECURITY CLASSIFICATION Unclassified	
3. REPORT TITLE  Low Frequency Scattering by Plasma Coated Objects		2b. GROUP	
4. DESCRIPTIVE NOTES (Type of report and inclusive dates) Final Report January 1969 - January 1970			
5. AUTHOR(S) (First name, middle initial, last name)  R. E. Kleinman, T. B. A. Senior and P. L. E. Uslenghi			
6. REPORT DATE  January 1970	7a. TOTAL NO. OF PAGES  156	7b. NO. OF REFS  35	
8a. CONTRACT OR GRANT NO. DAAH01-69-C-0875	9a. ORIGINATOR'S REPORT NUMBER(S)  2425-1-F		
b. PROJECT NO. ARPA Order 709	9b. OTHER REPORT NO(S) (Any other numbers that may be assigned this report)		
c. Program Code Number 8 E 40	d.		
10. DISTRIBUTION STATEMENT Each transmittal of this document outside the Department of Defense, must have prior approval of U. S. Army Missile Command, Redstone Arsenal, Alabama 35809, ATTN: AMSMI-RNA			
11. SUPPLEMENTARY NOTES		12. SPONSORING MILITARY ACTIVITY Advanced Research Projects Agency Monitored by U. S. Army Missile Command Redstone Arsenal, Alabama 35809	
13. ABSTRACT  The scattered field produced by a plane electromagnetic wave incident on a plasma coated re-entry vehicle is studied, in the low-frequency limit. When the collision frequency is large with respect to the operational frequency, the determination of the electric and magnetic dipole moments of the scatterer is reduced to the solution of two standard potential problems for perfect conductors.  For axially symmetric bodies, only three of the six dipole moment coefficients are independent. The dipole moments are found for a variety of scattering shapes, and the low-frequency radar cross section is obtained for any direction of incidence and for different combinations of the shapes of the bare vehicle and of the outer surface of the plasma sheath.			

14.

KEY WORDS

Re-entry vehicle  
Plasma sheath  
Electromagnetic scattering  
Low frequency  
Radar cross section  
Dipole moments

LINK A

LINK B

LINK C

ROLE

WT

ROLE

WT

ROLE

WT